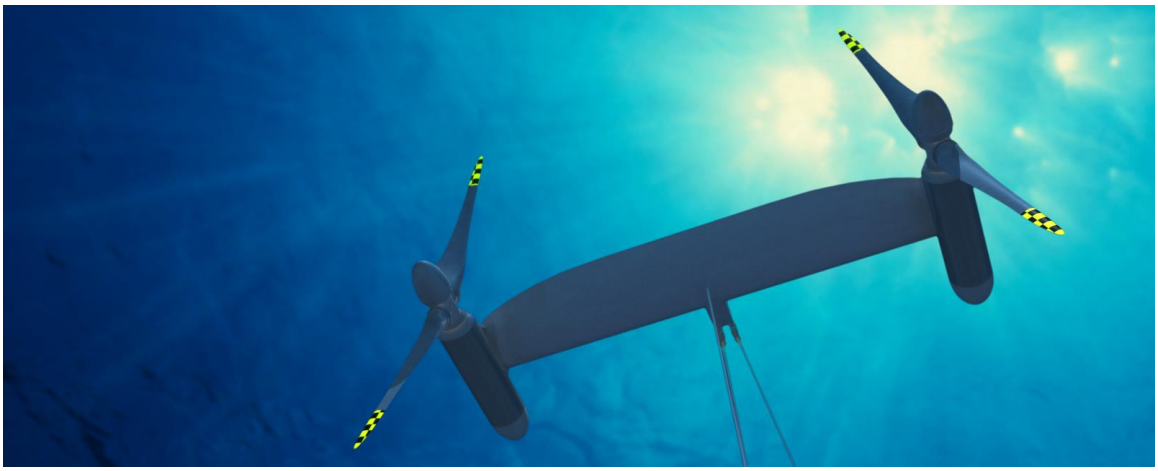

Aquantis C-Plane Ocean Current Turbine Project

Marine Hydrokinetic Power Generation
September 1, 2009 – December 31, 2014

Alex Fleming
Dehlsen Associates, LLC
Santa Barbara, California

NOTICE

U.S. Department of Energy Disclaimer

This report was prepared as an account of work partially sponsored by an agency of the United States Government. Neither the United States Government nor any agency thereof, nor any of their employees, makes any warranty, express or implied, or assumes any legal liability or responsibility for the accuracy, completeness, or usefulness of any information, apparatus, product, or process disclosed, or represents that its use would not infringe privately owned rights. Reference herein to any specific commercial product, process, or service by trade name, trademark, manufacturer, or otherwise does not necessarily constitute or imply its endorsement, recommendation, or favoring by the United States Government or any agency thereof. The views and opinions of authors expressed herein do not necessarily state or reflect those of the United States Government or any agency thereof.

Project Consortium Legal Notice/Disclaimer

This report was prepared by Dehlsen Associates, LLC pursuant to a Grant funded by the U.S. Department of Energy (DOE) under Instrument Number DE-EE0003643. NO WARRANTY OR REPRESENTATION, EXPRESS OR IMPLIED, IS MADE WITH RESPECT TO THE ACCURACY, COMPLETENESS, AND/OR USEFULNESS OF INFORMATION CONTAINED IN THIS REPORT. FURTHER, NO WARRANTY OR REPRESENTATION, EXPRESS OR IMPLIED, IS MADE THAT THE USE OF ANY INFORMATION, APPARATUS, METHOD, OR PROCESS DISCLOSED IN THIS REPORT WILL NOT INFRINGE UPON PRIVATELY OWNED RIGHTS. FINALLY, NO LIABILITY IS ASSUMED WITH RESPECT TO THE USE OF, OR FOR DAMAGES RESULTING FROM THE USE OF, ANY INFORMATION, APPARATUS, METHOD OR PROCESS DISCLOSED IN THIS REPORT.

For further information about Dehlsen Associates, LLC, call 805-845-7575
or e-mail Alex J. Fleming at afleming@ecomerittech.com

This publication is a corporate document that should be cited in the literature in the following manner: "Aquantis C-Plane Ocean Current Turbine Project" Dehlsen Associates, LLC, Santa Barbara, CA and U.S. Department of Energy, Washington, DC: 2015.0003643

This report describes research sponsored by Dehlsen Associates, LLC and the U.S. Department of Energy. The U.S. Department of Energy, Energy Efficiency and Renewable Energy Office, Wind & Water Power Program provided 60% of project funding via grant number DE-EE0003643, "Aquantis C-Plane Ocean Current Turbine Project". Long-term development of the Aquantis turbine including the accomplishments discussed herein would not have been possible without the support and vision of many DOE project managers.

Table of Contents

ACCOMPLISHMENTS

PROJECT OBJECTIVES

The principal objective of the Aquantis Project is development of technology to harness the vast Gulf Stream energy resource with innovative breakthrough power generation technology, projected to be cost competitive with thermal power generation in early deployment.

PROJECT DELIVERABLES

This effort will result in six conclusive products:

1. Experimental Validation of Analytical Tools/Design: Use of Scale (1/20th to 1/25th) Models and Full Scale Component Testing, Subsystem Integration and Global System responses will be used to validate analytical tools and gain confidence in device performance and loads.
2. Cost of Energy Model: Robust model factoring in Capital Expenditure (CAPEX) and Operational Expenditure (OPEX). This Techno Economic model will evolve, giving specific design goals for serviceability, maintenance intervals, and reliability.
3. Garner Certification and Permitting Approvals.
4. Drawing Package: Scaled Proof of Concept and Full Scale Prototype drawings.
5. Subsystem Evolution: Critical subsystem scaled testing and integration.
6. Final Report: Design, Trade Studies and Validation via Virtual Prototyping using the latest Computer-Aided Engineering tools and leveraging a significant experience base in marine renewable energy conversion and the design of offshore structures

PROJECT SCOPE

The Aquantis 2.5 MW Ocean Current Generation Device technology developed by Dehlsen Associates, LLC (DA) is a derivation of wind power generating technology (a means of harnessing a slow moving fluid) adapted to the ocean environment. The Aquantis Project provides an opportunity for accelerated technological development and early commercialization, since it involves the joining of two mature disciplines: ocean engineering and wind turbine design. The Aquantis Current Plane (C-Plane) technology is an ocean current turbine designed to extract kinetic energy from a current flow. The technology is capable of achieving competitively priced, continuous, base-load, and reliable power generation from a source of renewable energy not before possible in this scale or form.

The C-Plane operates 50m below the ocean surface and is tethered to the ocean floor at 200m to 300m of depth. The design allows for operational surfacing for periodic maintenance of the units. While C-Plane deployment would be phased with appropriate environmental milestones for expansion to proceed, it is estimated that 6,500 MW of generating capacity could be in operation within 10 years from start; similar to the deployment experienced by early stage wind power in several European countries.

SYSTEM DESCRIPTION

Early conceptualization of the C-Plane is shown in **Figure 1** which illustrates the dual rotors, nacelles, and the connecting transverse structure. The overall system is intended to be moored to the seafloor in a relatively fixed position in an ocean current resource 50m below the surface in 200m to 300m of water depth. The rotor diameter in this early concept is on the order of 42m. Each nacelle contains a main shaft, wet brake, hydrostatic drivetrain, generator, transformer, filters, heat exchangers, condition based monitoring equipment, and a cable connection to the onshore electrical grid. These nacelle design features are shown in **Figure 2.** Operation of the system consists of the rotor being driven by the ocean current flow which in turn rotates the main shaft. Two hydraulic pumps are attached to the main shaft and these power two hydraulic motors. The hydraulic motors turn a generator of which the speed is kept constant through valving and variable displacement of one of the motors. Generator voltage is stepped up with the transformer to an appropriate level for long distance transmission.

Further development of the concept and levelized cost of energy (LCOE) economic analysis resulted in the shift to a single rotor, gearbox driven and pitched rotor control hub system**.** The final configuration that DA down selected at the end of the MHK reporting period is a 500kW, 27m diameter single rotor, pitch controlled turbine with a conventional main bearing, gearbox, and permanent magnet generator drivetrain. The LCOE of this configuration presented the most promising initial commercial cost of energy and allows for future cost of energy (COE) reductions with larger rotors and higher power ratings.

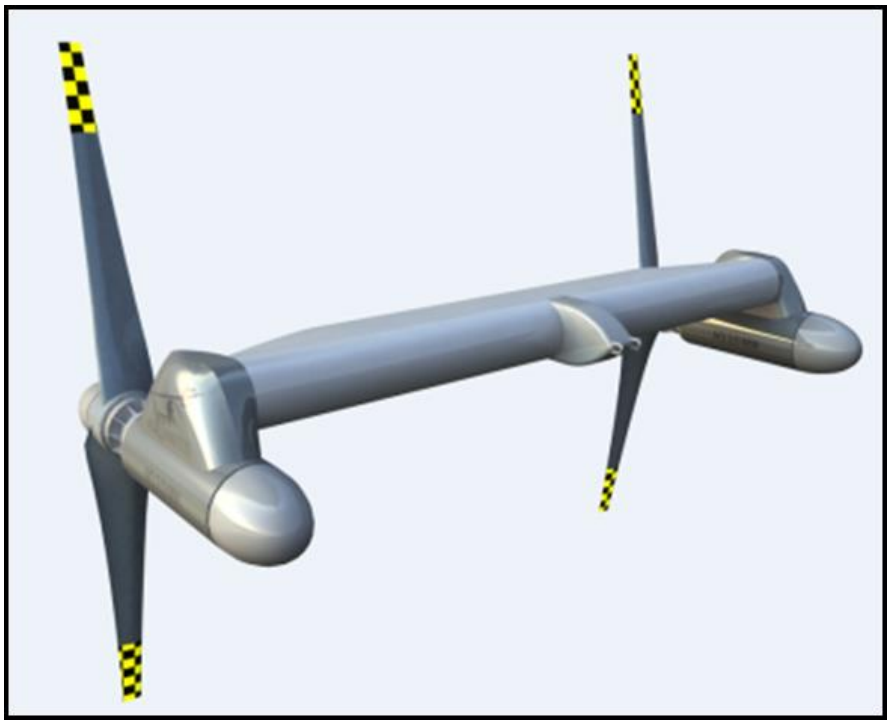

Figure 1 - Dual Rotor C-Plane Concept

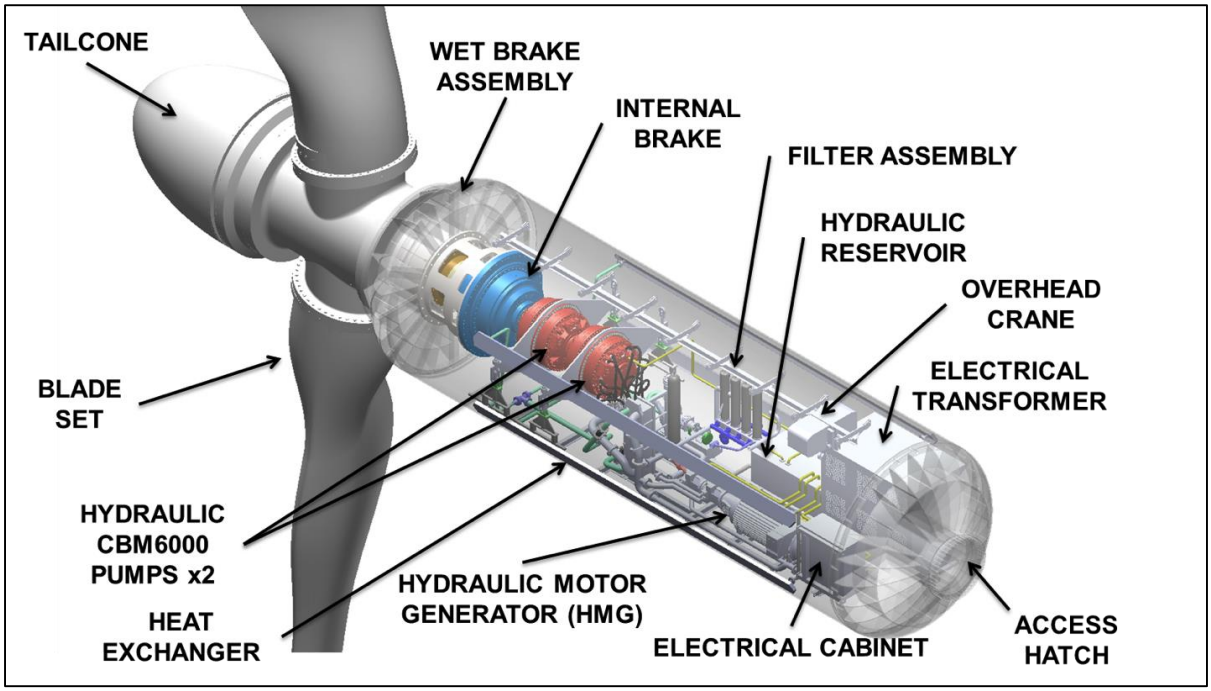

Figure 2 - C-Plane Nacelle Assembly

PHASE 1: SCOPE OF WORK

The following scope of work items were planned under Phase 1 of the project.

Task 1: Dynamic Stability and Simulation

Task 1.1 Naval Architecture

The C-Plane design will be developed and matured through the implementation of naval architecture principles. Analysis will be completed to determine center of gravity, center of buoyancy, and overall center of lift as well as weight in air, weight in water, displacement, and calculated moments of inertia.

Task 1.2 Hydrodynamic Analysis

The team will perform detailed hydrodynamic analyses of the C-Plane platform to assess the platform characteristics in terms of basic hydrodynamic and static forces (i.e. lift, drag, buoyancy, weight) and moments developed for various current speeds flowing through/over the platform.

Task 1.2.1 Hydrodynamic Coefficient Development

Hydrodynamic coefficients will be the principle input for the dynamic simulation of the C-Plane configuration. The dynamic simulation will be capable of analyzing vehicle motions, control surface sizing, resultant loads imparted to the Aquantis system from the C-Plane, and other information of concern. Coefficients will be developed analytically through computer modeling and empirically through Tow Tank testing. Comparisons of coefficients between the two methods of development will be made.

Task 1.3 C-Plane Dynamic Simulation Analysis

The hydrodynamic design and performance of the C-Plane will be evaluated. Information to be provided is: hydrodynamic performance, resultant forces to the system, etc.

Task 1.4 Mooring Analysis

A time domain analysis procedure is to be used to calculate maximum design tensions for the mooring system of the turbine, mooring cables, and anchor system. The dynamic simulation analysis is to be used as input to calculate time histories of dynamic mooring line tensions.

Several realistic simulations are to be used to derive design values of maximum tension at all points in the mooring system.

Task 1.4.1 OrcaFlex

OrcaFlex will be used to model the moorings. OrcaFlex is a nonlinear time domain, finite element software program principally used for the static and dynamic modeling of systems used in offshore construction environment, including marine risers of the flexible and rigid types, mooring systems and towed arrays.

Task 1.5 System Modeling, Stability, Computational Fluid Dynamics, and Finite Element Analysis

An external function that defines the complex hydrodynamic relationship between the turbine and the surrounding fluid will be incorporated into the OrcaFlex simulation to define the performance of the complete system.

Task 1.6 Go/No-Go Decision Meeting

PHASE 2: SCOPE OF WORK

The following scope of work items were planned under Phase 2 of the project.

Task 2: Tow Tank Tests

Task 2.1 Scale C-Plane Model Platform and Mooring Fabrication- 1/20th

The 1/20th-scale model will be designed and fabricated based on the results of the hydrodynamic analysis and analytical codes BODXYZ, DCAB and Flightlab. The team will provide the C- Plane center pod, the support spars, instrumentation and their required pressure housings of in- water operations (in the test facilities) as well as the interface capability for external pods.

Task 2.2 Platform Instrumentations: Inertial Measurement Unit, Transducers Load Cell. Instrumentation within the center pod of the model will include: an inertial measurement unit which provides direct measurements of accelerations in the x, y, and z directions as well as roll rate, pitch rate, and yaw rate. The inertial measurement unit will also provide processed angular measurements for roll and pitch. A pressure gage will also be installed to provide measured depth during the basin evaluations.

Task 2.3 Scale Turbine Blades Fabrication - 1/20th

Towing-tank testing will include instrumentation to address the important issues of energy extraction and fatigue. The blades will be laid-up and cured in halves (pressure and suction side) using a laminate. If the scale of the prototype permits, a mechanical interlocking feature will be included in each blade half laminate to accommodate the infusion of a foreign object damage resistant leading edge.

Task 2.4 Basin Test Towing Hardware

A towing bridle with end terminations designed specifically for the basin test will be completed The bridle will be made of an electro-mechanical cable capable of transmitting data signals from on-board instrumentation and electrical power transmission as required by the instrumentation packages.

Task 2.5 Tow Tank Tests: Basin Evaluation

A basin evaluation of a 1/20th-scale C-Plane model will be performed to validate the hydrodynamic design and loads imparted on the mooring system. Total costs include follow-on studies from Task 1.3 dynamic stability analysis in preparation for the tank testing, testing costs, post-processing, and report writing.

Task 2.6 Mechanical Turbine Design

The mechanical turbine design for Aquantis will be completed including the bearing and seal design selection and the wet brake.

Task 3: Marine Composite Material Testing

Further refinement of the rotor's through-hub spar concept will evaluate suitable material selection and test the spar with and without joints.

Task 3.1 Spar Testing (with and without joints)

The spar testing will include design of the test articles, response prediction, fabrication of two test articles, static testing of one article, fatigue testing of the second article, and correlation of experimental results and predictions.

Task 3.2 Pass-through-Spar-to-Hub Attachment

The spar testing will include design of the test articles, response prediction, fabrication of two test articles, static testing of one article, fatigue testing of the second article, and correlation of experimental results and predictions.

Task 3.3 Skin-to-Spar Attachment

To test the skin attachment to the spar, two articles will be designed with their responses predicted prior to testing. One test article will be fabricated and used for static testing, while the second will be fabricated and fatigue tested. The experimental results will then be correlated with the original predictions.

Task 3.4 Identification of Critical Failure Modes and Effects

The results of the through-hub spar testing, hub attachment and skin to spar attachment will be used to identify critical failure modes and effects for the blade hub attachment.

Task 4: Platform Design

Platform design analysis will determine the most suitable connective structure between the nacelles. Both a truss structure and a wing structure will be evaluated according to static and dynamic stability design requirements, capital costs, and structural requirements. Finite element analysis modeling tools and Navy stability codes will be used to evaluate both designs. The connective structure will be evaluated in the tow tank and efforts will be made to measure the wake fraction impact on downstream rotors

Task 5: Hydrodynamic and Bearing Design

The rotor will continue to be evaluated in terms of hydrodynamics using NREL codes: Wind Turbine Performance Predictor (WT_Perf), Horizontal Axis Rotor Performance Optimization (Harp_Opt), and Xfoil and compared with computational fluid dynamics (CFD) results. These results are to be used in the structural, finite element analysis (FEA) models and mechanical design.

Task 5.1 Bearing Design

Design of the rotor bearing design will determine an appropriate bearing based upon the rotor thrust and torque loading applied to the shaft. The bearing design will evaluate wet and dry concepts, cost considerations, and robustness of each option.

Task 6: Final Design Review

Dehlsen Associates, LLC will participate in a final design review meeting with representatives from the DOE.

PHASE 1: WORK ACCOMPLISHED

The following scope of work tasks and results were accomplished under Phase 1 of the project.

Task 1: Dynamic Stability and Simulation

1.1 Naval Architecture

The C-Plane design has matured through iterative development including initial conceptualization of device stability parameters consisting of center of buoyancy (CB), center of gravity (CG), device overall mass, device inertias, component flow drag, and mooring design architecture.

Initial development for the naval architecture subcategory consisted of adjusting the system level tabulation of the component weights, buoyancies and the centers of these two parameters in accordance with the latest CAD models. This tabulation and the ensuing static analysis of all forces formed the basis for the overall system static stability. These parameters were used in the design of the tow tank test model to assure that the model exhibits the same stability characteristics as the full scale system.

Later iterations continued to focus on refining the weight and buoyancy analysis of the Aquantis C-Plane. Further refinement was conducted for the anticipated C-Plane tow tank test program. Detailed engineering work involved DA reviewing the current masses of all components and their placement within the system. An illustration of the full scale and model buoyancy analysis results are shown in **Figure 3** and **Figure 4**.

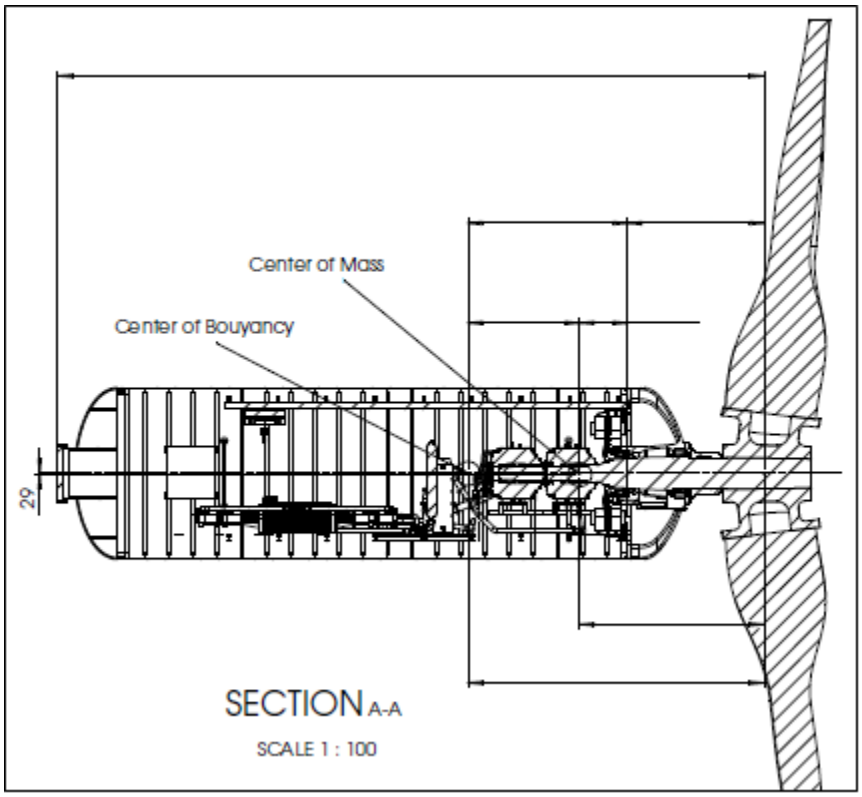

Figure 3 - Full-Scale Design CG and CB Locations

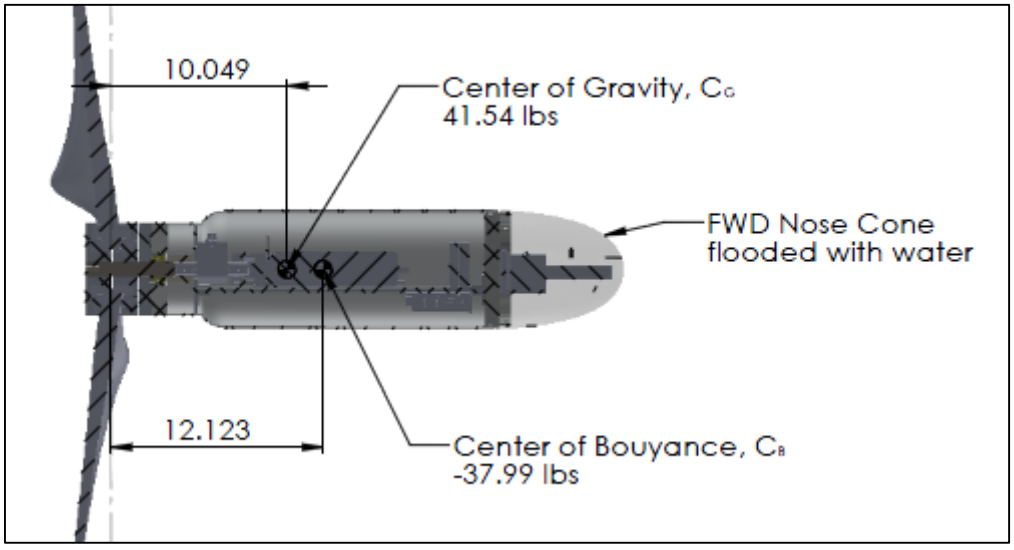

Figure 4 - Tow Tank Model CG and CB Locations

Further optimization of the C-Plane naval architecture parameters were conducted in preparation for the static and dynamic tow tank test. These efforts were focused on obtaining parameters by which to tune the tow tank model for optimum mass and buoyancy stability and in turn the inertial properties of the model. With respect to the single rotor and nacelle captured test model this process is fairly straight forward however, with the two rotors, dual nacelle moored model this analysis becomes more critical as the overall stability of the C-Plane is impacted. Several hand calculation and software tools were used in this process including DCAB, Flightlab and Tidal Bladed. A graphical representation of the significant points of interest is shown in **Figure 5**.

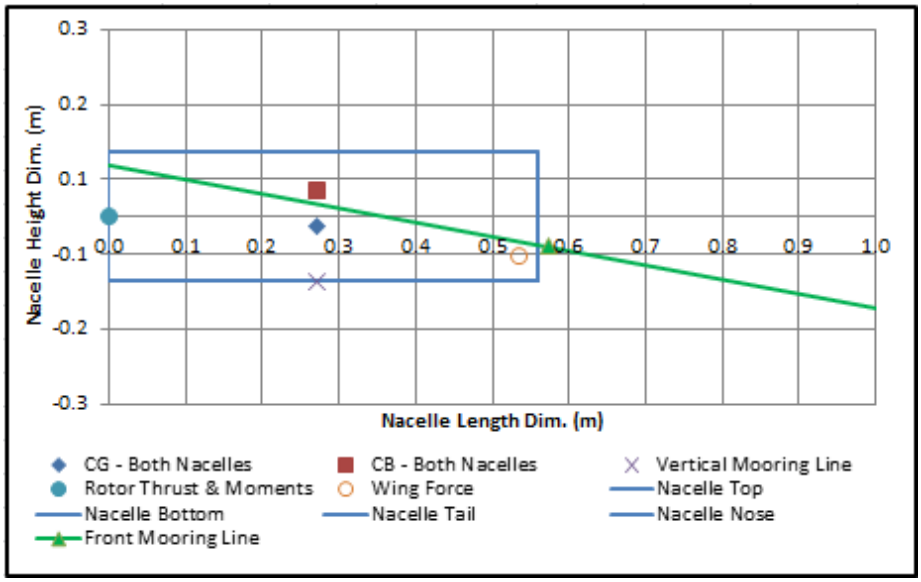

Figure 5 - Dynamic Test Model Mass and Buoyancy Analysis

Several computational methods were utilized to predict the stability of the C-Plane. The simplest of these is a steady-state platform pitch and depth calculation used to quickly iterate on model design parameters such as the locations of the mooring attachments, center of gravity (CG) and center of buoyancy (CB). At the center of this calculation is a force and moment balance which takes inputs from the NREL Blade-Element-Momentum (BEM) code WT_Perf and iterates on the platform depth and pitch to compute the resulting body and mooring forces and moments necessary to achieve a stable depth and pitch attitude. A representation of these forces and moments can be seen in **Figure 6**.

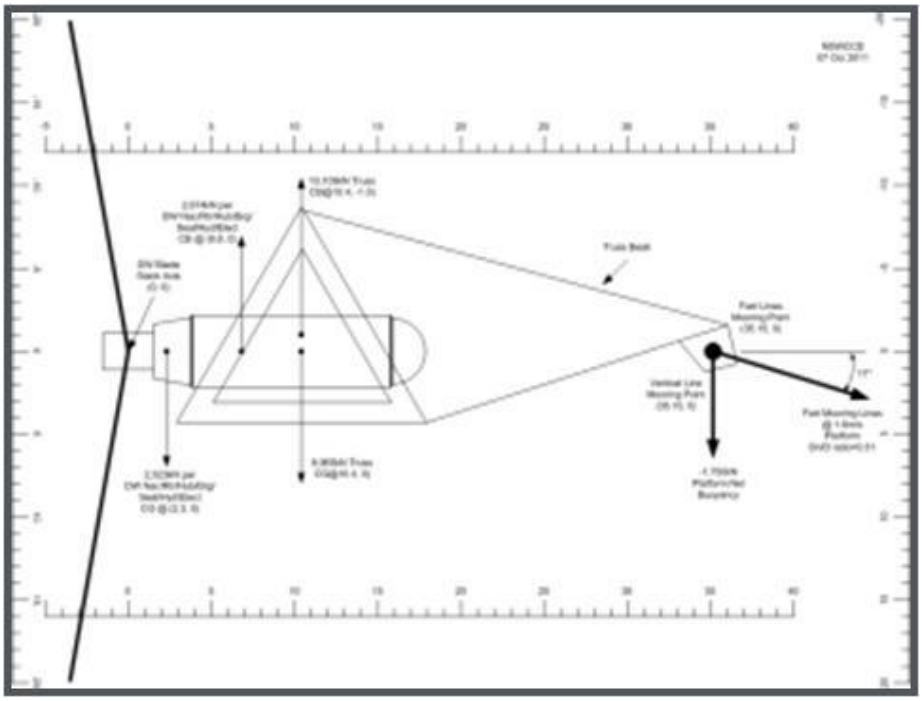

Figure 6 - C-Plane Body and Mooring Forces and Moments

DA has further developed the multi-body dynamics model of the single rotor C-Plane with present CAD measurements for the device center of gravity, center of buoyancy, structural mass, structural stiffness, and inertias to reflect the current design. The converged upon model characteristics were used to further refine the Tidal Bladed model to predict device response for the single rotor C-Plane.

In order to understand variance in construction, additional sensitivity studies were carried out to quantify the impact on device stability to variation in as-built tolerances. One such correlation, which is of specific interest to device stability, is the coupling of yaw error and mean roll vs. restoring moment. As expected, additional roll stability generated by separating the CG and CB reduces the device yaw and roll.

In conclusion, the C-Plane MHK device has undergone a coordinated product development path in regards to the device stability. The sensitivity analyses in conjunction with the tow tank tests have converged on a design which provides stability of the device during varying flow conditions through accurate location of the center of buoyancy, center of gravity, and device Inertias. CAD models were developed and validated in a tow tank test (TTT) to confirm accurate modeling of the Aquantis device. These tools are being used to develop a full scale prototype for deployment in the Florida Gulf Stream.

1.2 C-Plane Hydrodynamic and Dynamic Simulation Analysis

Due to substantial content overlap between the Statement of Project Objectives (SOPO) tasks 1.2 Hydrodynamic Analysis; 1.2.1 Hydrodynamic Coefficient Development; 1.3 C-Plane Dynamic Simulation Analysis and 1.5 System Modeling, Stability, Computational Fluid Dynamics and Finite Element Analysis it was decided to merge the final technical report content in these areas into this single section for clarity.

The C-Plane system level model was developed by DA in conjunction with its partners and validated through tow tank testing to multiple state of the art system codes. Model results were prepared and presented in the following sections. Throughout this multi-faceted development process, multiple configurations were analyzed and down selected to converge on a commercially viable low cost of energy product.

The simulation tools developed include multiple sub-system models covering the resource modeling, hydrodynamic interactions, structural response, and controller integration. Resource modeling was tuned from a comprehensive data collection plan and resolved into inflow characteristics to determine the boundary conditions impacting the stability, fatigue and performance of the C-Plane.

An evaluation of the flow boundary conditions that present stability and fatigue concerns for the C-Plane within the Florida Current or Florida Gulf Stream was conducted. These concerns include turbulence, internal waves, surface waves felt within 50m depths and below, current meandering, horizontal shear, and local current reversals. **Table 1** outlines the resource characteristics for the Florida current with specific characteristics affectivity stability highlighted in green, and characteristics affecting device fatigue highlighted in light blue.

Table 1 - Resource Characteristics and Influences on Stability and Loads

Concern in Florida Current	Cause	Length Scale	Speeds	Period
Seasonal upwelling, downwelling	Upwelling in trough of frontal eddies, lifts the density structure of the front in upper 200m	Amplitude = 10m	10m/day	day
Continental shelf waves	Seasonal winds cause upwelling/downwelling, flow over topography generates north/south along FL coast	100km	28cm/s	4days
		200km	15cm/s	14days
Internal waves – baroclinic inflection points	Where lines of constant density meet contours of constant pressure	Amplitude: 10m		30min Min. period = 10s. Max period = 24hrs
Inertial waves	Due to winds	Not of great concern	-	-

Concern in Florida Current	Cause	Length Scale	Speeds	Period
Solitary internal wave – SFOMF measured	Multiple phenomena	-	-	-
Meanders	Primarily barotropic instabilities	λ=100-250km	40 cm/s	2-14 days
		λ=160-240km	50 cm/s	4-6 days
		λ=340km	30cm/s	12, 5 days
		λ=170km	40cm/s	12, 5 days
		Amp = 5km	-	-
Eddies	Meander in current causes spin-offs at outer edges of core, Can occur from generation in Loop Current, baroclinic instabilities; D=meander amplitude, varies depending on bathymetry	-	50cm/s	11 hrs.
		D=10-30km, λ=75-122km, d=200m Miami	-	-
		D = 23km, L = 34km	39cm/s	2.2 days
		Spin-Offs, D=10km, L=20-30km	25cm/s	Interval 1-2days

Initial resource measurements were developed with DA's CRADA partner NSWC-CD. The resource data collection system includes a mooring system (**Figure 7**) composed of an array of acoustic instruments including acoustic Doppler current profilers (ADCP's) and Doppler volume samplers (DVS), which are able to provide velocity profiles through the water column. In general, sampling rates decrease with an increase in measurement region. A combination of a 150 kHz, 300 kHz, and 600 kHz ADCPs were proposed to acquire all three components of the mean velocity profile through the entire water column with varying levels of spatial and temporal characterizations (increasing acoustic frequency has finer spatial resolution but smaller measurement range). These measurements were installed at two separate locations spaced 150m apart in the cross-stream direction to avoid entanglement and provide horizontal sheer. Additionally, the 600 kHz ADCP would was used to monitor the surface waves.

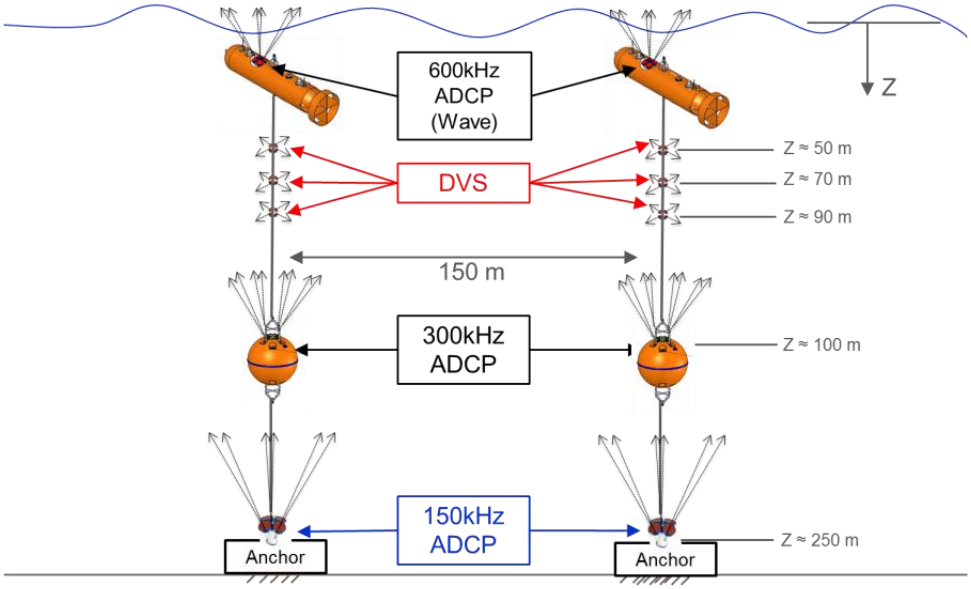

Figure 7 – Proposed Resource Assessment Instrumentation Arrangement

The ADCP measurements provide information about the mean flow of the ocean current, but lack sufficient temporal resolution to resolve smaller scale flow phenomenon that impact blade design (turbulence), fatigue (in-phase turbulent motions), and stability (out-of-phase turbulent motions). Consequently, a proposed array of six (6) Doppler volume sampler (DVS) instruments was planned to span the relevant length scales of the planned turbine system. The DVS (velocity) profiles are sufficiently small that they can be treated as point measurements within this flow environment. They can sample the three components of velocity at up to 3 Hz, which is sufficient to resolve flow structures smaller than 1 meter. Use of cross correlation (spatially and temporally) between the six DVS signals enabled the identification of relevant flow structures that impacted the system design.

The DVS was planned to measure a 2-5m range and positioned at the depth of the C-Plane rotor hub and tips. The sampling frequency was set to 1 Hz and the DVS is equipped with an accelerometer providing roll, pitch, and yaw. The accelerometer averages two samples for every time step for the DVS. The pressure measurements from 600kHz (at 50m) and 300kHz (at 100m) were used to determine the approximate catenary and therefore the position of the DVS sensors. Data analysis and quality assurance was carried out for the collected data and resolved into meaningful flow characteristics which were modeled into the stability models.

After careful planning and costing of such an instrumentation deployment and data gathering program it was determined that the cost was too prohibitive given the limited scope and budget of the program. Instead a resource measurement and characterization program was conducted using just mid-water ADCPs and an ocean surface based ADCP equipped glider. Both of these instruments measured gross flow in the Florida Gulf Stream to provide generic design and

economic data for the C-Plane. This data was gathered under the DA AWP –T1 grant program and fed into the various analysis programs used on this project.

System modeling was completed through the use of multiple codes in parallel for model validation. These included:

- NSWC-CD DCAB
- Flightlab
- Tidal Bladed

Much of the initial hydrodynamic stability work was conducted by the NSWC-CD. This work used a proprietary Navy code called DCAB developed in the 1990s to analyze dynamic stability of typical navy towed systems. DCAB was further improved including:

- Ability to handle multiple bodies such as nacelles, rotors and wings.
- Inclusion of rotor gyroscopic forces and moments.
- Estimates of current reduction over the structure due to the rotor induced drag.
- A second cable that is used to model the vertical line.

A comparative study of the hydrodynamic forces, moments, and overall stability as calculated from DCAB were cross checked with those calculated earlier from Flightlab and from an accurate Reynolds Averaged Navier Stokes solver run by an expert at ARL Penn State. The results showed good correlation between the three codes providing significant confidence in the standard coefficients used in U.S. Navy DCAB for simulations of ships and towed systems.

NSWC-CD DCAB code was used initially for a 2.0 MW, 2 down-flow rotor configuration. This analysis included both static and dynamic simulations.

Six ideal inflow conditions were used in the DCAB model as different flow regimes at different depths for variable shear profiles.

The device demonstrated the following behavior:

- Undoubtedly hydrostatically stable with vertical line attached, with trim near zero pitch
- Undoubtedly will dive to evade higher currents in most if not all conditions
    - Outlier conditions, of high currents and reverse shear require further study and is a project risk
- Changing flow directions is a stability risk
    - Rotor model of the platform shows the C-Plane can handle this affect for most inflow conditions
    - Examination of potential outlier conditions needs to be completed

  - Fallback is to install tails or other devices to increase stability
  - Changing flow directions should be considered for the tow tank test
- Simulations in waves show the following
  - Storm waves, in head and following seas, can cause high pitch values and requires further study
  - 7 m SWH head seas appear to result in acceptable forward mooring line tensions
  - 7 m SWH beam seas results in much less motion in this model (which has no truss)
- Complete hydrodynamic stability for all flows measured to date appears achievable, but has not been demonstrated in numerical simulations to date
- Stability without rotors turning, and lateral plane motions in general, are risks
- Motion based loads require further study

Additional analysis was completed to understand the capabilities of the C-Plane device to passively control power regulation by seeking the correct flow speed vs. depth. Hydrodynamic analyses were performed using the Navy NSWC-CD program DCAB for various vertical shear velocity gradients as determined from resource assessment velocity profile data. The work performed for the Preliminary Design Review (PDR) of October 2011 was based on an ideal shear profile of 0.0057mps/m. Investigation of resource data shows the nominal vertical shear to be approximately 0.004mps/m and could be as high as 0.015mps/m in extreme events (hurricanes, high swirl eddies, etc.). In some cases reverse shear was seen.

The C-Plane passive depth control operating methodology is such that the increased drag of the rotors in high velocity flow reduces the overall lift (net buoyancy)-to-drag ratio of the device, thereby reducing the mooring line angle (with respect to horizontal) and causing the device to lower (dive) in the water column to seek a lower velocity flow due to the vertical shear profile.

Analyses using the lower nominal vertical velocity shear profile, indicates that the C-Plane does not passively seek the lower depth/velocity flow as quickly as originally expected. Therefore, with reverse shear profiles, the C-Plane has a tendency to rise or stay at the nominal depth due to the vertical line restraint and will tend to produce more than anticipated and allowed forces on the rotor system. These analyses were conducted to refine the profiles and maximum velocities of the off-design flow events, and to determine a solution (i.e., a large-chord wing at a significant angle of attack and different mooring attachment locations) that will enhance the depth/velocity seeking tendency of the C-Plane and not overstress the rotor structure.

In order to validate the system models, Hydrodynamic and dynamic simulation analyses were conducted in support the tow tank test program. DCAB and Flightlab analysis runs were completed to simulate conditions that will be tested in the tow tank. Results demonstrated the

stability parameters of the C-Plane in a static mode with respect to the buoyant, drag and mooring forces. Primary focus was applied to the dynamic conditions which will also be tested in the tow tank.

Further validation of device stability was achieved through work completed by The U.S Navy Naval Surface Warfare Center – Carderock Division under the direction of DA contributing by:

1. Conducting all DCAB dynamic simulations used to help design the C-Plane.
2. Consulting with DA personnel to arrive at a simplified two dimensional model that predicted diving behavior;
3. Predicting yawed flow simulations that resembled the captured test behavior.
4. Reviewing the captured test plan.
5. Supplied guidance to the test conditions by suggesting additional testing, including running just the nacelle at higher speed in the captive model test and in conducting the reverse flow runs during the moored test.

The simulations have shown that the C-Plane would be stable. This in fact was validated by the moored model test. The moored test, as it turned out, was in fact a vindication of all the simulation work conducted by NSWC-CD since the inception of the C-Plane CRADA with regard to stability and overall performance.

Upon completion of the above stability validation, a thorough software trade off study was conducted comparing multiple system level dynamic codes to bring the system dynamic modelling in house. Tidal Bladed was chosen and purchased by DA to provide a comprehensive analysis (global integration model) of the C-Plane. DNV – GL's (Garrad Hassan) Tidal Bladed was chosen because it has been thoroughly validated for marine and tidal current turbine modeling and is based on the industry leading wind turbine analysis software Bladed.

Tidal Bladed is a time-domain simulation with full hydro-elastic modeling based on multi-body dynamics. It allows modeling to describe 'added mass' effects on both the rotor and support structure. Custom drivetrains and controls can be modeled as external dynamic link libraries (DLL's) which is particularly important in the case of the C-Plane's hydrostatic transmission. The ability to model multiple rotors, as in the C-Plane, is included. Tidal Bladed is equipped to model quasi-static moorings presently however the inclusion of dynamic moorings is being pursued. The Tidal Bladed standard input parameters are as shown in **Figure 8**.

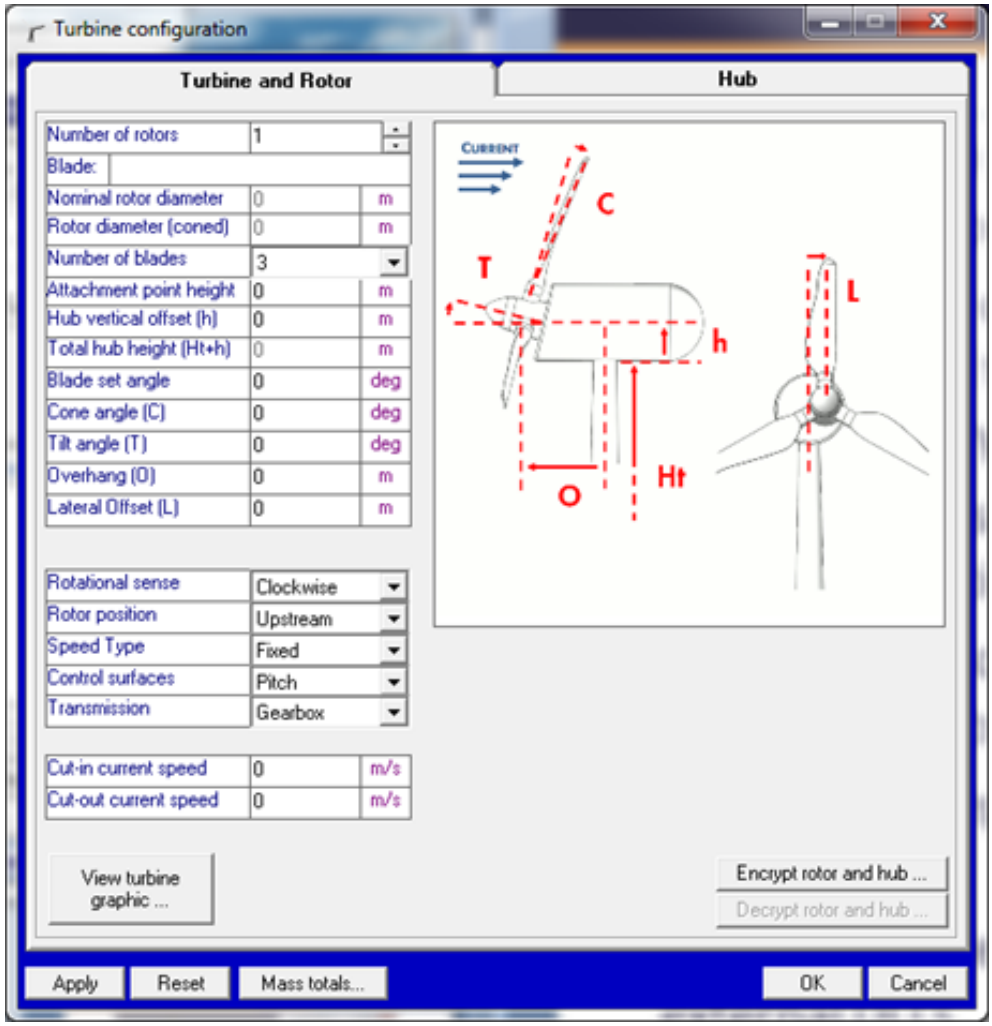

Figure 8 - Tidal Bladed Input Parameters

The remainder of the hydrodynamic and dynamic (stability) simulation analysis conducted utilized Tidal Bladed. The initial Tidal Bladed modeling results used the single, captured nacelle (**Figure 9**) and these data were checked for accuracy using the captured tow tank test results. Modeling and analysis of the captured test configuration involved tuning masses according to the actual test model. The blades (**Figure 10**), nacelle and strut were assumed to be infinitely stiff. The component volumes were based on solid models and matched the observations from the captured test. The simulations were conducted for various tip speed ratios and yaw error sweeps.

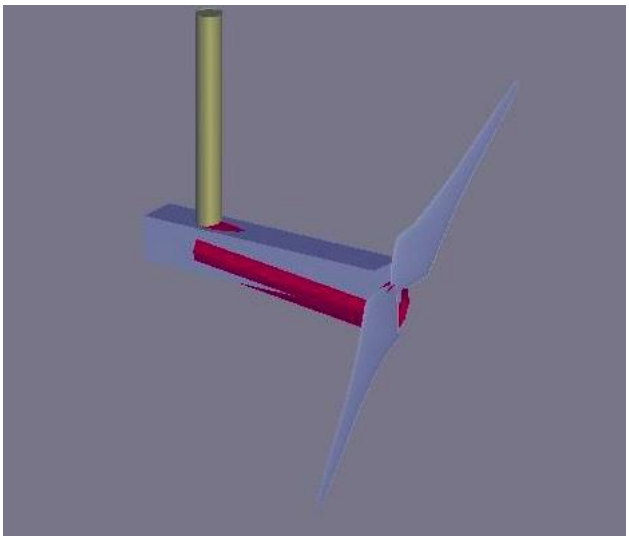

Figure 9 - Tidal Bladed Captured Test Model

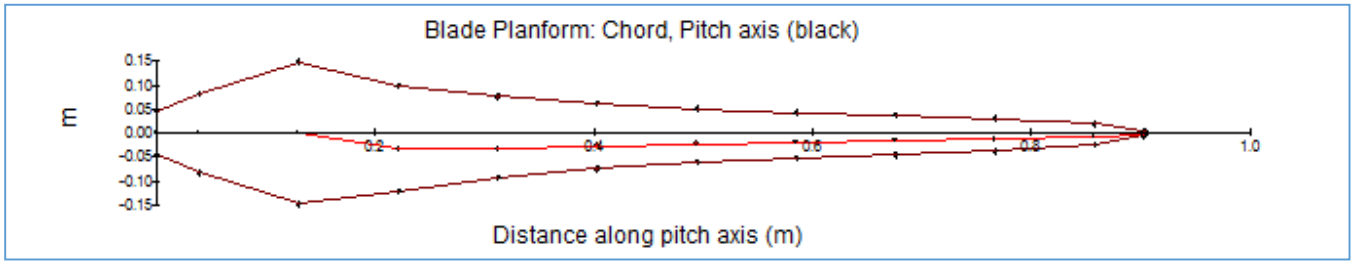

Figure 10 - Tidal Bladed Rotor Input Parameters

The next phase of modeling involved building a dynamic test scaled model and then comparing the predictions against tow tank test measurements to validate stability and loads for a floating system. Multi-rotor modeling is available in Tidal Bladed and was utilized for this task (**Figure 11**). Small modifications to the program were made by DNV - GL for the C-Plane's counter-rotating rotors. Calculations were made of the mooring stiffness, inertia and mass properties for the custom scaled test moorings. Preliminary simulations were completed with rotors rotating in the same direction using a fixed (non-moored) system. Load transfers were confirmed using the fixed system.

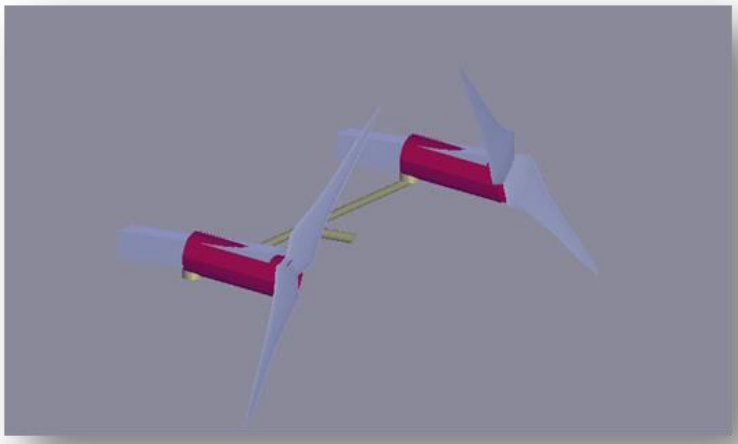

Figure 11 - Tidal Bladed Dynamic (two rotors) Test Model

Cross code validation was completed for the Tow tank test results by using both DCAB and Tidal Bladed. The Navy's Cable-Body (DCAB) code was utilized extensively for model refinements. DCAB utilized stability coefficients generated for the rotor by a commercial BEM code called FlightLab. Body hydrodynamic and hydrostatic coefficients are generated by other Navy codes called BODXYZ and BSTAT respectively. Cable inputs are generated in another Navy code called CAB3PC. DCAB is capable of computing time-domain simulations for a ridged representation of the C-Plane structure.

The yaw and pitch moments calculated by Tidal Bladed and FlightLab show similar correlation to the test data for varying inflow yaw angles (**Figure 12** and **Figure 13**).

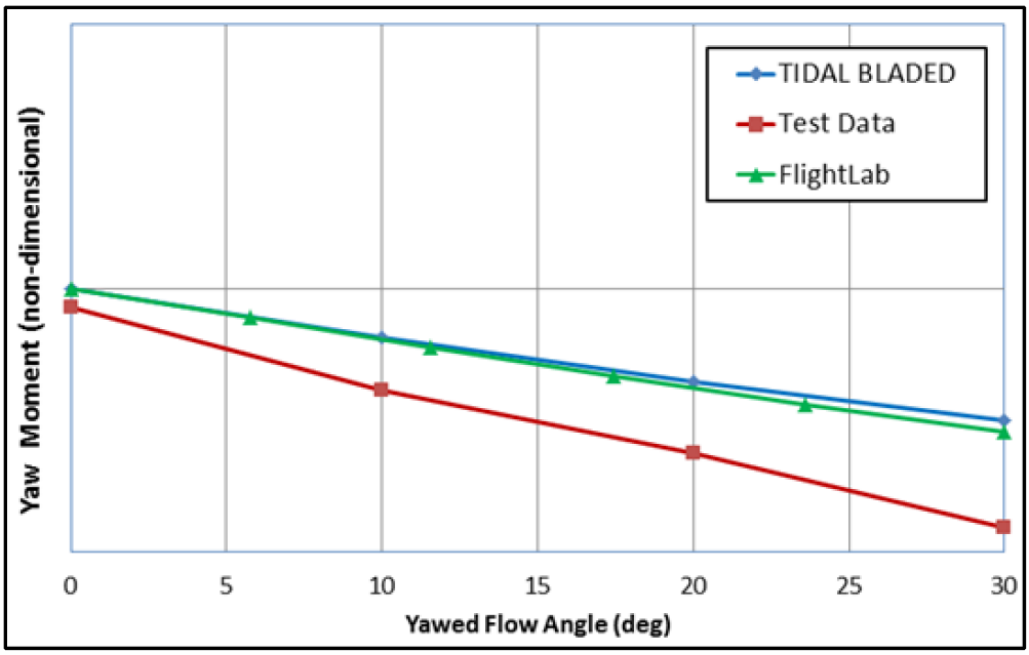

Figure 12 – System Model Comparison, Yaw Moment vs. Yawed Flow

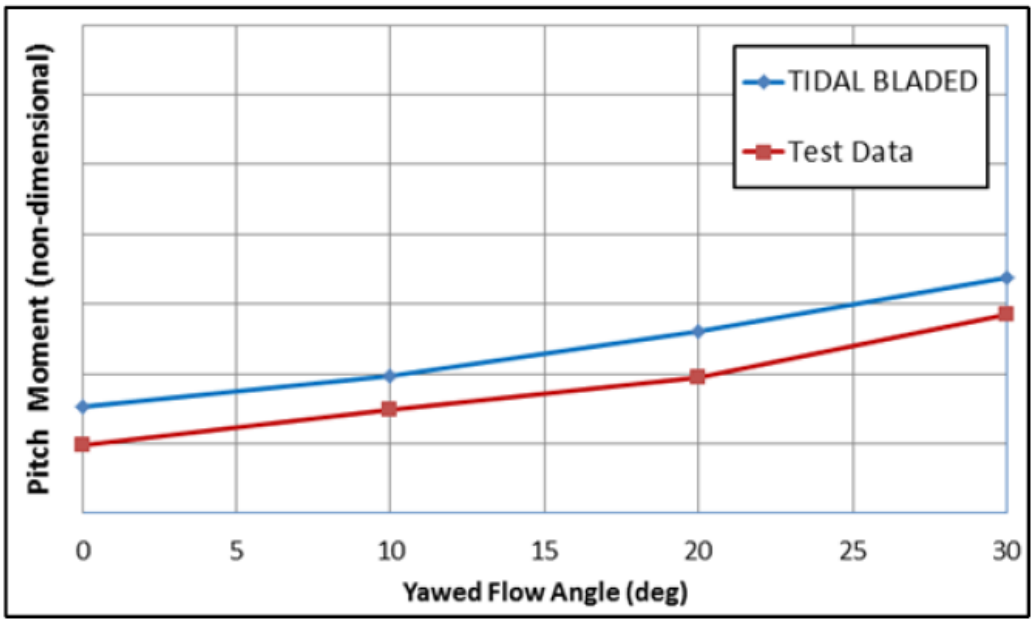

Figure 13 – System Model Comparison, Pitch Moment vs. Yawed Flow

Additionally DA, in conjunction with its consultant Garrad Hassan and Partners (GH), now known as DNV-GL, have conducted analysis of the dynamic tow tank test scale model of the C-Plane device using Tidal Bladed. This work has consisted of:

- A review of machine design parameters required to build a model of the C-Plane device,
- A review of a model of the C-Plane device as supplied to DNV-GL by DA,
- Updating the Tidal Bladed model,
- Performing a range of steady flow simulations and;
- Comparing to data measured from the dynamic tow tank tests using a physical scale model.

Overall, the C-Plane model is able to move in six degrees of freedom in space (three translational and three rotational) however the components of the structure are assumed to be rigid in that there is no flexibility between the various components.

The simulations undertaken for validation of the tow tank results have all used a steady flow speed, a fixed rotor speed, tension mooring legs, and stiff structural members including blades, rotor, drivetrain and support, which allows for an easier comparison with measured data. This is a reasonable first step in a validation exercise for complex systems.

Tidal Bladed is capable of modeling catenary mooring lines (**Figure 14**) and tension leg mooring lines. All moorings were modeled as tension legs connected to the same anchor and attachment points as in the physical model. The tension legs are assumed to contribute no load when the simulation is initialized, then as the buoyancy and thrust loading is applied to the structure, the moorings impart load to maintain equilibrium.

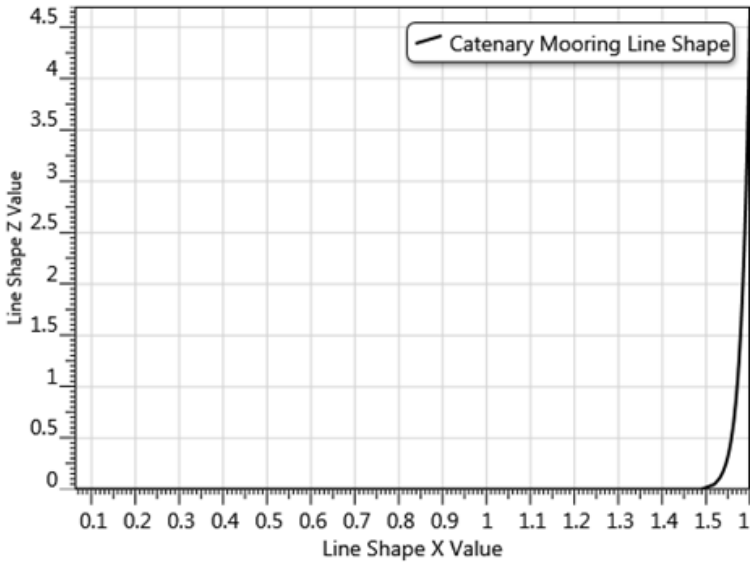

Figure 14 - Tidal Bladed Mooring Representation

It is possible in Tidal Bladed to model the mass and buoyancy for the blades, hub, support structure and nacelle. However, mass and inertia were only attributed to the nacelles allowing the magnitude and location of the center of gravity to be easily modified while matching with measured data. Buoyancy was only enabled for the nacelles, allowing the magnitude and position of the center of buoyancy to be easily modified. A representation of the updated C-Plane Tidal Bladed model can be seen in the **Figure 15**.

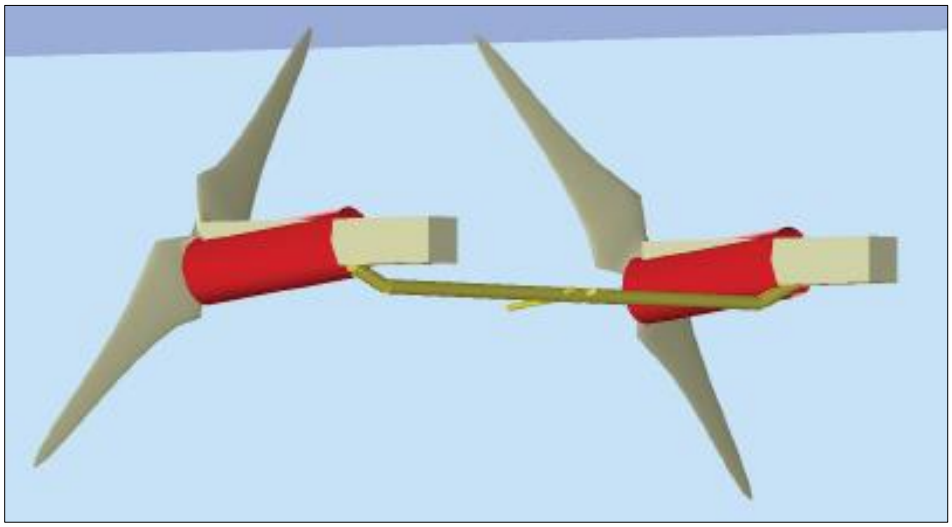

Figure 15 - Updated Tidal Bladed Dynamic (two rotors) Test Model

Upon tuning the Tidal Bladed model to the physical tow tank model, specific simulations were carried out to compare against tow tank measured data. The simulations were undertaken for steady flow conditions with no shear profile, that is, the flow speed is uniform throughout the water column. The density of water used for the calculations is 1027 kg/m^3. The results for some outputs of Tidal Bladed are compared with the measured data in the figures below.

The rotor speed is fixed in the simulations so it is expected to match those prescribed in the physical experiments. A further key parameter to judge rotor performance is the rotor torque. **Figure 16** shows that the torque seems to have matched well between Tidal Bladed and the measured data. Tidal Bladed slightly over-predicted the rotor torque; however, this may be due to additional boundary layer tripping features added to the physical model. To facilitate a more thorough comparison, the geometric and hydrofoil definition within Tidal Bladed should be reviewed against dedicated hydrofoil measurements.

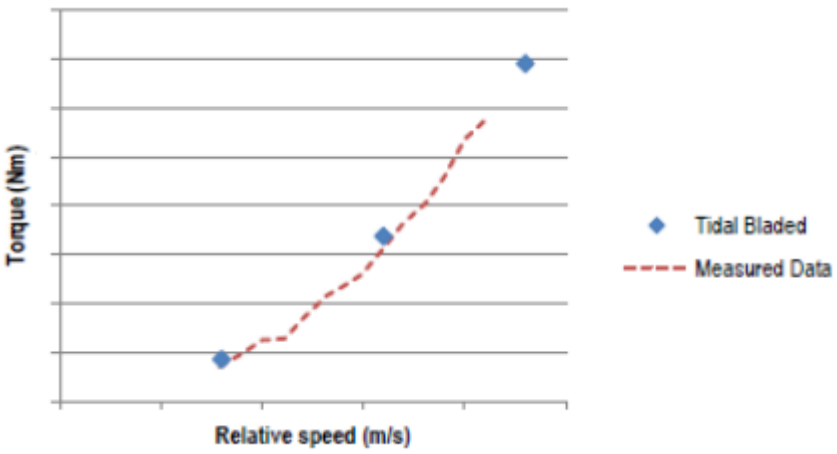

Figure 16 – TTT vs. Tidal Bladed Torque

Figure 17 shows that the depth of the device below the water surface (i.e. vertical displacement) seems to be matched very well to the Tidal Bladed model. At low flow speeds the change in vertical displacement is small with increasing flow speed. As the change in vertical displacement was small and similar to the tow tank test data, the overall depth of the water column in the Tidal Bladed model was set to 6.25m to give the same device depth as the tow tank tests. At higher flow speeds the trend has been predicted well.

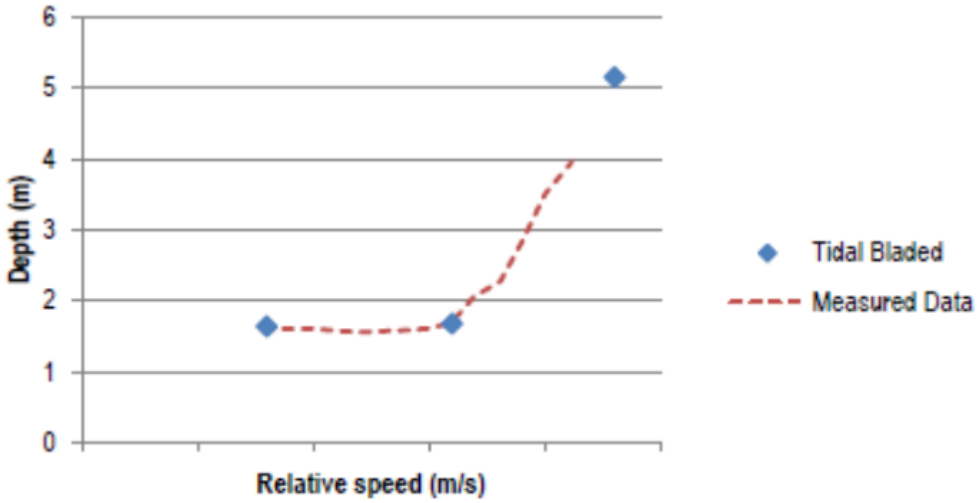

Figure 17 – TTT vs. Tidal Bladed Depth

Figure 18 shows that Tidal Bladed over-predicts the loading on the aft mooring line compared to the measured data. The forward line loading is strongly dependent on the rotor thrust, which may have been modified with the additional boundary layer tripping features added to the blades in the physical tests when compared to the Tidal Bladed model. At a given level of rotor thrust the aft

mooring line should go slack as the device is forced to greater depth by the constraints imposed by the forward moorings. This suggests that the rotor thrust is lower in the Tidal Bladed simulations than in the measured data.

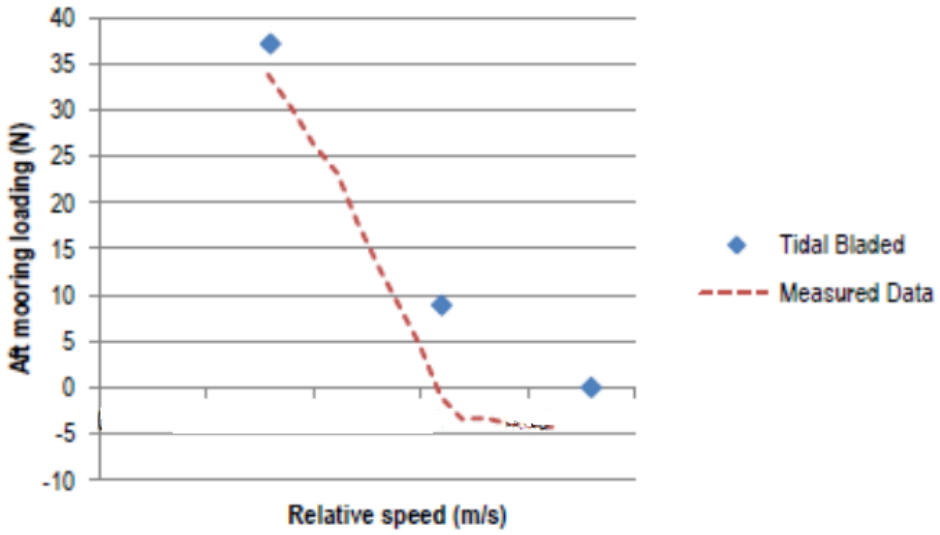

Figure 18 – TTT vs. Tidal Bladed Aft Mooring Load

The tensile loading measured in the experiments becomes negative at flow speeds just over 0.30 m/s. It would be anticipated that the loading would tend to zero and then remain at zero while the aft mooring line was slack above rated flow speed, i.e. that no compressive load would be exerted. This could be explained either by inaccurate calibration or by the mooring line being partially pre-tensioned. The differences are relatively small in terms of the overall loading on the system when compared with the loads acting on the forward moorings.

Figure 19 shows the combined loading contributed by the forward moorings. The values were summed as in the measured data and there is a significant asymmetry shown between the mooring line loads. It can be seen that Tidal Bladed partially under-predicts the forward mooring loads. Given that the forward moorings primarily resist the thrust loading from the rotors this agrees with the suggestion above that the thrust loading contributed by the rotors in Tidal Bladed is less than that seen in the tow tank tests, causing the device to require a greater vertical load to restrain it.

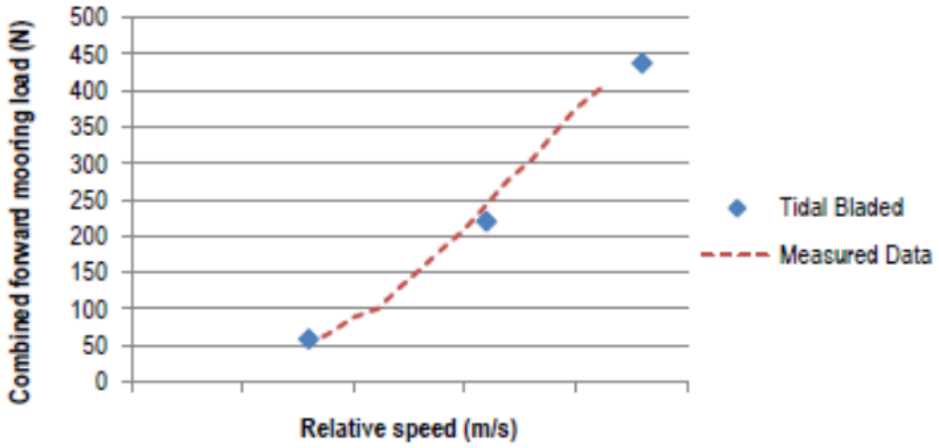

Figure 19 – TTT vs. Tidal Bladed Combined Forward Mooring Load

Figure 20 shows that Tidal Bladed predicts the trend in pitch relatively well, however the offset at low flow speeds is around 2 degrees. The difference may be due to a difference in trimming between the center of gravity and center of buoyancy in the Tidal Bladed model when compared to the real model (hydrostatic loads), particularly as once hydrodynamic affects take over (at higher relative speeds) the match between simulated and measured data appears to improve.

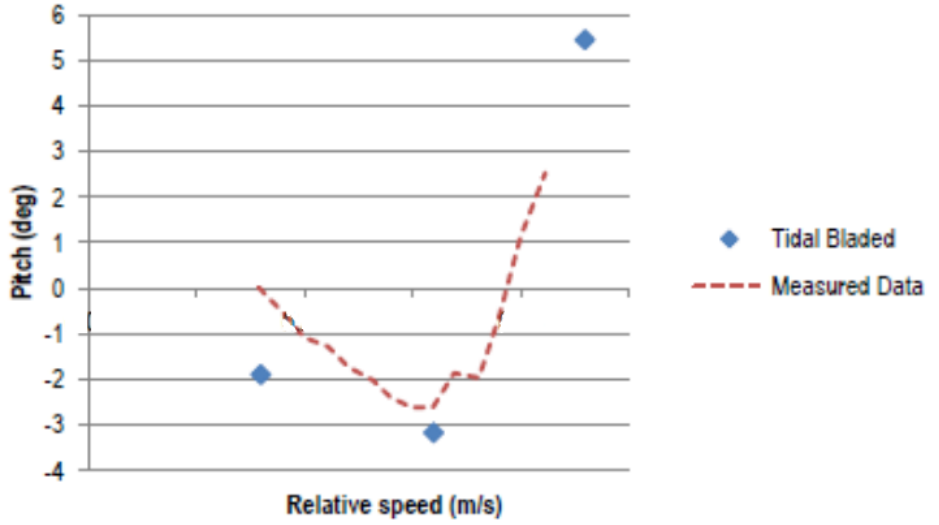

Figure 20 – TTT vs. Tidal Bladed Pitch

Turbulent simulations were not carried out for the validation campaign of the tow tank tests due to the difficulty of creating representative turbulence in the tow tank test and was deemed to be

outside the scope of this campaign. Additionally vertical shear was not validated in the tow tank test due to difficulty of creating a shear profile. An initial look at vertical shear was carried out to understand the effect on passive depth control using a quasi-static approach alluding to potential issues with negative shear driving the device deeper in the water column, and is one of the reasons why DA is moving away from passive depth control (PDC). Ongoing design is analyzing device sensitivity to shear and turbulence in the simulation environment and is being included in the design loads.

In lieu of tow tank testing to better understand the impact of turbulence and shear, the design team is incorporating these factors through Tidal Bladed simulations. For example, during the resource campaign vertical shear data was collected and found over a range of depths and flow speeds. This data was consolidated down into histograms and is being used for design load cases.

Turbulence data has been incorporated into the design cases by use of turbulence intensity vs. flow speed. Unfortunately during the resource campaign data collection frequency was too low to resolve turbulent coherent length scales and is an ongoing challenge for ocean current resource characterization.

Mesoscale flow reversals due to core meander are not expected at the deployment location off the Florida coast due to the funneling affect created by the Florida coast and the Bahamas bathymetry. Nevertheless, microscale eddies could create flow reversals which have not been modelled and their contributions are hopefully covered by safety factors. Directionality of the flow speed is being considered to vary ±5° during operation and is included in the design requirements.

After the tow tank and model validation had been completed, work was initiated on the development of a controller for analysis of the full scale C-Plane in Tidal Bladed. Controller development was necessary to begin outlining design load cases for further component design. Some issues arose with development of the start-up external controller and consisted of the following:

- TIDAL BLADED, after v4.4, have changed the way the external controllers interfaces are written. The legacy external controller interface was still available and was the fallback position instead of trying to figure out the new interface. However, this approach has not been successful and errors had been received. It was possible that the multi-rotor turbine is not supported in the previous controller interface.
- It was thought that the torque demand and RPM ramp would be applied to both rotors but it was possible that the two rotors need to be sent different commands. It was suspected that this could be the issue.

Investigations were undertaken in Tidal Bladed to determine the wave effects and the loads from them that would be imparted on a MHK device. A summary of the work conducted and the preliminary findings are as follows:

- The time period for waves used (1.8s and 2.4 s) in combination with rotor 1P time period of ~2s creates a beating kind of phenomenon for the water particle velocity and blade loads follow that.
- Tidal Bladed uses a stream function formulation of regular waves instead of the Airy function. This is recommended for extreme loads analysis.
- Different starting wave azimuth angles were also simulated. No differences in extreme loads were noted except for a time shift in the time series.
- A close approximation of linear shear of 0.01 (m/s)/m was used and results were found to be acceptable.

DA focused on refining the Tidal Bladed model, including controls development and loads analysis work in the area of hydrodynamic and dynamic simulation. This work was conducted as a collaborative effort between DA and its partners DNV – GL (Garrad Hassan) and Helios Engineering, Inc.

In order to further define the system operational requirements, design situations were outlined for the single rotor C-Plane. Following DNV-GL guidance on design loads, DA created a set of operational load cases to be simulated for the device. These load cases included normal operation, start up, shutdown, fault cases, emergency shutdown, parked, and O&M applications.

A multitude of load cases and seeded events were simulated for the single rotor device. From these design situations, extreme and fatigue results were processed and produced into load inputs for component design.

A fatigue histogram for the drive shaft was also used for component design outlines the duration at load for a device over 20 years.

One of the driving load cases which was found to govern much of the component design was a grid outage event.

At present continued convergence of system model properties is being conducted and additional refinement of the operational cases are being considered to be incorporated into component design.

In conclusion, the C-Plane dynamic simulation model was modeled and refined throughout the process using multiple codes in parallel to gain confidence in the device stability, loading, and performance. The codes used included Navy DCAB, Flightlab, and DNV GL Tidal Bladed. The simulation model included the resource modeling, hydrodynamics, structural dynamics, and controller together to simulate the response of the device. These codes were used to validate the tow tank test results and continue to provide vital information for creating a commercially viable and understood ocean current MHK device.

1.3 Mooring Analysis

A comprehensive mooring analysis was completed for the C-Plane in order to model the mooring characteristics accurately. OrcaFlex was used for the simulation, analysis and specification of the C-Plane mooring system.

The mooring system has a direct correlation to the stability of the system, performance of the device, and overall cost competitiveness of the C-Plane. One major cost reducing technology employed by the C-Plane is the use of an optimized mooring system. Multiple approaches were used during the design process to develop, analyze, and validate the mooring system in a cost competitive manner. Both Orcaflex and Tidal Bladed were used to develop the mooring system and validated from the tow tank results. From these analysis tools mooring line loads were developed and integrated into the design.

DA developed the mooring requirements and installation concepts for the 2.5 MW twin rotor Aquantis C-Plane ocean-current device. These requirements included the findings of a feasibility study to determine if reducing the two forward mooring lines to one forward mooring would be achievable. This line reduction would reduce opportunities for entanglement or clashing between the power cabling and mooring line, and ease of installation. OrcaFlex, a 3D non-linear time domain code commonly used in the oil and gas industry for simulation of mooring systems, was used to determine the mooring line tensions as a function of various current speeds and environmental loading. The mooring lines also provide the greatest constraint in placement of the C-Planes. To reduce leasing costs, the mooring line lengths and components were evaluated such that they require minimal spacing between C-Planes, while still maintaining adequate spacing in the event of a failure of one line. The OrcaFlex model of the dual rotor C-Plane can be seen in **Figure 21**.

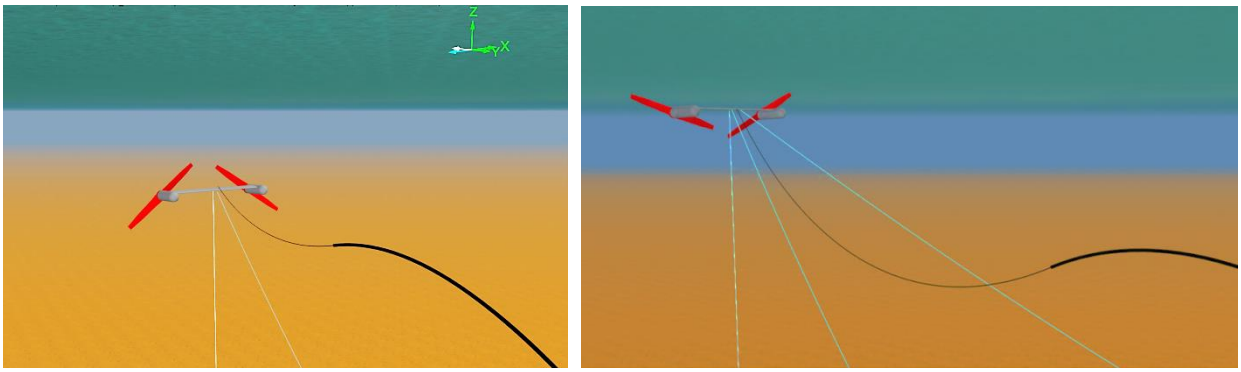

Figure 21 - Dual Rotor C-Plane Mooring OrcaFlex Model

From Q2 to Q3 of 2013 further mooring analysis was completed preparing for the tow tank dynamic test. This included an Orcaflex model consisting of the mooring and power cable. Detailed tasks included:

1. Scaling of the current Orcaflex C-Plane model to reflect a 2.5 MW, two rotor configuration.
2. Based on the results of the two rotor scaling, a 1:25 scale mooring system and power cable components, sizes, lengths and layout were generated for use in dynamic tow tank testing at NSWC-CD.
3. Collaboration with NSWC-CD personnel as required to arrive at a scaled mooring system and power cable components, specifications and layout.
4. A listing and specifications for the scaled mooring system and power cable components was generated.

Upon the acquisition of Tidal Bladed, a mooring model was developed using input matrices which included mooring system stiffness, damping and mass matrix information. Line stiffness's were estimated for the 2-rotor C-Plane.

Initial analysis quantified the device displacement. Device translation was measured from -0- defined at the steady-state equilibrium position at rated flow speed. For all mooring lines, positive-X displacement is the C-Plane moving away from the anchor, negative-X displacement is the C-Plane moving toward the anchor. For example, at the equilibrium position, the aft anchor is ~10m in front of the C-Plane, so negative displacement is forward towards the anchor (similar global direction as the forward lines). Z is defined as positive upward. The net results of these efforts are depicted in **Figure 22** through **Figure 25**.

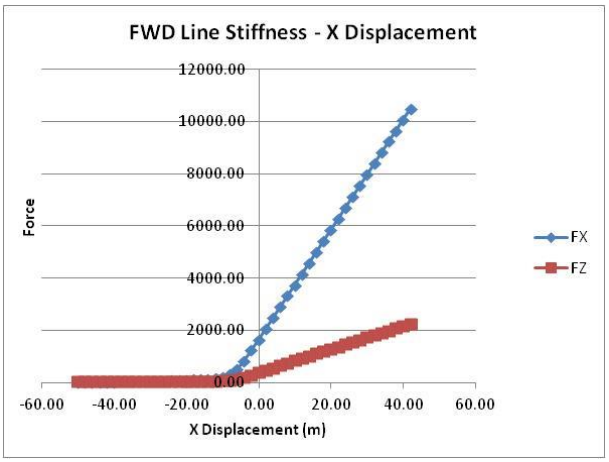

Figure 22 – Forward Line Stiffness – X Displacement

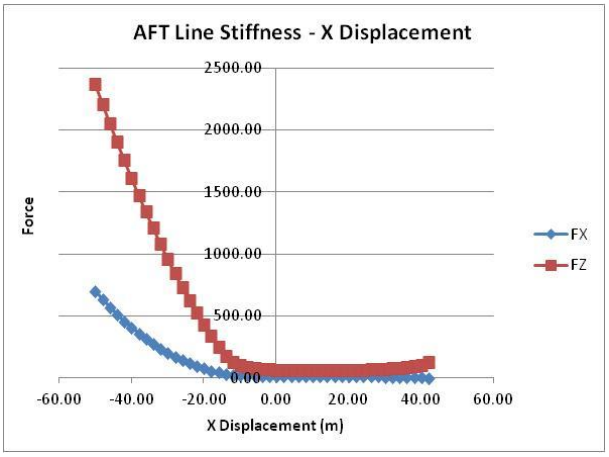

Figure 23 – Aft Line Stiffness – X Displacement

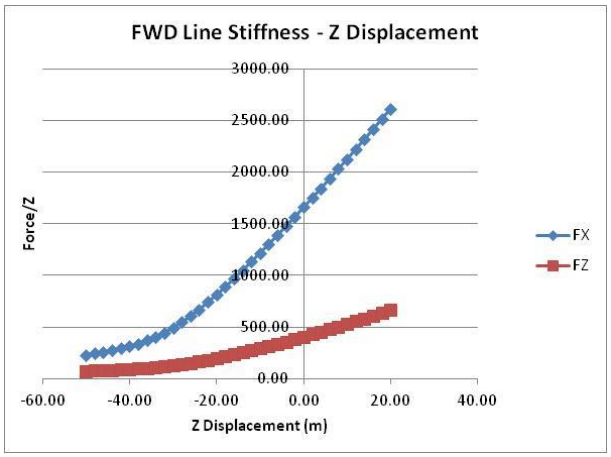

Figure 24 – Forward Line Stiffness – Z Displacement

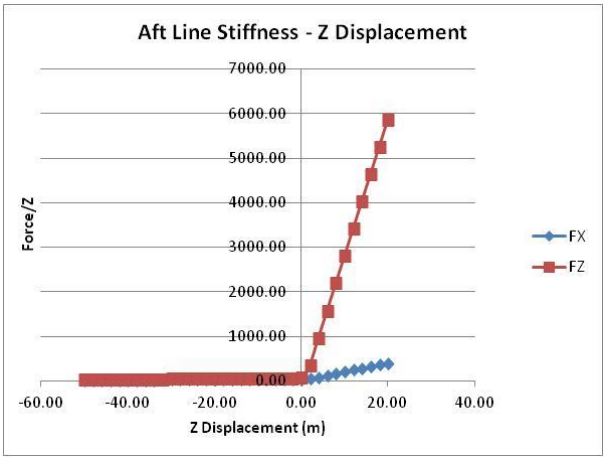

Figure 25 – Aft Line Stiffness – Z Displacement

Upon completion of the tow tank tests, results were used to further refine the mooring system into Tidal Bladed with a more accurate approximation. This allowed for more realistic results to be obtained from the Tidal Bladed simulation.

The single rotor C-Plane mooring system was modeled in Tidal Bladed using the findings from the tow tank test and representing those findings for the single rotor system. This mooring development has enabled DA to model the dynamic implications of the device during operation and other design situations. Multiple mooring configurations were carried out; the most promising achieving both stability and reduced cost of energy.

The first consists of two forward lines which provide additional stability; however, this configuration requires two lengthy forward mooring lines (**Figure 26**). The second minimizes device cost by utilizing a single forward mooring line and supplying additional stability in the device by separating the center of buoyancy and center of gravity **Figure 27**. The mooring lines are then attached to the stinger locations, represented in yellow.

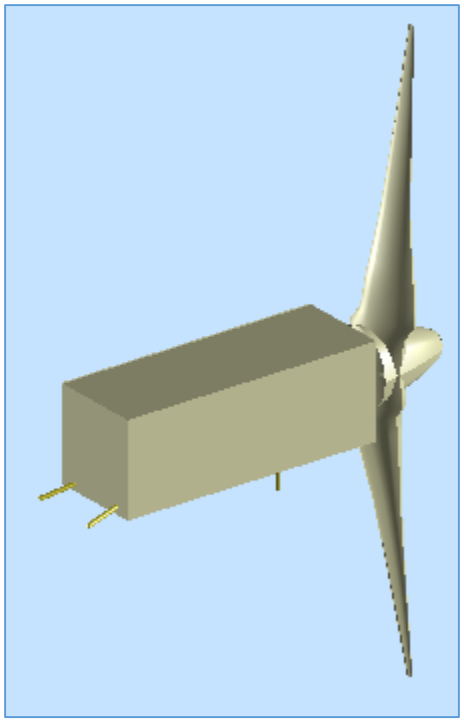

Figure 26 – Double Forward Mooring Line Model

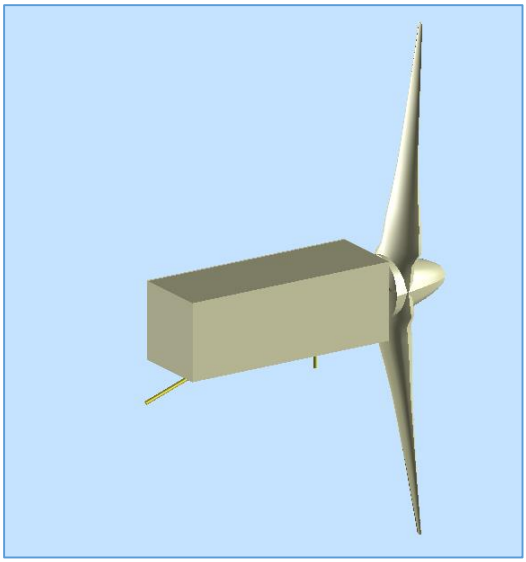

Figure 27 – Single Forward Mooring Line Model

It was found that the double forward line provided stability yet had additional cost; therefore, the single forward line was further investigated. Appropriate stability could be achieved by sufficient separation of CB and CG in order to increase the rolling moment.

In summary, the mooring analysis was conducted using industry standard tools including OrcaFlex and Tidal Bladed to understand the sensitivity of the device under operation and to develop the mooring system. Further validation was achieved through tow tank testing. DA is continuing the development of a marine turbine further refining the design details taking advantage of the thoroughly validated system modelling tools.

PHASE 2: WORK ACCOMPLISHED

The following scope of work tasks and results were accomplished under Phase 2 of the project.

Task 2: Tow Tank Tests

2.1 Scale C-Plane Model Platform and Mooring Fabrication - 1/25th Scale

The 1/25th scale model C-Plane platform and mooring system was designed, developed and fabricated in a collaborative effort between DA and NSWC-CD. Design issues considered in the development effort included: Froude and Reynolds number scaling, mass and trim resolution, torque control and rotor synchronization. Physical system issues such as where to locate instrumentation packages and matching the scaled weight, buoyancy and trim of the full scale system were addressed. The model weight and trim scaling can be seen in **Figure 28**.

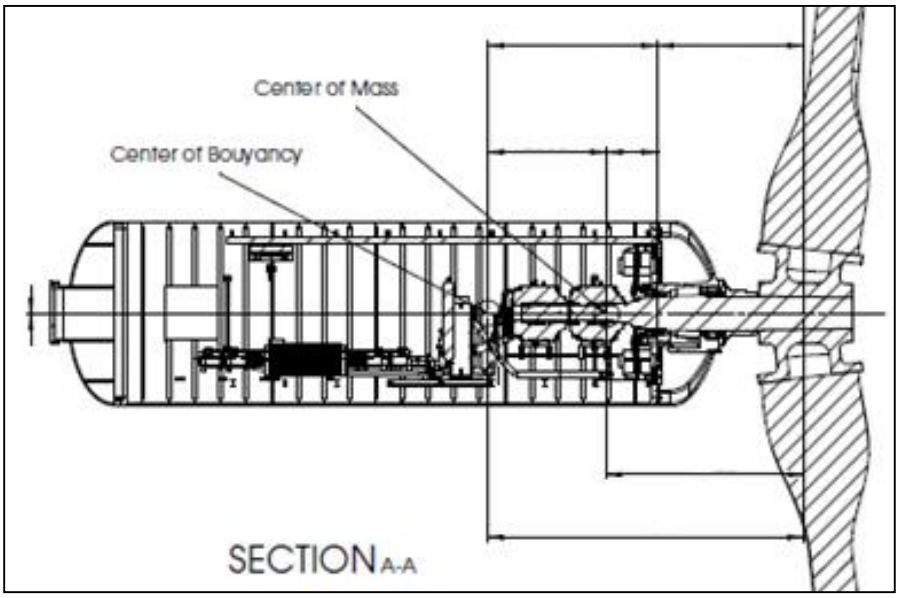

Figure 28 - Model Weight and Trim Scaling

The final configuration and components of the tow tank test model for a single unit can be seen in **Figure 29**. The C-Plane model as used for the dynamic test program is composed of two identical 6061 aluminum alloy nacelles; two counter-rotating, two-bladed, carbon fiber rotors; a 6061 aluminum transverse structure and Accura60 plastic rapid prototyped buoyancy pods and fairings. The extensive use of Accura60 allowed for very expedient development and produciton of complex components that also had structural requirements. The complete C-Plane model as used in the dynamic or moored testing program can be seen in

Figure 30. **Figure 31** shows the complete model assembled with the mooring and umbilical in the basin.

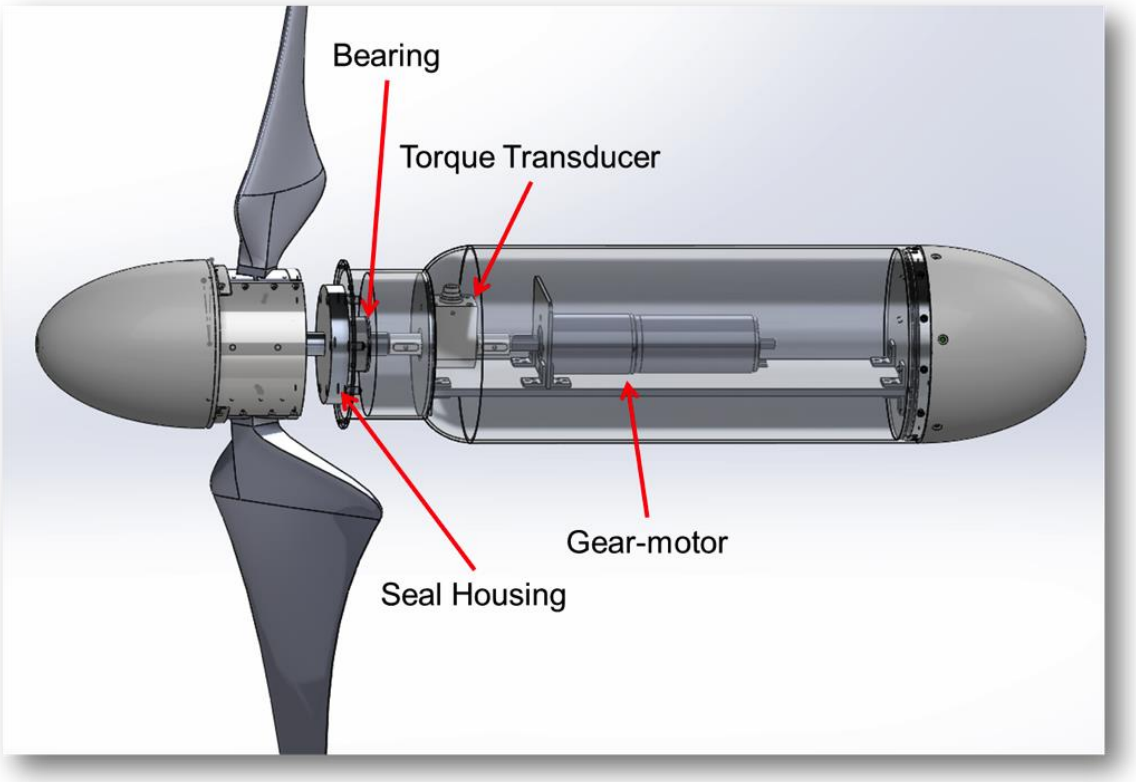

Figure 29 - Nacelle Model Layout

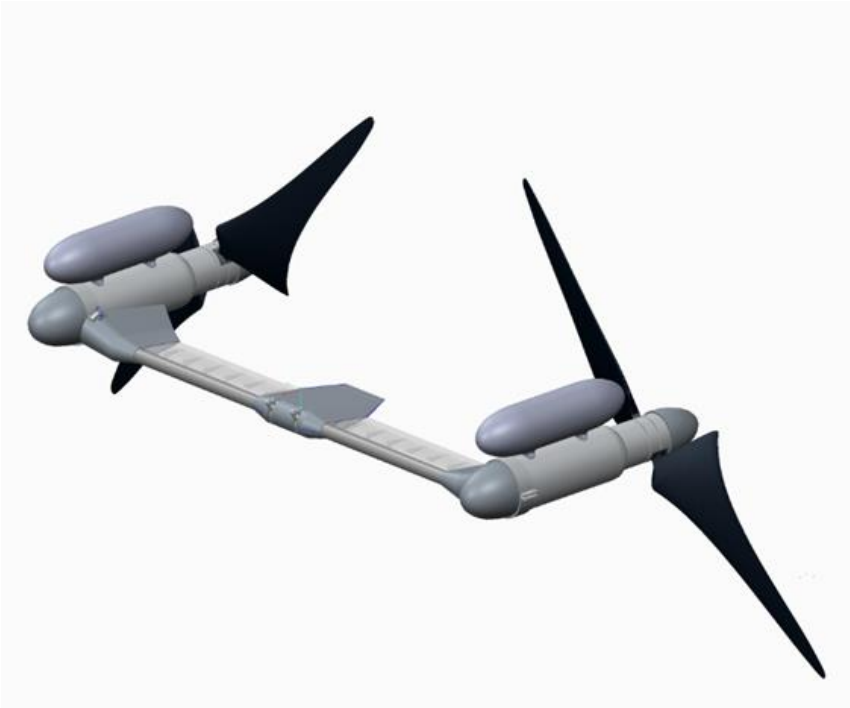

Figure 30 - Complete Tow Tank Test Model

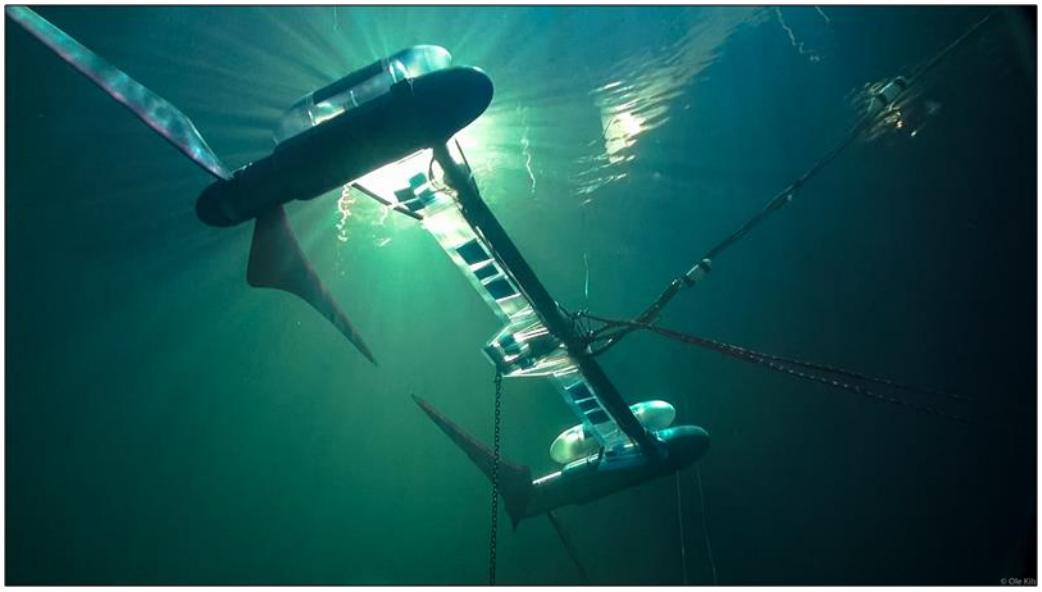

Figure 31 - Complete Tow Tank Test Model as Installed for Testing

An additional final configuration of the tow tank test model was developed using only a single nacelle, buoyancy pod and rotor assembly, and a keel for stability. This model configuration was assembled using components from the dual rotor model with the exception of the keel. The existing mooring system and electrical and control umbilical were affixed to the keel assembly The completed model as used in the testing can be seen in **Figure 32** . The model was developed and assembled to allow basic stability testing of a single rotor C-Plane system.

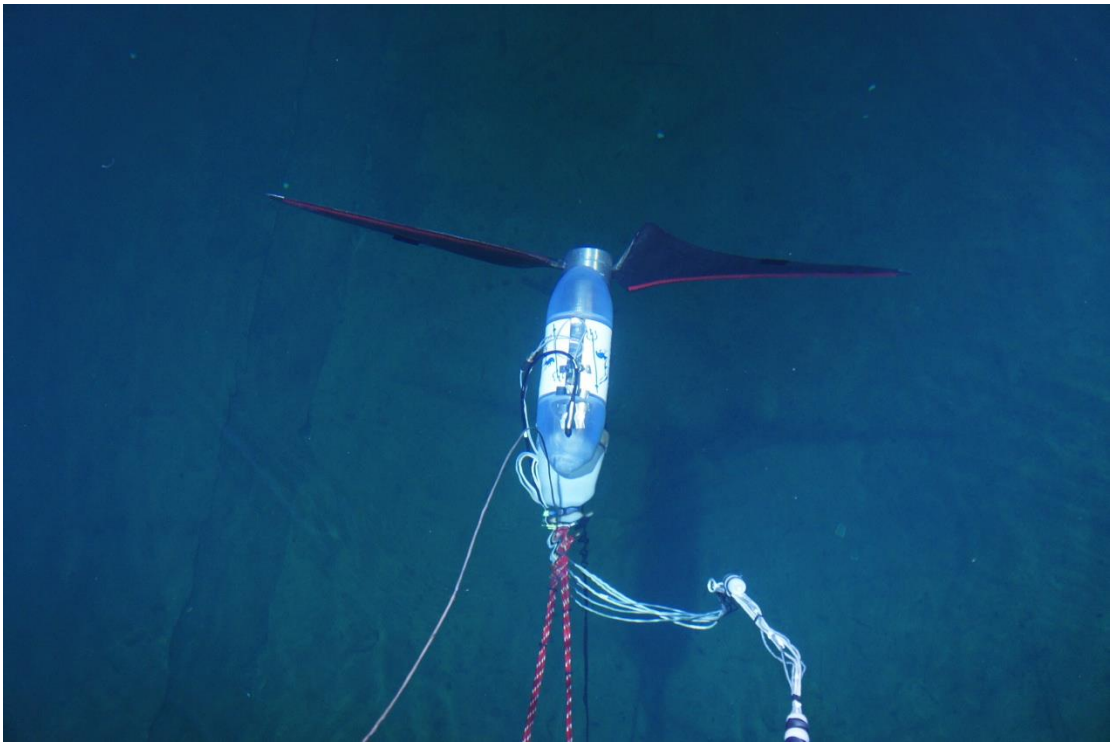

Figure 32 - Single Rotor C-Plane Tow Tank Test Model

2.2 Platform Instrumentations: Inertial Measurement Unit, Transducers Load Cell

In collaboration with DA, NSWC-CD specified and designed the tow tank test model instrumentation package. The instrumentation was required to gather rotor motions and loads, structure loads and motions of the collective model. Key concerns were that the instrumentation met the data gathering requirements and that the physical size and mass could be accommodated in the scale model.

The instrumentation installed in the model and used for the test consisted of the following items with discrete specifications as follows:

Captive model testing:

- 6 component Load cell
  - Mx Limit: 1000 in*lb.

  - My Limit: 1000 in*lb.
  - Mz Limit: 500 in*lb.
- GX3 Inertial Measurement Unit (IMU)
- Tachometer(s)
  - Rotor Speed Limit: 57 RPM
- Carriage speed
- Depth gage
- Thrust on shaft
- Torque on the shaft
  - Mx Limit: 25.5Nm (18.8 ft.*lbf)

Dynamic model testing:

- GX3 Inertial Measurement Unit (IMU)
- Tachometer(s)
- Carriage speed
- Depth gage
- Thrust on shaft
- Torque on the shaft
- Video adequate for yaw measurement
- 2 or 3 tension gages, one at each mooring point

A 3-D CAD layout of all the instrumentation components was conducted to determine the packaging arrangement and accurate mass and location information. A FEA analysis was then conducted using this layout to assess the rotor drive motor torque inputs into the model structure. The respective layout and the FEA stress results can be seen in **Figure 33**.

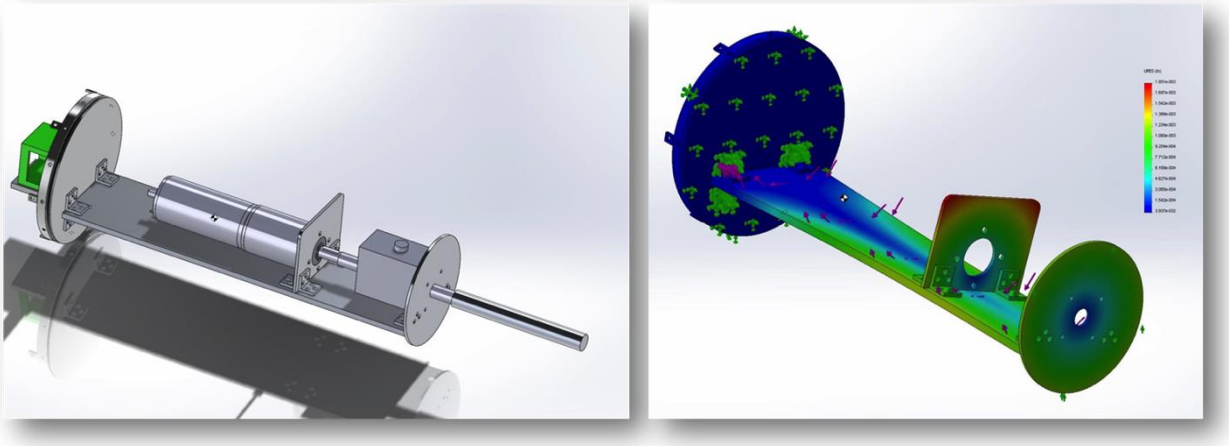

Figure 33 - Instrumentation Internal Layout and Support Structure Stress Analysis

2.3 Scale Turbine Blades Fabrication - 1/25th Scale

Design of the scaled rotor for the tow tank test program aimed to duplicate the full scale rotor effects, primarily rotor drag on the system in the tow tank test. The scaling effort focused on reconciling Froude and Reynolds number scaling of the rotor through a design study utilizing low Reynolds number airfoils (**Figure 34**). This study demonstrated a design approach, which can address these issues and provide proper force scaling while meeting constraints on rotor diameter and speed and minimizing performance instabilities due to the formation of laminar separation bubbles. These are key parameters for validation of platform stability.

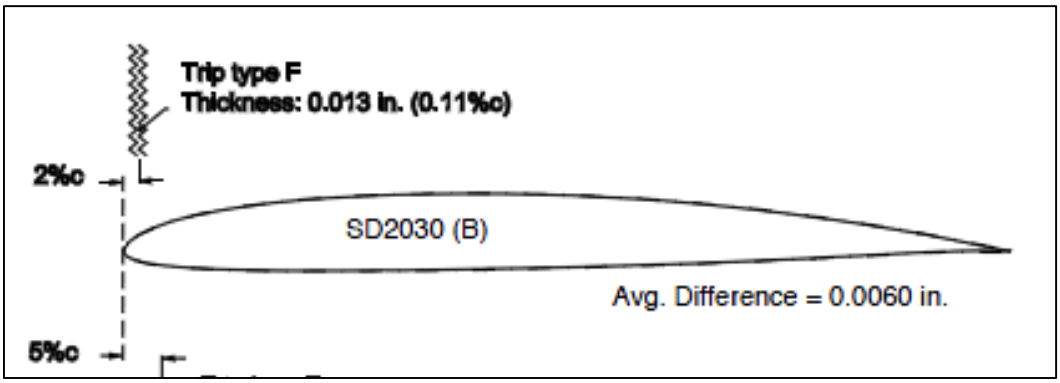

Figure 34 - Low Reynolds Number Airfoil Developed for Small Wind Turbines

In developing the tow tank test model rotor, the full-scale rotor had to be re-designed for model scale using airfoil and test data appropriate for the low tow tank Reynolds Number of 100k-200k. The design objectives included:

- Minimize performance instabilities due to laminar separation bubbles
- Maintain Froude scaling of thrust, diameter and RPM for dynamic stability tests

A single SD2030 airfoil was selected for the entire rotor for which it was designed and tested at test data at relevant Reynolds Numbers. The airfoil parameters can be seen in **Figure 35**.

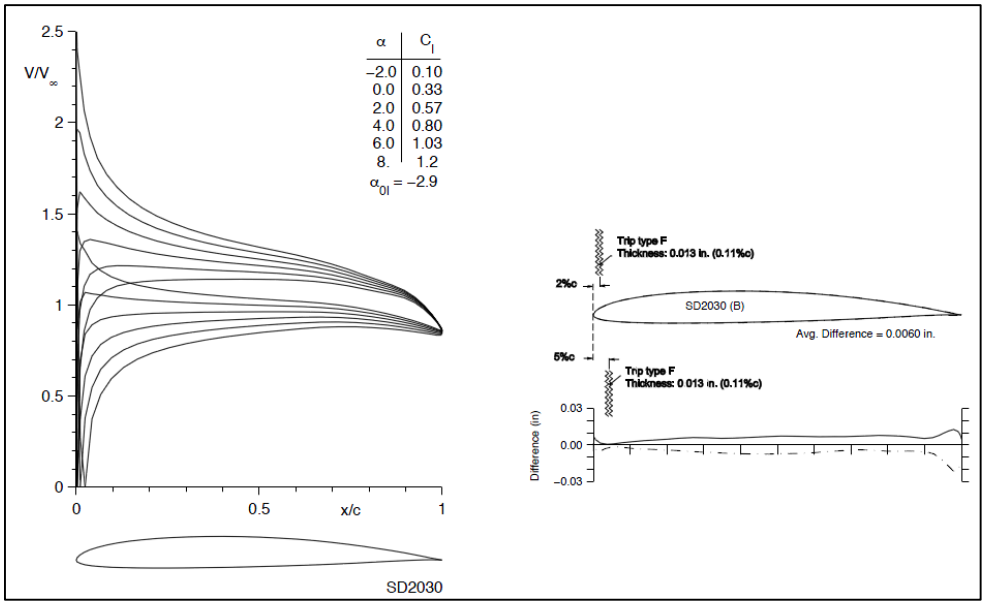

Figure 35 - Tow Tank Test Model Rotor Hydrofoil Parameters

The rotor was designed using the airfoil test data which incorporated a boundary layer trip as this served to eliminate evidence of boundary layer instabilities such as laminar separation bubbles in the drag performance. The boundary layer trip design details can be seen in **Figure 36**. Clean versus tripped boundary layer performance data can be seen in **Figure 37**.

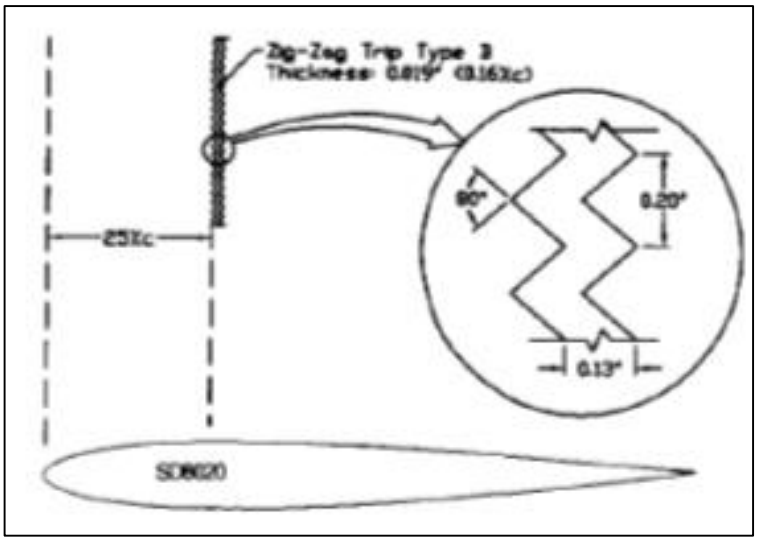

Figure 36 - Boundary Layer Trip Detail

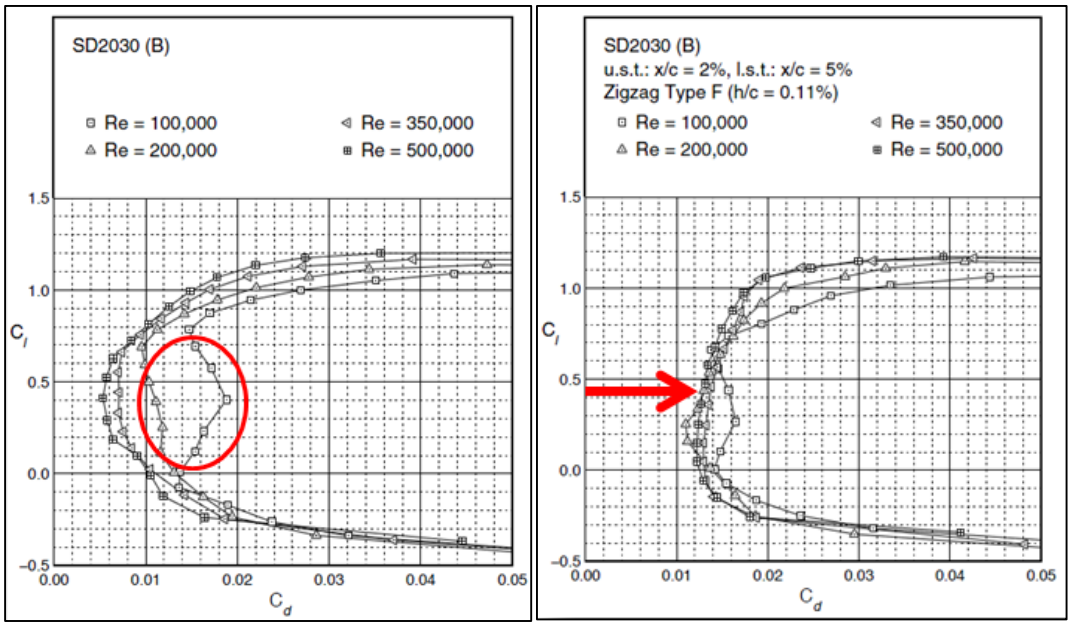

Figure 37 - Clean vs Tripped Boundary Layer Airfoil Performance Test Data

A low Cl of 0.43 was selected for rotor design optimization to increase blade chord length thereby increasing blade Reynolds number and further avoid boundary layer instabilities. Rotor design data and hydrodynamic characteristics can be found in
Figure 38 and
Figure 39 respectively.

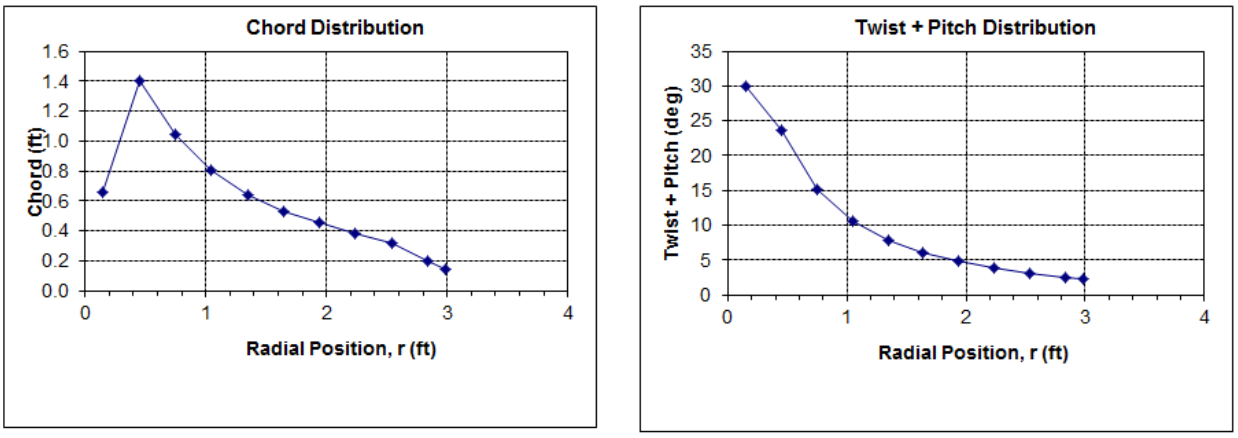

Figure 38 - Tow Tank Test Blade Design Plots

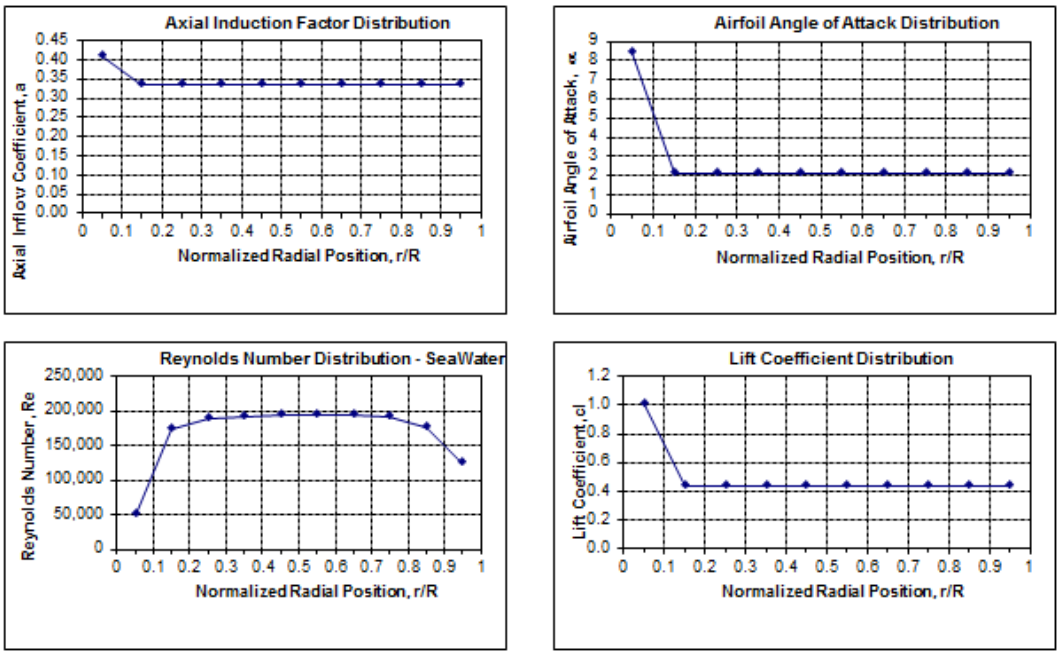

Figure 39 - Tow Tank Test Rotor Hydrodynamic Characterization

The hydrodynamic scaling resulted in a very thin blade with hydrofoils (8.56% T/C) as outlined below in **Table 2**. Extreme loads for this blade design were calculated at the extreme operating point.

Table 2 – Scale Blade Definition and Loads

#	r/R	Relm (m)	Twist (deg)	Chord (m)	Relative Thickness (t/c %)	Absolute Thickness (m)	Thr/Len (N/m)	Trq/Len (N)
		0		0	100%	0.092		
1	0.050	0.046	23.553	0.092	100%	0.092	9.1	0.365
2	0.150	0.137	23.553	0.155	40%	0.062	37.5	2.784
3	0.250	0.228	15.078	0.218	8.56%	0.0186608	79.3	5.23
4	0.350	0.319	10.558	0.167	8.56%	0.0142952	111.0	7.286
5	0.450	0.41	7.833	0.134	8.56%	0.0114704	142.7	9.173
6	0.550	0.501	6.032	0.111	8.56%	0.0095016	174.1	10.904
7	0.650	0.592	4.758	0.094	8.56%	0.0080464	204.4	12.438
8	0.750	0.683	3.812	0.08	8.56%	0.006848	230.6	13.608
9	0.850	0.774	3.083	0.066	8.56%	0.0056496	242.7	13.763
10	0.950	0.865	2.503	0.042	8.56%	0.0035952	192.1	10.44

To generate the 3D loft, a spreadsheet was used to modify the input airfoil coordinates to the appropriate chord lengths, offsets and twist at 11 stations which were subsequently imported into a 3D model for lofting (**Figure 40**, **Figure 41** and **Figure 42**).

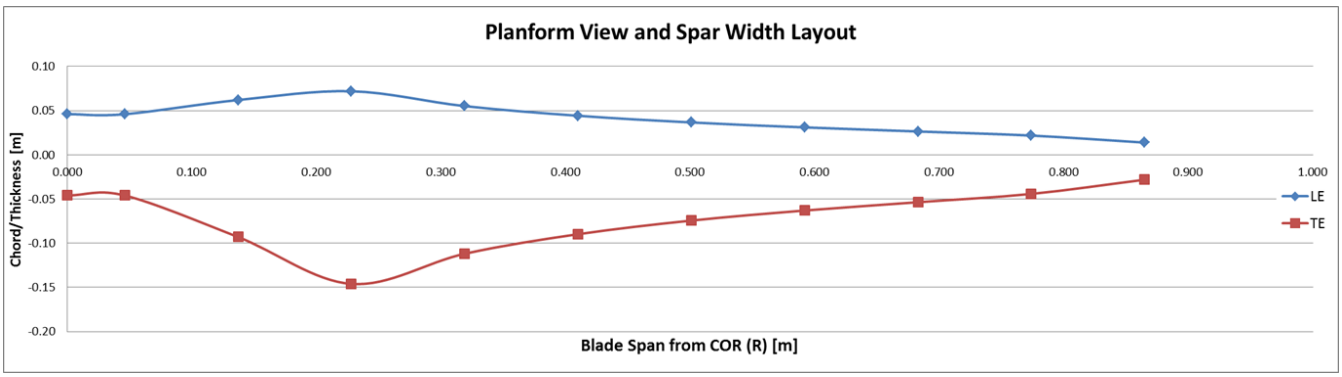

Figure 40 - Scale Blade Chord Distribution

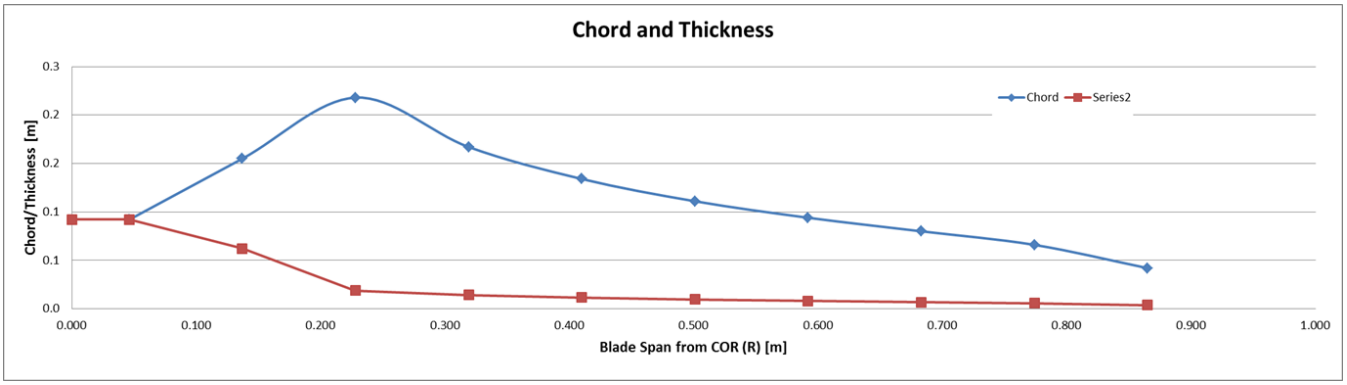

Figure 41 - Scale Blade Chord and Thickness Distribution

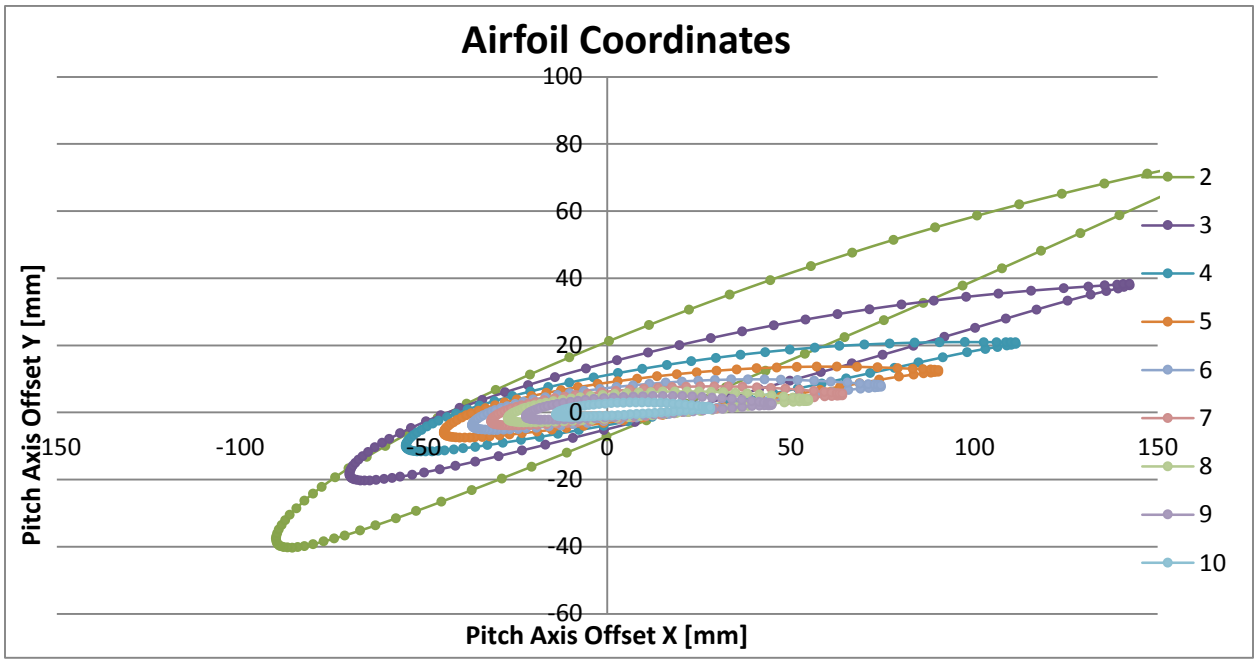

Figure 42 - Scale Blade Airfoil Coordinates

Basic beam-calculations were performed to evaluate several potential material choices ranging from 3D rapid prototype materials to compression molded composites as shown below in **Figure 43** and **Figure 44**

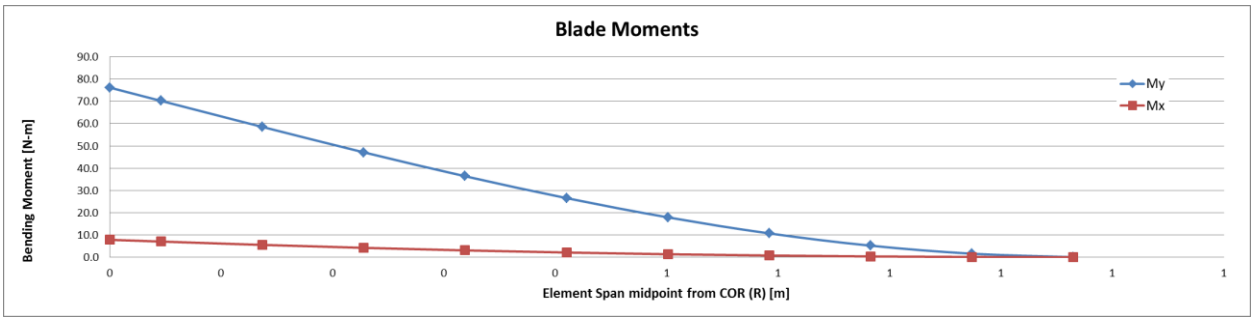

Figure 43 - Scale Blade Moment Distribution

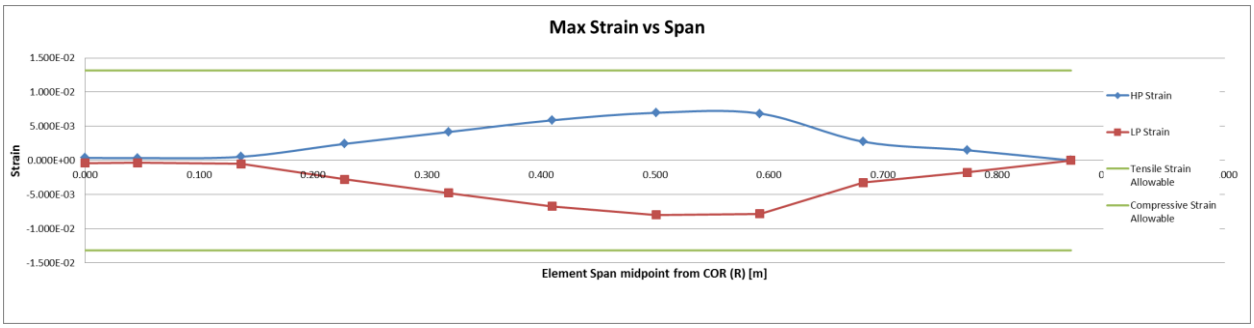

Figure 44 - Scale Blade Strain Levels for Watershed Xc11122

Upon completion of the 3D loft, more detailed structural calculations were run to compare various materials (**Figure 45**, **Figure 46** and **Figure 47**).

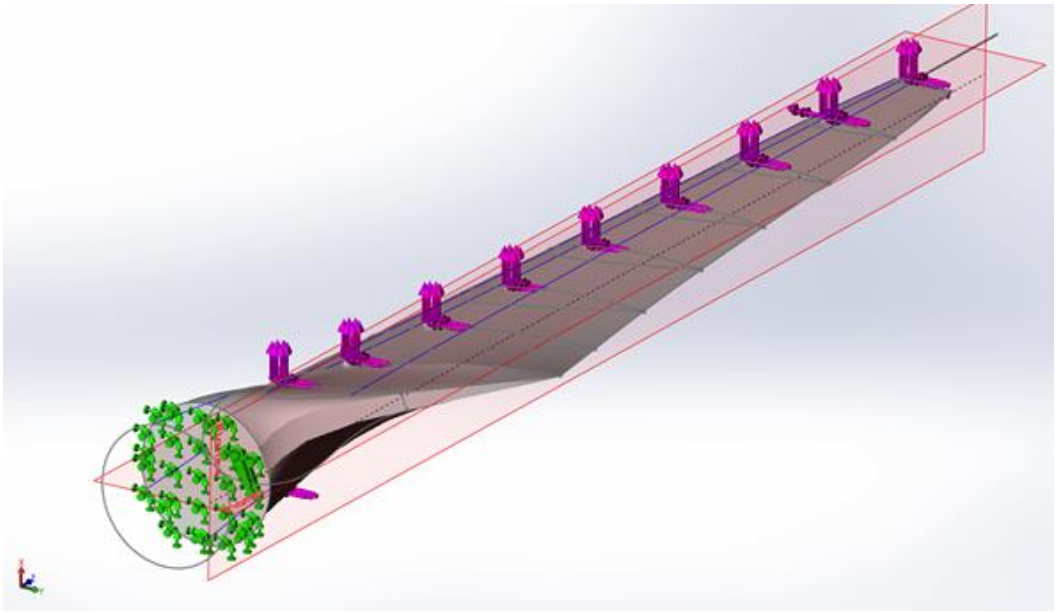

Figure 45 - Scale Blade 3D Loft and Loading/Constraints

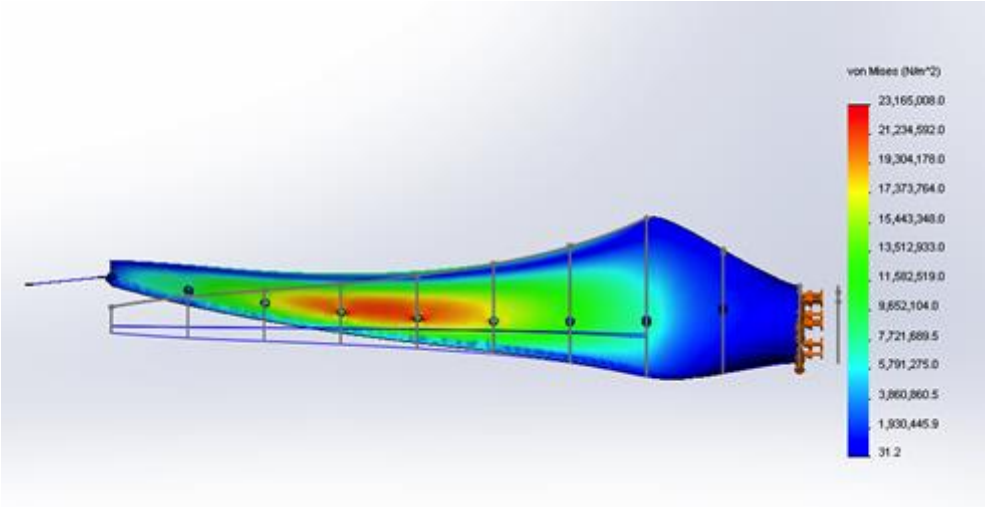

Figure 46 - Scale Blade Stress Analysis

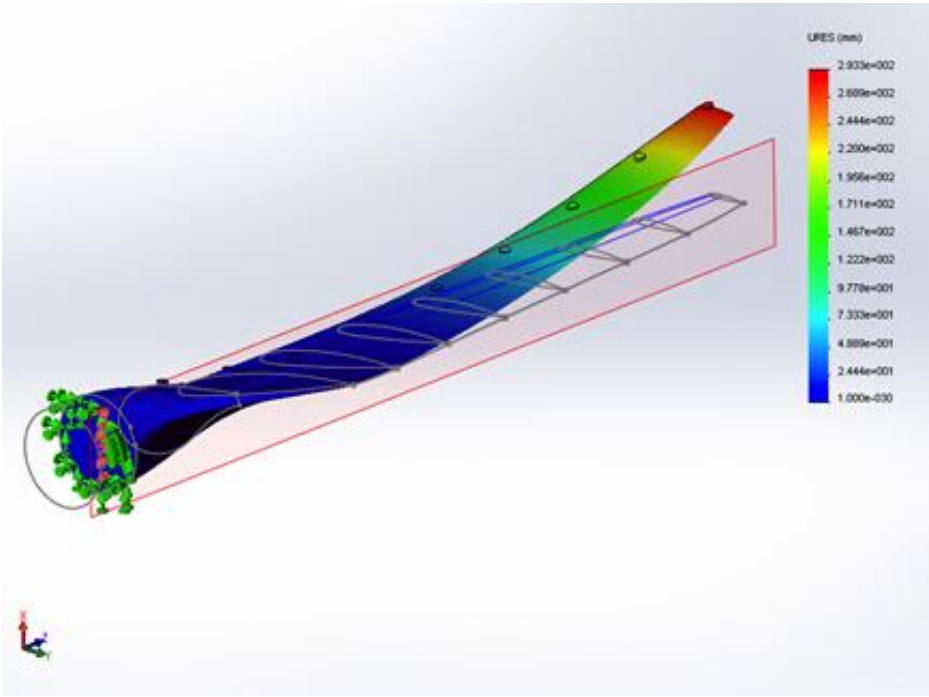

Figure 47 - Scale Blade Deflection Analysis

While 3D-printing appeared feasible from a structural standpoint, the anticipated tip deflection (~18cm) was deemed too high, so compression molded carbon fiber was selected as the material of choice. This would result in a very stiff blade which correlated well with the baseline asssumptions used in the Tidal Bladed model.

To achieve highly accurate pitch adjustments (.5deg) in the model between tank test runs, the root geometry was modified to a convex spud design, held in compression inside of the hub via exchangeable inserts. Several inserts were produced that could very accurately position the test blade at various rake and pitch angles (**Figure 48**).

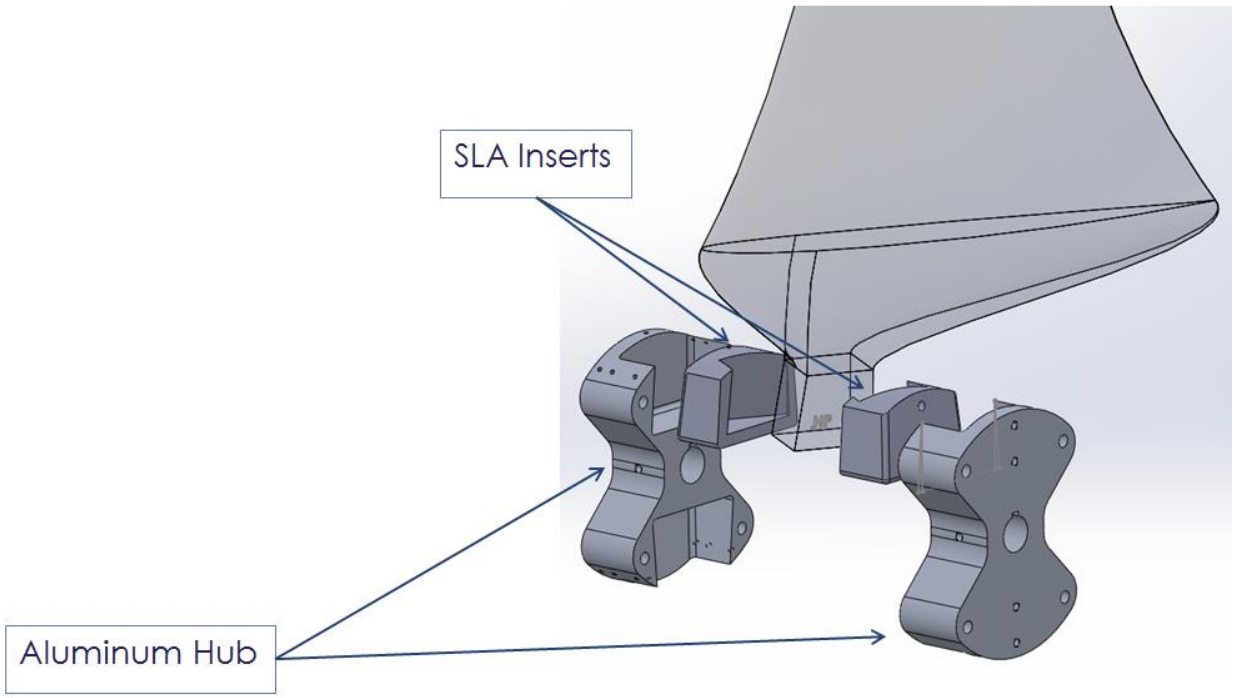

Figure 48 - Updated Scale Blade Root Geometry and Hub Connection

While this spud was initially positioned at 0 degree pitch (left), it was subsequently aligned to the innermost station for manufacturability improvements (right) (**Figure 49**).

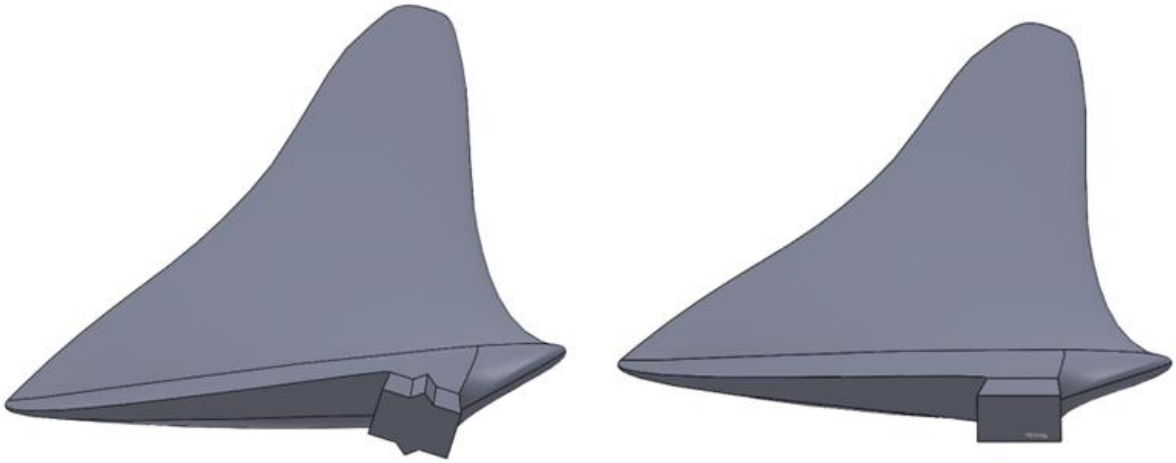

Figure 49 - Updated Spud Geometry

With this new blade geometry, the structural analysis was repeated to assure acceptable margin in the root area and validate the layup (**Table 3** and **Figure 50**).

Table 3 - Scaled Rotor Composite Lay-up Schedule

Aquantis C-Plane 1/25-scale Model Rotor Blade Ply Lay-up Schedule

NSWC Rich Banko, Code 8810, 301-227-1811 Date: 10-Jul-13 Issue: Orig

						Lower (Pressure) Surface													sym	Upper (Suction) Surface)												
Section	Span (%)	Span (in.)	Chord (in.)	Tmax (in.)	Plies (max #)	Outer Wrap (lwr surf)	Ply 1	Ply 2	Ply 3	Ply 4	Ply 5	Ply 6	Ply 7	Ply 8	Ply 9	Ply 10	Ply 11	Ply 12	Ply 13	Ply 14	Ply 15	Ply 16	Ply 17	Ply 18	Ply 19	Ply 20	Ply 21	Ply 22	Ply 23	Ply 24	Ply 25	Outer Wrap (upr surf)
Hub (innr)	3.0%	1.08	1.50	1.000	25	X	0	± 45	0/90	0	0/90	0	0	± 45	0/90	0	± 45	0	0/90	0	± 45	0	0/90	± 45	0	0	0/90	0	0/90	± 45	0	X
Hub (outr)	7.5%	2.71	1.50	1.000	25	X	0	± 45	0/90	0	0/90	0	0	± 45	0/90	0	± 45	0	0/90	0	± 45	0	0/90	± 45	0	0	0/90	0	0/90	± 45	0	X
A - A	15.0%	5.42	11.70	0.992	25	X	0	± 45	0/90	0	0/90	0	0	± 45	0/90	0	± 45	0	0/90	0	± 45	0	0/90	± 45	0	0	0/90	0	0/90	± 45	0	X
B - B	25.0%	9.03	8.66	0.735	18	X					0/90	0	0	± 45	0/90	0	± 45	0	0/90	0	± 45	0	0/90	± 45	0	0	0/90	0				X
C - C	35.0%	12.64	6.66	0.564	14	X							0	± 45	0/90	0	± 45	0	0/90	0	± 45	0	0/90	± 45	0	0						X
D - D	45.0%	16.25	5.36	0.454	11	X								± 45	0/90	0	± 45	0	0/90	0	± 45	0	0/90	± 45								X
E - E	55.0%	19.86	4.41	0.374	9	X									0/90	0	± 45	0	0/90	0	± 45	0	0/90									X
F - F	65.0%	23.47	3.78	0.321	8	X										0	± 45	0	0/90	0	± 45	0	0/90									X
G - G	75.0%	27.08	3.23	0.274	7	X										0	± 45	0	0/90	0	± 45	0										X
H - H	85.0%	30.69	2.64	0.223	5	X											± 45	0	0/90	0	± 45											X
J - J	95.0%	34.30	1.65	0.140	3	X												0	0/90	0												X
Tip	100.0%	36.10			2	X												0	0/90													X

Notes:

1. Outer Wrap is Zoltek fabric (highly flexible woven yarn) with a ply thickness of 0.015 in.
2. 0° plies are VECTORPLY C-LA 1812 unidirectional carbon fiber (598 gsm areal weight) knitted to glass veil with a ply thickness of 0.040 in. per ply at 45% fiber volume
3. 0/90° plies are VECTORPLY C-LT 1800 carbon fiber bidirectional knitted fabric (315 gsm areal in each 0° and 90° directions) with a ply thickness of 0.039 in. per ply at 45% fiber volume
4. ±45° plies are VECTORPLY C-BX 1800 carbon fiber double bias knitted fabric (290 gsm areal in each +45° and -45° directions) with a ply thickness of 0.036 in. per ply at 45% fiber volume
   Resin system is ProSet M1002 epoxy resin/135 hardener with a gel time of 10 - 14 hrs, room temperature
5. cure.

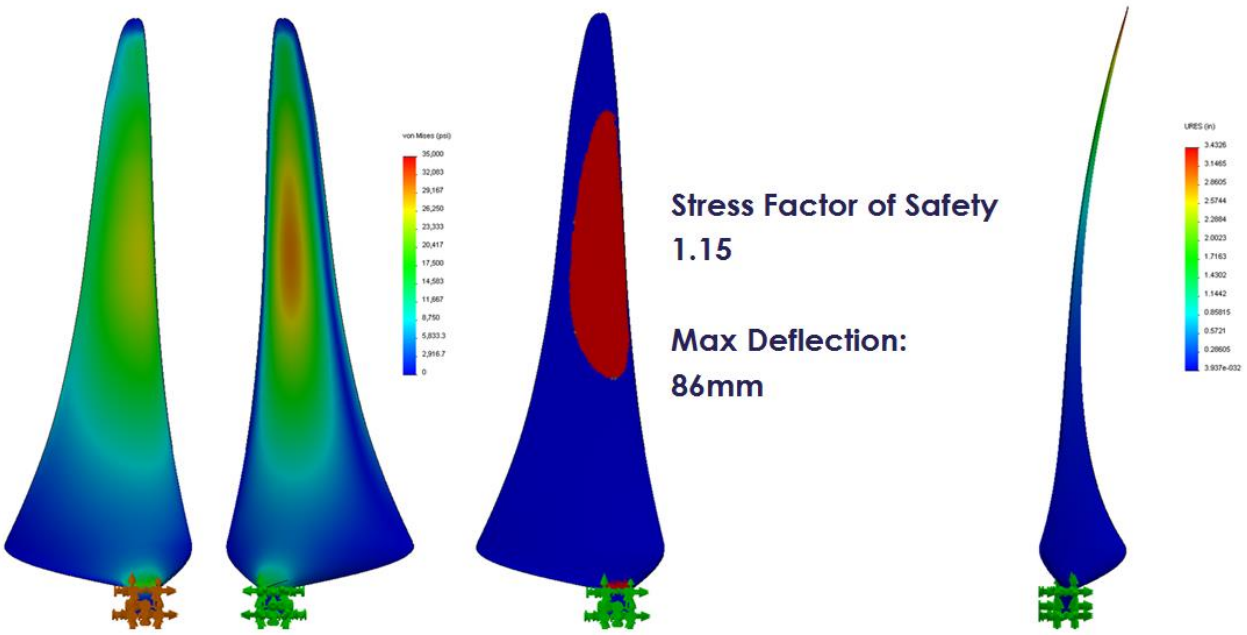

Figure 50 - Updated Scale Blade Analysis

While the spud-insert hub provided excellent adjustability, the compression-fit and large difference in stiffness between the composite blade and 3D-printed (Accura 60) insert was identified as an area of structural concern. A non-linear model was built for the joint and initial analysis showed stress concentrations in the corners that were exceeding the material strength of the insert material (**Figure 51**).

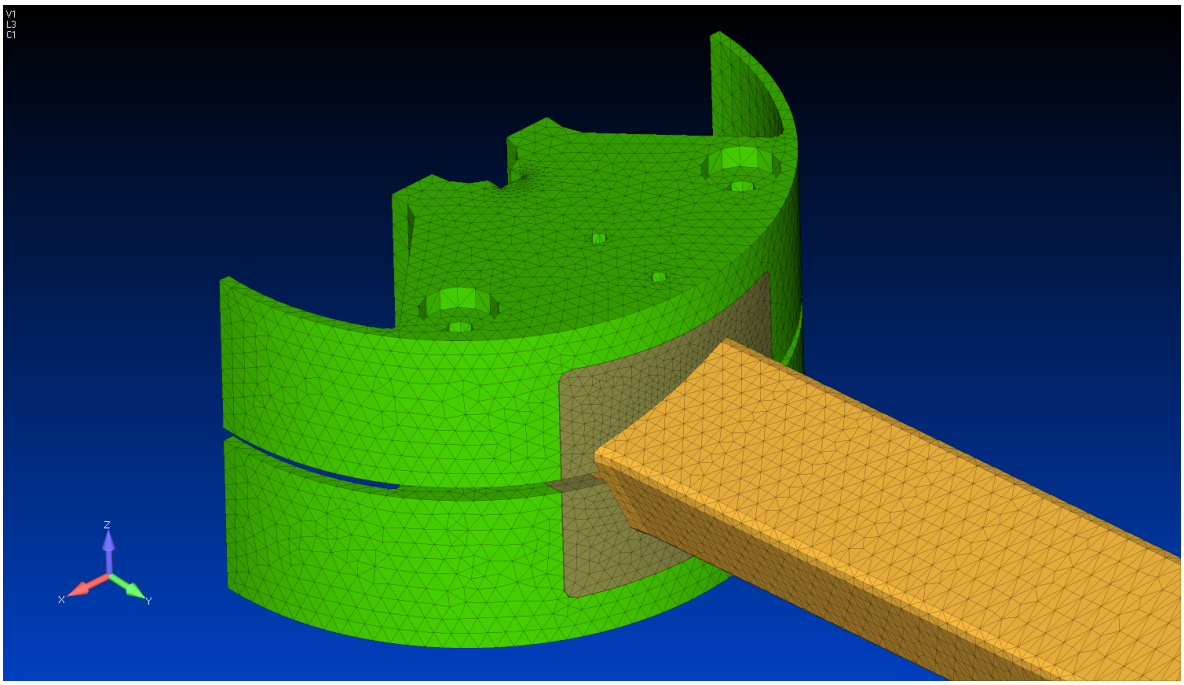

Figure 51 - Non-Linear FEA of Blade-Hub Connection

The model was run with various frictional coefficients and bolt pre-loads and after several design iterations, a 0.3" chamfer was applied to the blade spud to alleviate stress concentrations in the inserts (**Figure 52** and **Figure 53**).

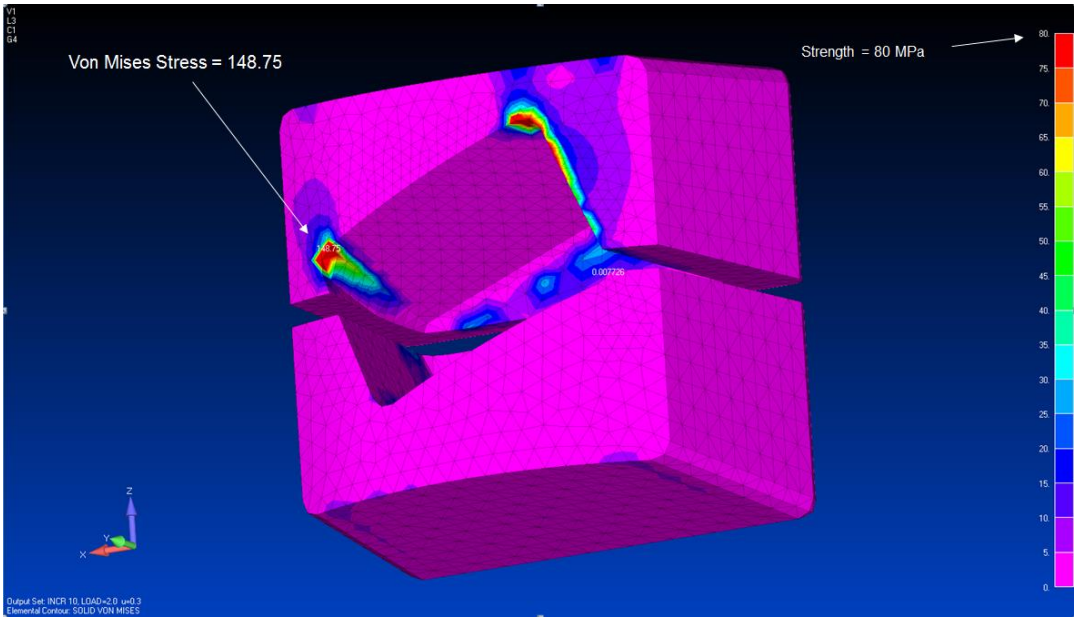

Figure 52 - Scale Blade Insert with Baseline Spud

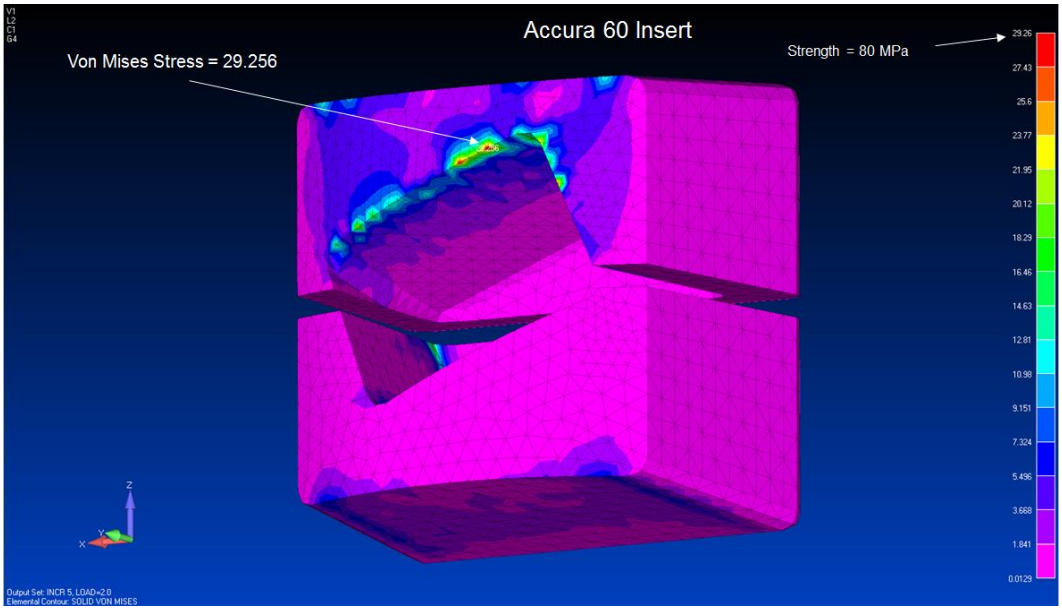

Figure 53 - Scale Blade Insert with Chamfered Spud

NSWC- CD was chosen to supply the first set of blades for the initial single-rotor checkout testing. The initial tooling effort proposed by NSWC-CD comprised Teflon-anodized aluminum molds which were projected to be extremely costly. NSWC-CD proposed a novel low-cost tooling process which involved 3D printing of the tooled surface and back-filling the tool with epoxy.

NSWC-CD designed and fabricated the SLA tooling. To save costly resin and reduce 3D printing time, material was removed from the back-side of the tool and subsequently filled with epoxy resin (**Figure 54**). The part-surface of the tool was sanded smooth and sealed with mold sealer.

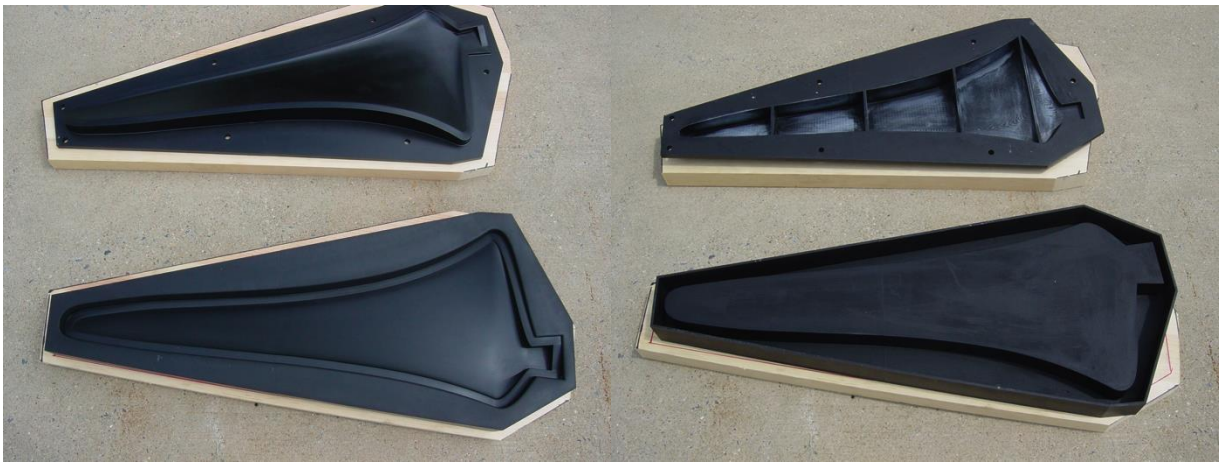

Figure 54 - SLA Tooling Set 1

To build the parts, layers were patterned by using template guides and wet-out on a separate table before being placed into the tool (**Figure 55**). Once all layers were correctly placed, the tool was closed and a breather cloth/vacuum bag was applied to the tool forcing it to close down to the flange (**Figure 56** and **Figure 57**). Excess resin was squeezed from the previously impregnated layers and absorbed in the breather/bleeder cloth. Tool closing was initially proposed to be achieved by mechanical press; however infrastructure problems prevented this from happening. The vacuum-compression provided adequate clamping force but resulted in a high level of porosity in the part due to the inability to keep the resin de-gassed during the manual wet-out process.

Figure 55 - Layer Templates

Figure 56 – Leading Edge Prior to Tool Closing

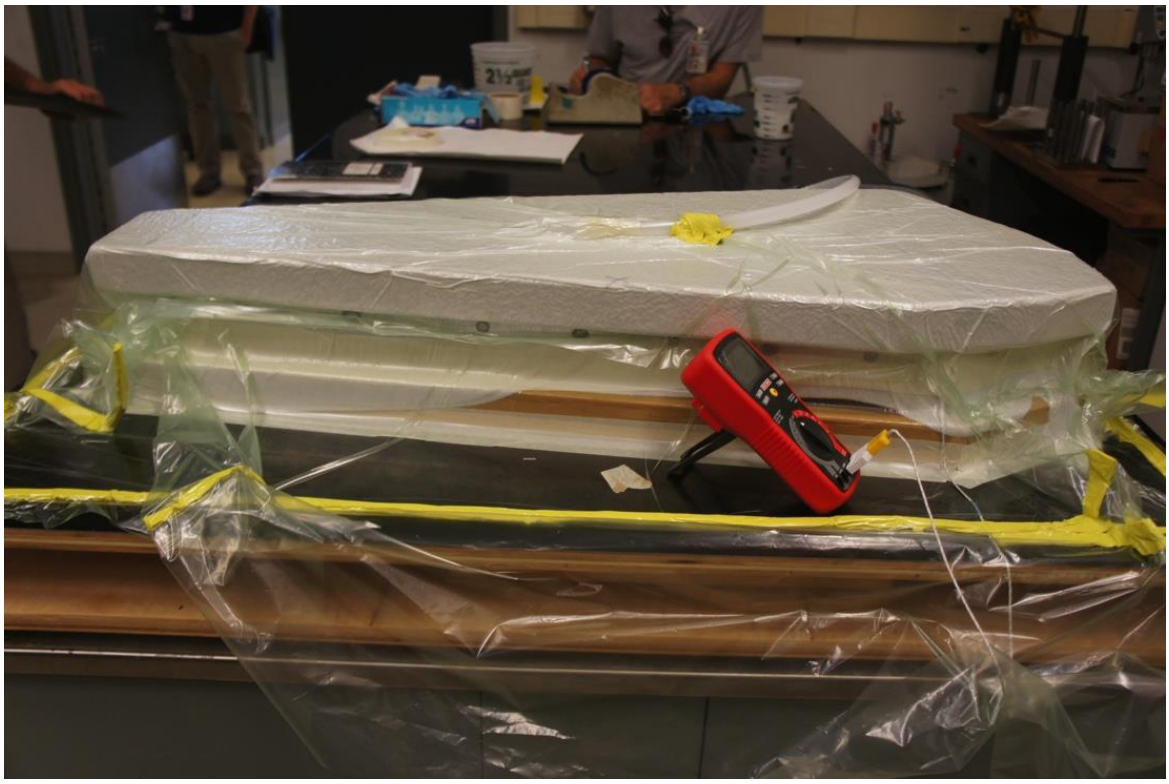

Figure 57 - Closed Tool with Vacuum Applied (Thermocouple to Monitor Exotherm)

After de-molding, the split-lines were trimmed and the part was finished with minimal use of epoxy filler (**Figure 58**). A final wet-sand was used to achieve a high quality surface finish (**Figure 59** and **Figure 60**).

Figure 58 - Blade during De-Molding

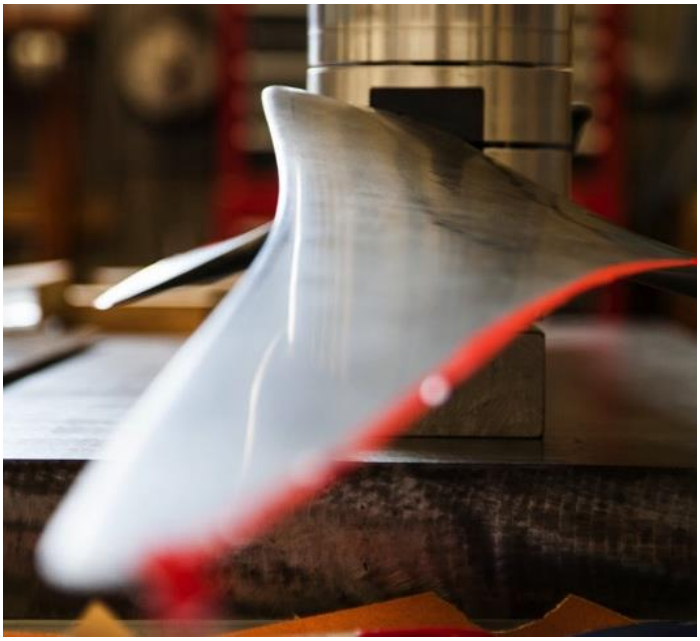

Figure 59 - Finished Blade Mounted to Hub

Figure 60 - Scale Blade Surface Finish

Unfortunately, the SLA tooling did not perform as expected and required substantial re-work between parts before cracking beyond repair on the third pull. To create the second (mirrored) set of blades, an alternate manufacturer was chosen to machine the tool from Perfect Pine with a hard tooling finish, bonded to a 1" aluminum plate (**Figure 61** and **Figure 62**). These tools proved to be very cost-effective and much easier to work with due to the improved performance of the release-system and less brittle material.

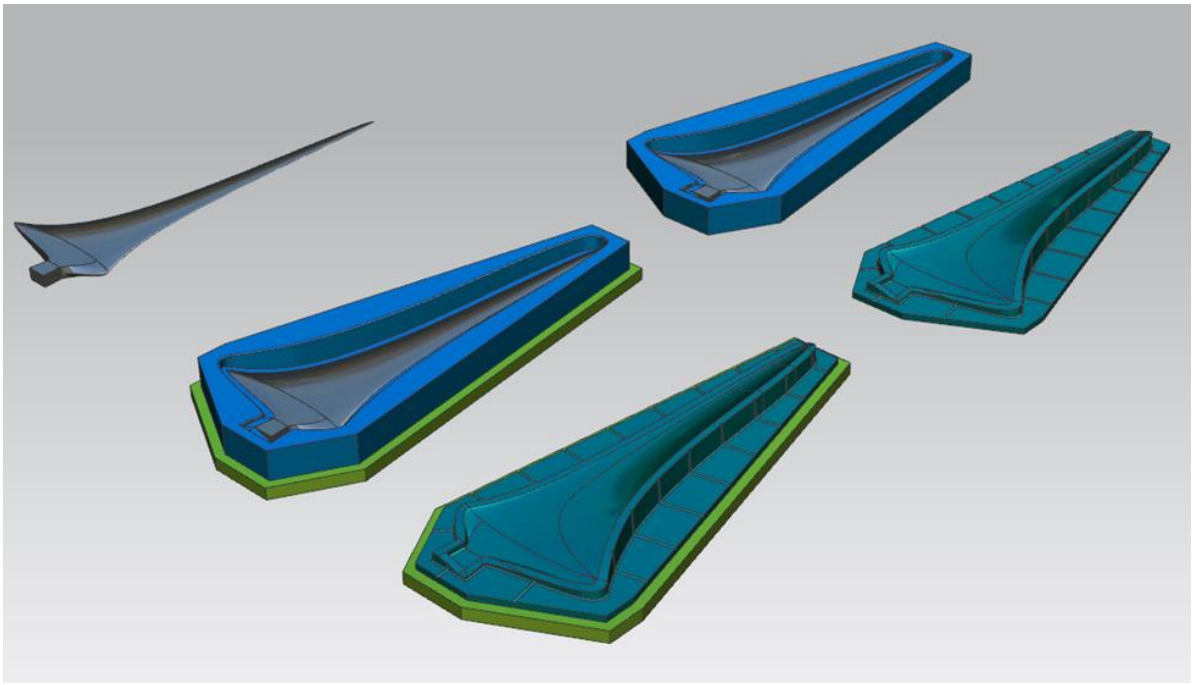

Figure 61 - Tooling Geometry for Second Set of Blades

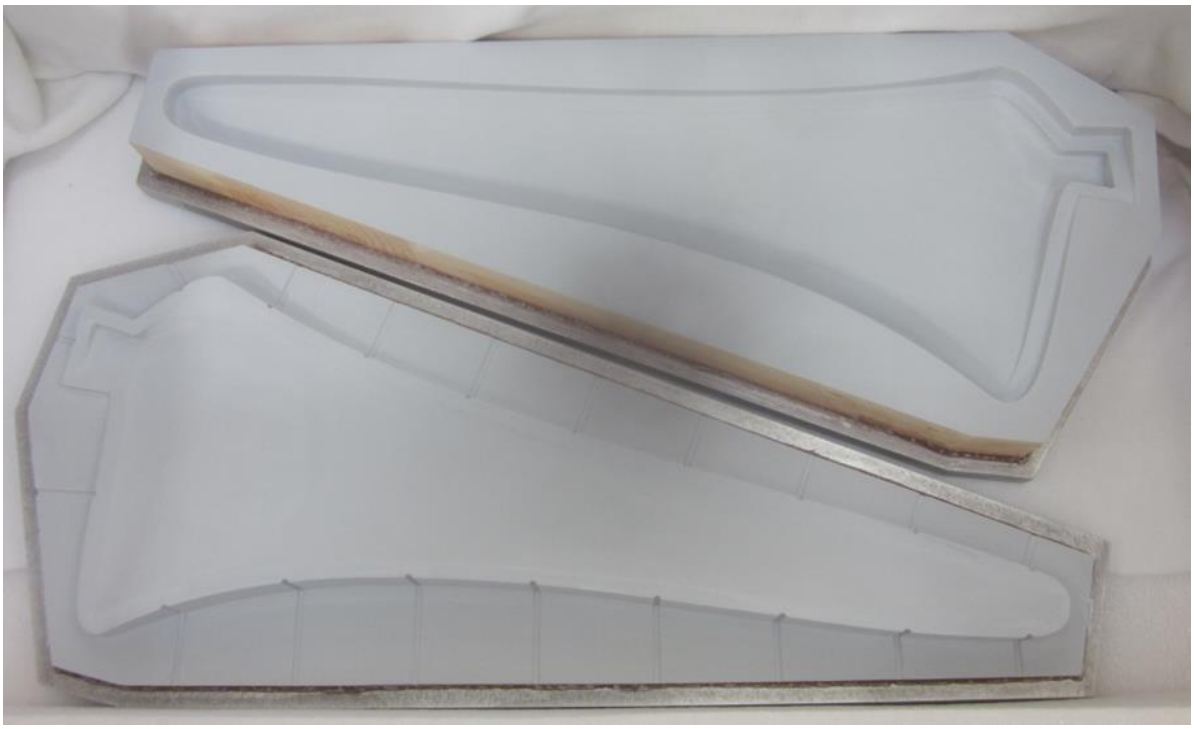

Figure 62 - Machined Tooling for Scale Blade Production

Production of the second set of blades was done at Aquantis and employed a similar process to the NSWC-CD blade fabrication in an effort to produce very similar blades (**Figure 63**). Upon inspection of blade mass and thickness, it was determined that sanding of the SLA tooling had increased the thickness of the first set of blades by ~4%. While not a structural issue, this may have led to a slight performance difference between the two rotors that was subsequently corrected with a trim tab.

Figure 63 - Complete Scale Rotor

2.4 Basin Test Towing Hardware

The deep water towing basin facility used for the scaled C-Plane testing is located at NSWC-CD in Bethesda, MD. The basin facility was designed and built to conduct stability and hydrodynamic property towing tests of scaled ship and submarine hulls. The facility features a powered and instrumented carriage which can tow models up to 25 m/sec. The basin has the following dimensions:

- Width: 15.5m (51 ft.)
- Depth: 6.7m (22 ft.)
- Length: 575m (1,886 ft.)

The overall basin layout with the towing carriage can be seen in **Figure 64**.

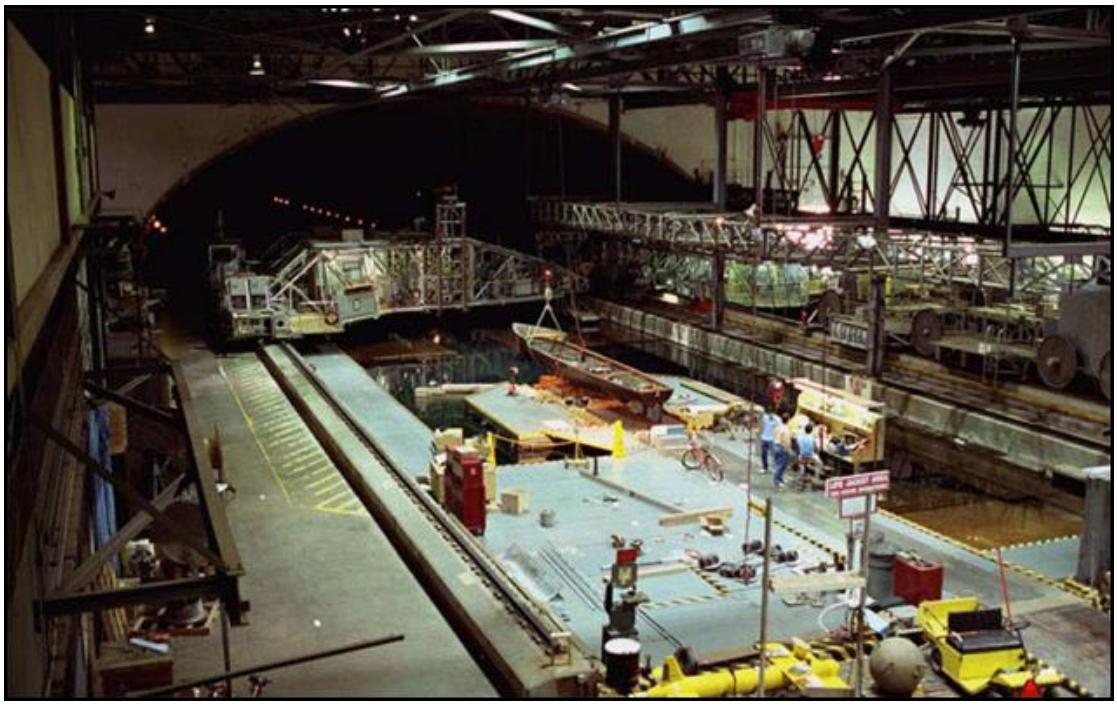

Figure 64 - Tow Test Basin

The tow tank test program required significant engineering of custom test hardware to create appropriate interfaces for the Aquantis C-Plane with the basin carriage. Specific test fixtures were designed to execute the two phases of testing; a captured test to validate the rotor hydrodynamic performance and a dynamic test that would validate the system performance and stability using the designed mooring points. The test hardware was developed collaboratively between NSWC-CD and DA. The final designs of the test hardware performed as anticipated and allowed for successful testing of the Aquantis C-plane. Initial concept designs of the static/captured and dynamic/moored rigs are shown in **Figure 65** and **Figure 66**.

Figure 65 - Concept Captured Rig Design

Figure 66 - Concept Moored Rig Design

The first phase of testing utilized a captured test rig (strut) to hold a single rotor and nacelle at constant yaw attitudes with respect to the flow. This phase was used to validate the rotor and nacelle hydrodynamic coefficients for a variety of configurations. The captured test rig design needed to provide a rigid attachment point with the ability to hold the model in various yaw

orientations. The initial concept design of the captured test hardware was conducted by NSWC-CD with some components such as the main support strut being supplied from their previous tests (**Figure 67**).

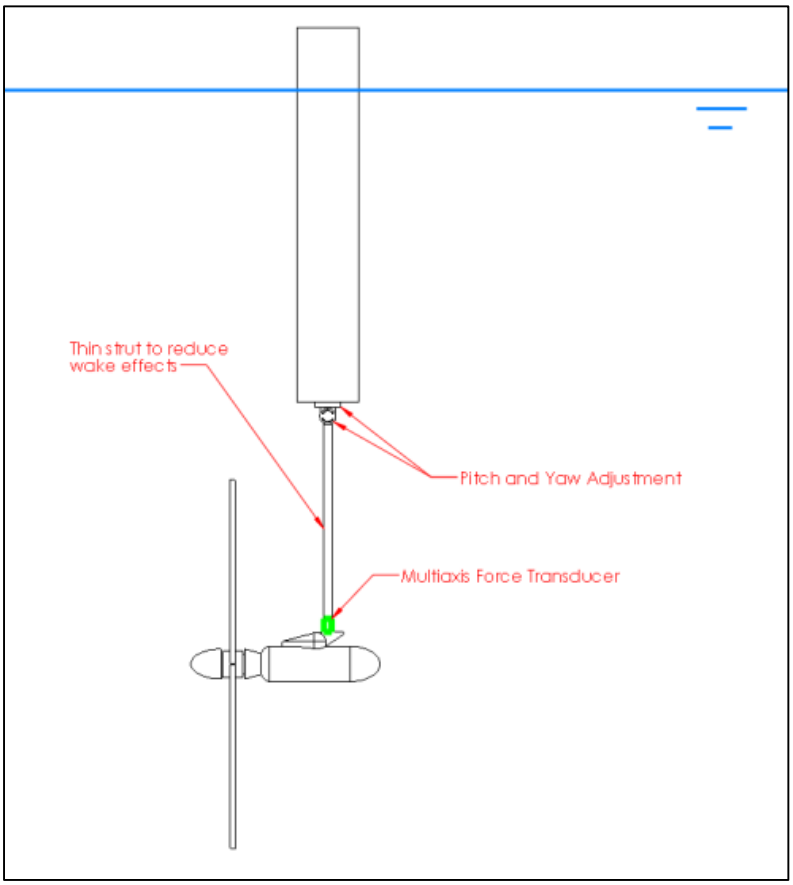

Figure 67 - Captured Tow Tank Test Rig Design

The final design of the captured rig was composed of a 304 stainless steel pipe attached to a set of calibrated discs at the upper end for setting the yaw angle. The configuration allowed yaw adjustability in 2.5 degree increments up to 45 degrees. The pipe was covered by a removable and freely articulating Accura60 fairing to form a streamlined strut. The removable fairing allowed testing of streamlined and cylindrical structure wake impacts on the rotor. Loads were measured using a 6-DOF load cell at the junction of the strut and the nacelle and by a torque sensor between the gear-motor and the rotor itself. Electrical power, sensor signal and control signal cables were internally routed through the stainless steel pipe from the nacelle to the control and data collection room on the carriage.

Figure 68 shows the captured test rig concept holding the 1/25th scale C-Plane model.

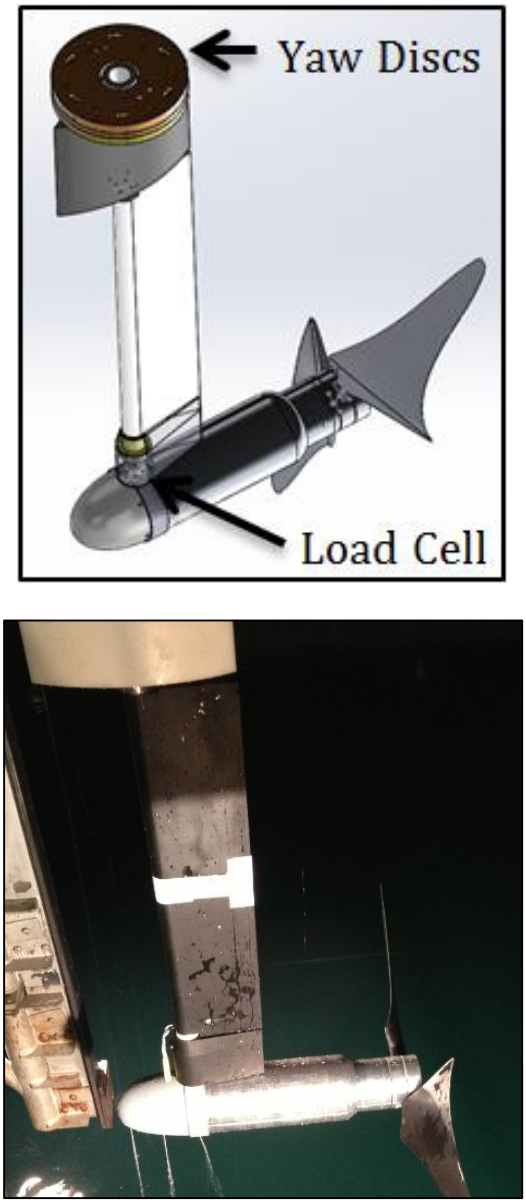

Figure 68 - Captured Tow Tank Test Rig Design

The initial goal was to have the entire c-plane with both rotors tested in the captured arrangement. However due to tow tank availability and manufacturing schedules the captured test was performed with a single rotor and nacelle. This test configuration proved to be simple and reliable while providing accurate rotor performance measurements.

The second phase of testing utilized a dynamic test rig to provide locations at the bottom of the basin to secure the C-Plane's three mooring lines. This phase was used to validate the system performance and stability under a variety of flow conditions, operational modes, failure cases, and model configurations. The test rig design needed flexibility to perform various tests repeatedly, have variable yaw positioning and not require divers for configuration changes. Various designs were investigated including a bottom running cart and a suspended frame structure. The final design was chosen due to its lowest cost, simplicity and non-interaction with debris on the bottom of the tank.

The final design of the dynamic rig was primarily constructed using a 6061 aluminum alloy truss system used normally for stage lighting and sound. The design consisted of a 12.5m wide, 7m tall and 17m long frame that mounted to the underside of the carriage structure. The truss system was stiffened with post tensioned Vectran cross-bracing of the vertical supports. The entire dynamic rig (and its submerged mooring points) attached to and moved with the carriage as shown in **Figure 69**. The design was analyzed for both stress and deflection to assure that the commercial truss structure was adequate for the drag and device loads applied as show in **Figure 70**.

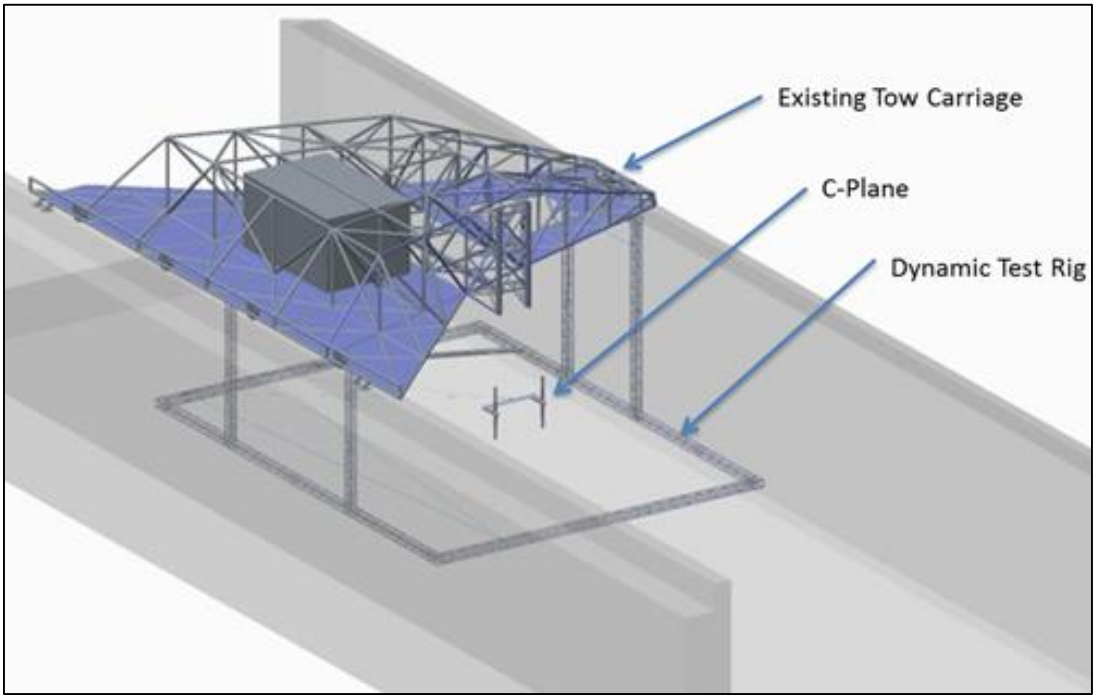

Figure 69 - Dynamic Test Rig

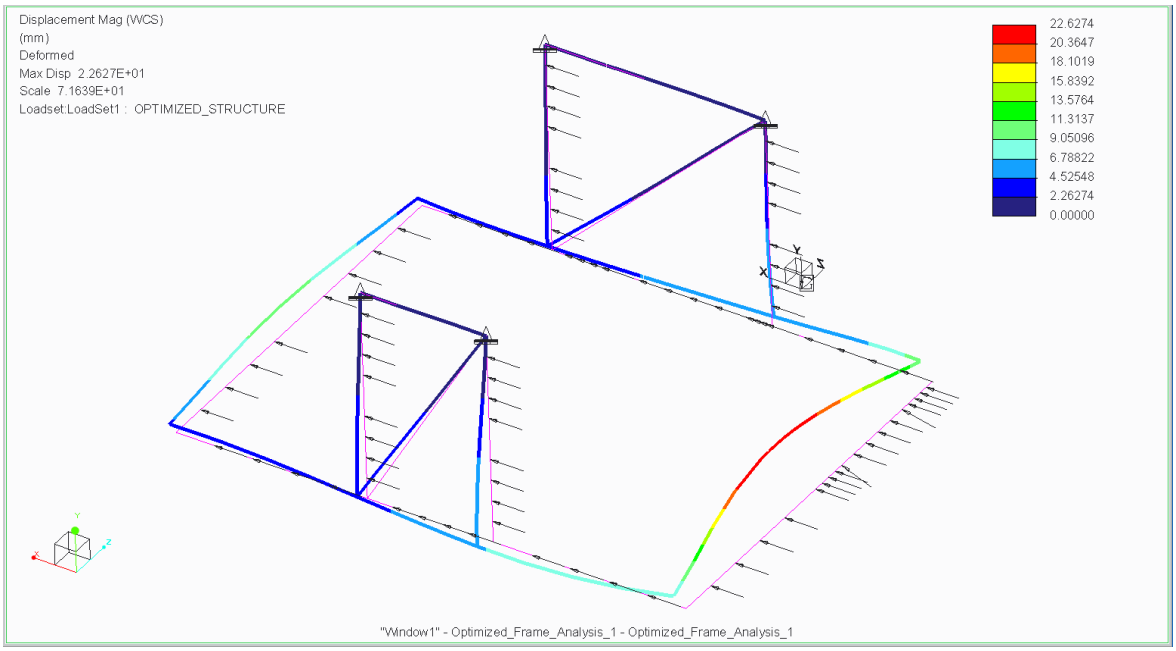

Figure 70 - Dynamic Rig Structural Analysis – Displacement at 0.6m/s Max Tow Speed

The forward mooring lines attached to traveler cars riding on a custom curved track which allowed them to be articulated around a fixed, aft, mooring location. This enabled setting the moorings at any angle up to 27.6 deg with respect to the tow (flow) direction without any impact on the dimensions of the mooring system architecture. The position of the forward mooing point was manipulated using a pulley system with low stretch Vectran lines (**Figure 71**).

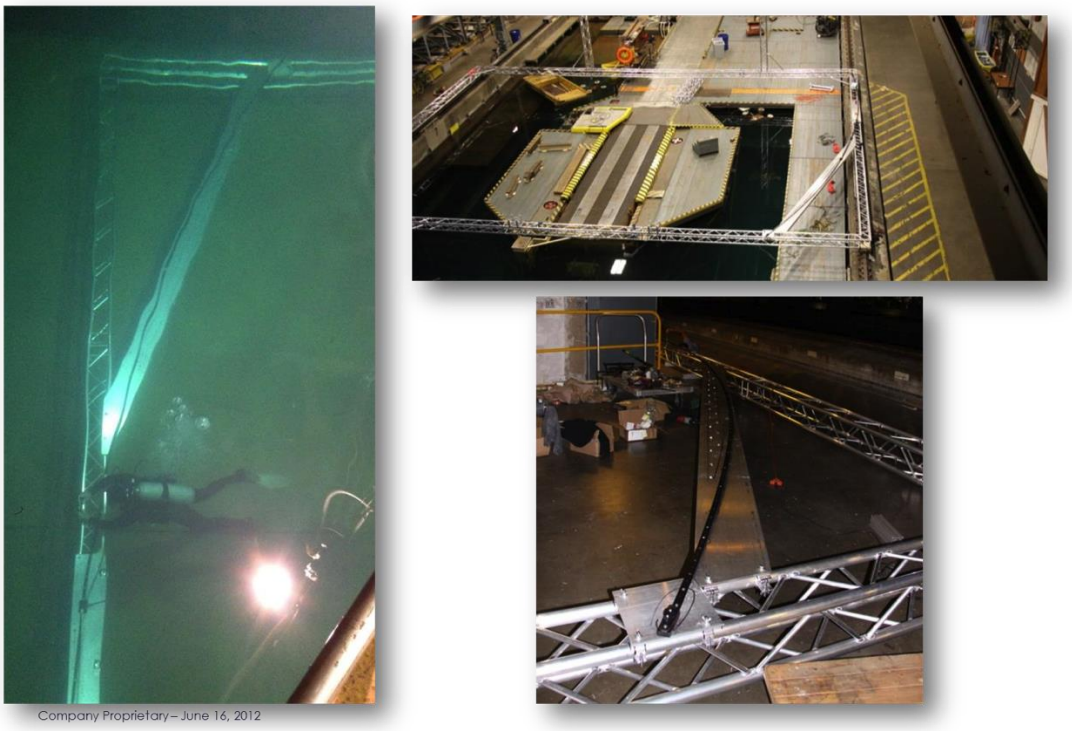

Figure 71 - Dynamic Test Rig Assembly and Installation

The test rig's forward mooring lines were designed to match the scaled stiffness, wet weight, and diameter of their full-sized counterparts. The depth of the tank limited the overall length of the mooring lines to approximately ½ of their scaled length. To account for this, specialized springs were implemented at the rig attachment point to supplement the stretch of the polyester lines themselves.

The entire tow structure was easily assembled in the basin facility and affixed to the existing carriage structure. During initial check out testing, a slight oscillation was detected by divers in the aft cross-member of the dynamic rig (where the aft mooring line attaches). This was eliminated through the application of damper plates to the underside of this member, and the solution was validated by the installation divers.

Electrical power, sensor signal and control signal cables were internally routed through the device and exited near the aft mooring attachment point. The cables were bundled into a buoyancy compensated umbilical similar in form and function to the required cabling of the full-scale device.

The dynamic rig proved to be an extremely cost-effective and easy-to-assemble solution and was successfully used in the dynamic test program without major modification or issue. At the completion of the dynamic test program the rig was detached from the carriage and set on the test basin bottom. The dynamic test rig remains partially intact for possible reattachment to the carriage for any future use needed.

2.5 Tow Tank Tests: Basin Evaluation

DA developed a detailed test plan for static tow tank testing based on the simulation work completed. The captured test was intended to verify and calibrate the hydrodynamic coefficients of the nacelle and rotor. For simplification, this test was conducted on a single power pod.

The captured test was intended to obtain the following results:

1. The following properties were measured and reconciled with the CAD and DCAB models:

    a. Weight, CG Location
    b. Buoyancy, CB Location
    c. 3-Axis Inertia
    d. Rotor Balance
    e. Rotor Rotational Inertia

2. The following properties were measured and used to calibrate the captured test results:

    a. 6 DOF loads of any supporting structure between the load cell and model
    b. 6 DOF loads of model without blades
    c. Torsional resistance of bearings and seals

The moored or dynamic test was intended to demonstrate all modes of operation including passive depth control and various, potential system failures, as well as validate, platform response as simulated in DCAB stability models. This testing program was conducted in September of 2013.

Data collected in the dynamic tow tank test basin evaluation activities was used for comparison with those data generated from the Tidal Bladed analyses of the full scale C-Plane. These data were useful in showing general trends in dynamics and loading.

Check out of the dynamic test rig and C-Plane model included:

1. Design, assembly, installation, and check-out of the dynamic test rig
2. Assembly of essential model components
3. Allowable level of testing investigating model functionality and preliminary stability cases

The test matrix executed during the check-out test is contained in **Table 4**.

Table 4 – Check-Out Test Cases

Preliminary Stability Cases:	Notes
Static Pitch & Roll Stability	Moment Measurement up to 30deg Pitch, Roll.
Pitch & Roll Natural Frequency & Inertia	IMU measurement of Pitch, Roll oscillation decay.
Tow Speed Sweep	TSR=8. Identify dive speed and pitch.
Yaw Behavior	27.6deg Max. Including transients. Above & below dive speed.
Reverse Flow	0.4m/s (2m/s full scale)
3 Center-Mooring Configurations	Fwd High, Fwd Low, CG
2 Bridled-Mooring Configurations	10cm Spread Fwd Low, 140cm Spread Fwd High
Torque & Thrust Imbalance	Starboard rotor RPM increased in increments of 5 up to 50. 26.86 Baseline on Port Rotor.

The check-out of the test rig and model and the preliminary test cases noted above indicated that the test rig was fully functional in its design intent. Check-out of the model further verified the need for additional functionality including additional rotor speed, start-up and shut down control and a functional yaw data measuring and gathering system. Video verification of the yaw behavior was a desired addition prior to conducting the dynamic testing program.

The full moored or dynamic test program was intended to demonstrate all modes of operation including passive depth control and various system failures as well as to validate platform response as simulated in the DCAB and Tidal Bladed stability models. An alternate C-Plane configuration using a single mooring with a simulated, reversing (tidal) flow was also tested. The final configuration consisting of a single nacelle and rotor was tested using the three point mooring configuration. This comprehensive testing program was conducted during the first two weeks in December 2013.

The dynamic testing program utilized the test rig structure to provide locations at the bottom of the basin to secure the C-Plane's three mooring lines. Measurements were taken using a comprehensive suite of sensors for the variety of flow conditions, operational modes, failure cases, and model configurations.

Data was collected for a minimum of 60 seconds for each case once the position of the C-Plane reached a steady-state to provide adequate time-series data as well as case-by-case statistics. In some cases, data was also recorded during transient events such as rotor and/or flow speed acceleration/deceleration, and flow angle changes. Data was recorded at either 100Hz or 400Hz depending on sensor and data logging capability. The higher sampling rate was utilized to investigate unsteady loading such as high yaw angles and passage of the rotor blades through upstream wakes.

The primary goals of the dynamic test were to validate computational stability simulations and loads avoidance, determine behavior during all modes of operation and failure events, and reduce technical risk in key areas of the C-Plane design. Testing the complete device required a significantly more complex model, controller, and sensor package than that used for the dynamic rig and model check out tests. One particularly challenging aspect was developing the Lab View controller to maintain rotor synchronization. This controller allowed for the rotor to be accelerated or decelerated at specified rates while maintaining any specified phase relationship between the two rotors. Alternatively, the rotors could be run at different speeds in order to vary the thrust and/or torque differential between them, or simulate a loss of torque control failure event.

Initial testing activities involved establishing the basic stability of the device and evaluating the pitch and depth response across a range of flow speeds. First, all sensors were zeroed and sensitivity studies were conducted. Secondly, the rotor thrust was balanced for synchronized rotors at the design speed to achieve near-zero yaw and sideslip using a trailing edge trim tab on the port rotor. The trim tab was used to achieve finer adjustment than was possible using the 1 degree blade pitch increments in the interchangeable hub inserts.

Speed sweeps at the design tip speed ratio (TSR) of eight demonstrated similar pitch and depth response compared to simulation as shown in **Figure 72**. Despite the lack of vertical shear in the tow tank, this validation is very useful for continued development of the passive depth control loads avoidance technique in the simulated environment.

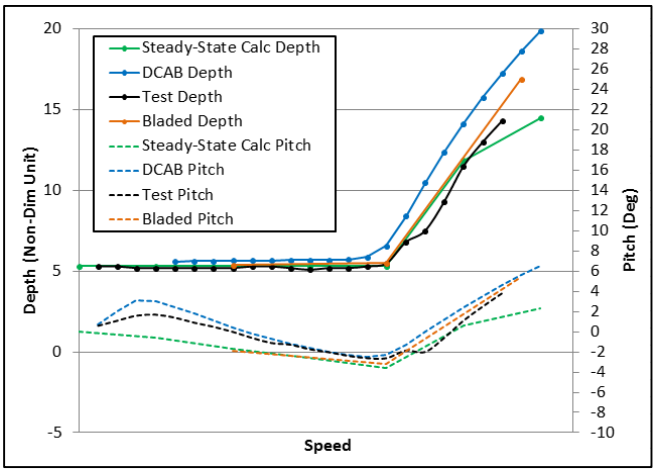

Figure 72 - Pitch and Depth Response

Testing included articulating the mooring anchor points up to 27.6deg with respect to the tow direction and collecting data over a range of speeds including reverse flow. In general, the C-Plane remains well aligned with the flow (less than 7 degree yaw), and becomes more aligned as flow speed increases.

Evaluating the C-Plane over the same range of flow speeds and directions with respect to roll, indicates its roll stability; capable of staying within 5 degrees of level regardless of the flow direction.

The initial captured test cases were designed to calibrate the rotor blade pitch to achieve the intended thrust at the design tip speed ratio (TSR). The model rotor is designed with boundary layer trips to minimize low Reynolds number flow instabilities, so the blade pitch must be calibrated for both the as-built rotor geometry and the boundary layer trip implementation. Once blade pitch and boundary layer trips were finalized, the remaining test matrix explored loading over a range of rotor cone angles, yaw angles, flow speeds, and rotor speeds.

The equation below indicates how the test data was reduced to a pure rotor yaw moment for comparison with FlightLab or WT_Perf. Tidal Bladed is capable of generating loads data at the location of the load cell, enabling a direct comparison with test data.

$$Mz_0 = (Mz_r - Mz_n) - [(Fy_r - Fy_n) * XposLoadCell]$$

Where (see **Figure 73**):
Mz_o = Rotor Yaw Moment
Mz_r = Platform Yaw Moment (Rotor & Nacelle)
Mz_n = Nacelle Only Yaw Moment
Fy_r = Platform Side Force (Rotor & Nacelle)
Fy_n = Nacelle Only Side Force
Xpos Load Cell = Longitudinal Distance from Load Cell to Rotor Reference Point

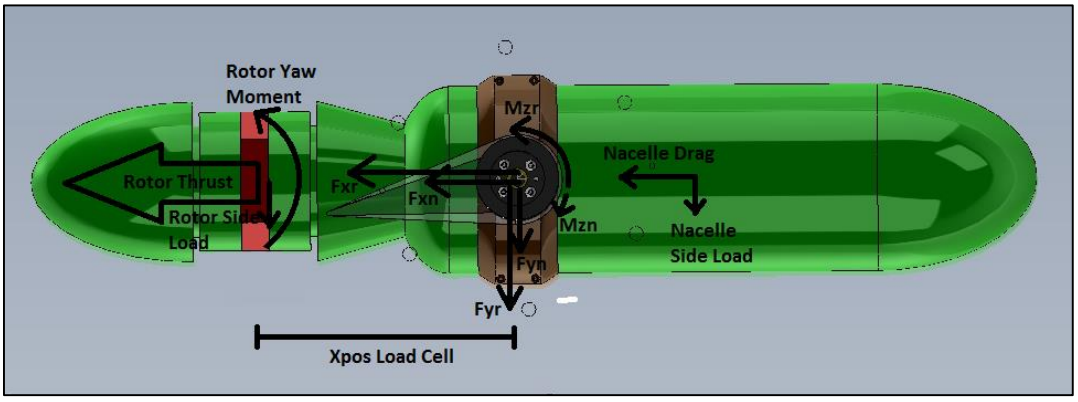

Figure 73 - Free-Body Diagram of Captured Test Model

Matching the trip geometry used in the 2D hydrofoil performance testing was desired to attain the best match between predicted and measured loads. **Figure 74** shows the as-built trip used on the rotor blades during tow tank testing. One challenge with re-creating the required trip geometry was reducing the width and thickness of the trip to match the reduction in chord of the rotor blade as a function of span. This was addressed by transitioning to fewer layers of tape over the span of the blade; however, the trip was still considerably larger than desired.

Figure 74 - Boundary Layer Trip

The application of the boundary layer trips had the dual effect of eliminating an unexpected reduction in thrust as a function of TSR, but also slightly reduced the thrust of the rotor over the entire range of TSR as seen in **Figure 75**.

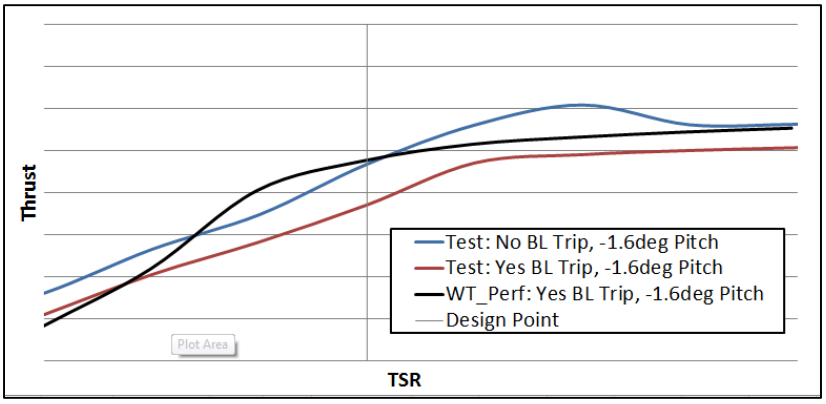

Figure 75 - Boundary Layer Trip Impact on Rotor Thrust

The model rotor was designed primarily to provide consistent thrust at very low Reynolds number rather than to optimize Cp. To achieve this design goal, some rotor efficiency was sacrificed. Tidal Bladed predicts a Cp_{max} for the rotor of 0.41 for the un-coned model rotor. Analysis of test data shows a similar shape of the characteristic Cp-TSR curve, but a lower maximum value for Cp_{max} of 0.38 as shown in **Figure 76**. This is expected because the boundary layer trip was much larger than the airfoil used in numerical simulations. This value is also uncorrected for mechanical losses in the rotor bearing and seal at this time.

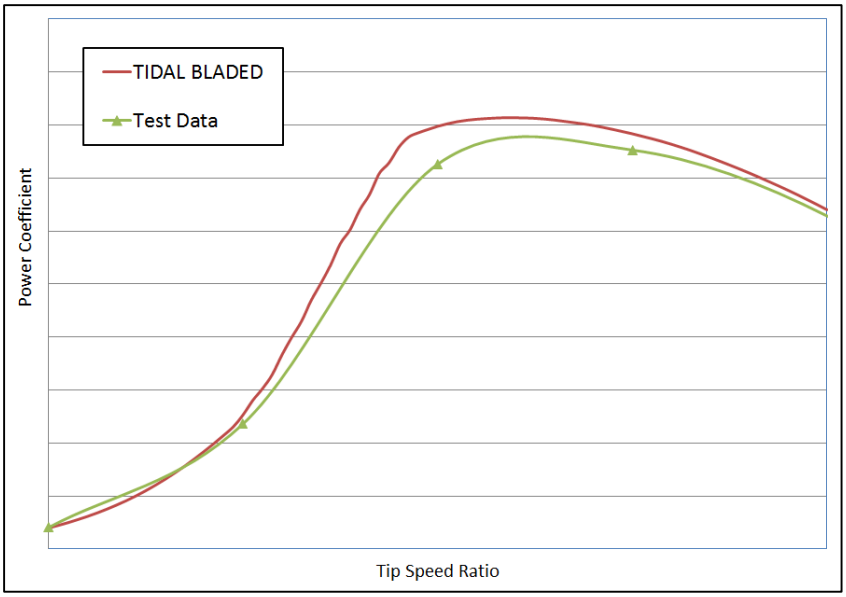

Figure 76 - Comparison of TIDAL BLADED Power Coefficient versus Tip Speed Ratio Predictions against Test Data and WT_PERF

Steady-state average rotor thrust is the largest loads factor in the overall stability and depth keeping of the C-Plane. **Figure 77** shows variation of thrust with tip speed ratio. Several pitch angle settings were tested during tow tank testing and thrust variation with tip speed ratio are shown for a pitch angle of -1.6 and -2.6 degrees. Predictions from WT_PERF have also been plotted. At the design tip speed ratio, the measured thrust values are within 10% of the predictions. This deviation is because of the dip in thrust values during testing for low pitch angles and the most probable cause is stall behavior of the tripped airfoils.

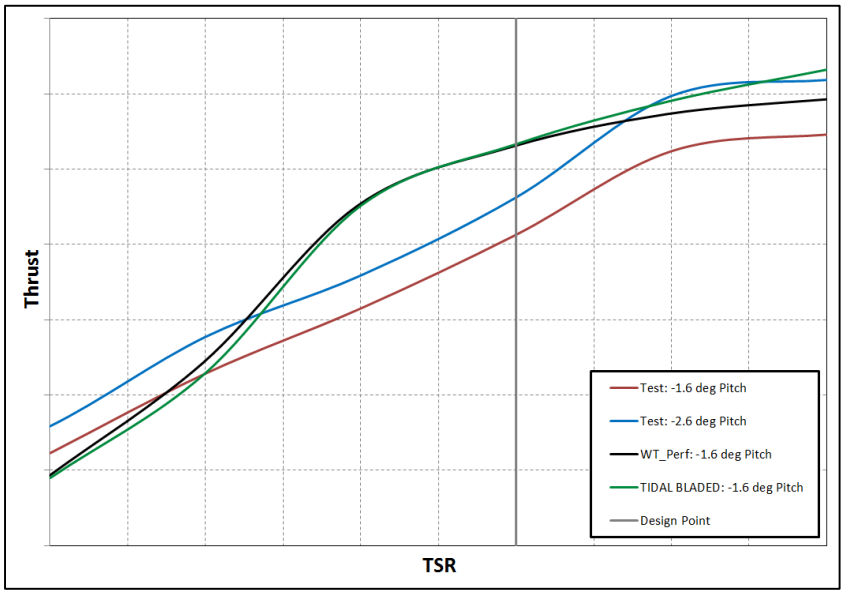

Figure 77 - Comparison of TIDAL BLADED Thrust versus Tip Speed Ratio Predictions against Test Data and WT_PERF

The next step was to compare loads predictions under yawed flow conditions. Data was collected for various yawed inflow conditions at the design tip speed ratio and current speed. This was done with the rotor configured downstream of the support strut and upstream. Predictions of thrust at the load cell location from Tidal Bladed are compared to test data and FlightLab for the upstream rotor configuration in **Figure 78**.

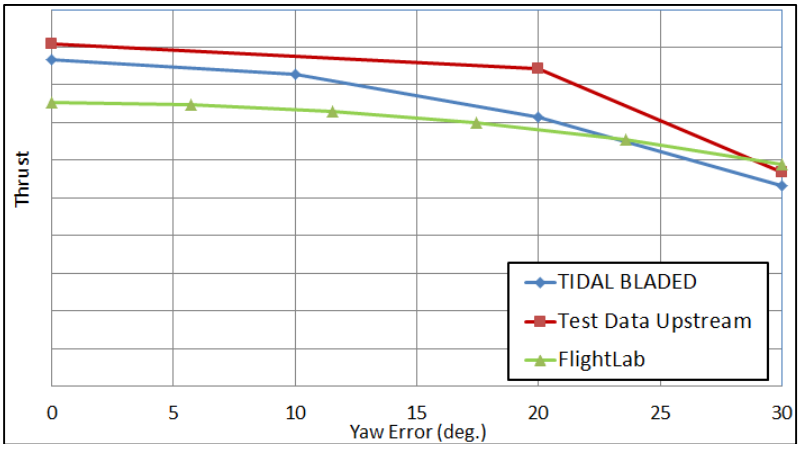

Figure 78 - Upstream Comparison of TIDAL BLADED Thrust versus Yaw Angle Predictions against Test Data and FLIGHTLAB

Figure 79 shows the variation of yaw moment at the load cell with yaw angle for the upstream rotor configuration. Simulations accurately predict the values measured during the test and show identical trends of increasing yaw moment with increasing yaw angle.

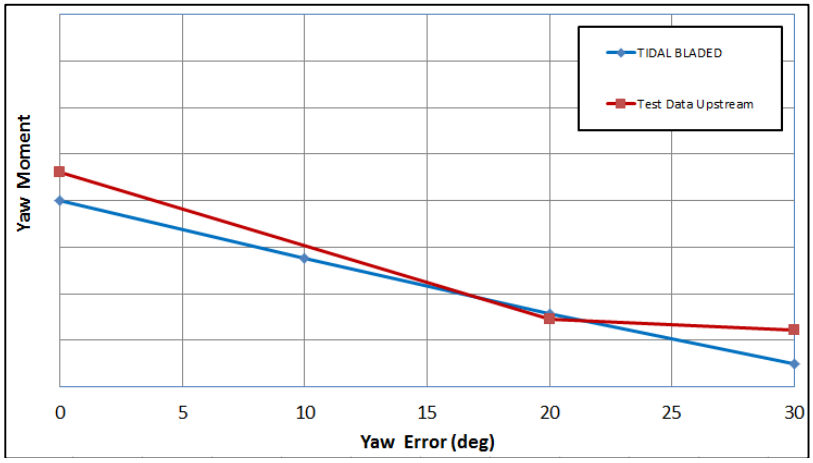

Figure 79 - Upstream Comparison of TIDAL BLADED Yaw Moment versus Yaw Angle Predictions against Test Data and FLIGHTLAB

Figure 80 shows the variation of yaw moment at the load cell with yaw angle for the downstream rotor configuration. Simulations show similar trends of increasing yaw moment with increasing yaw angle, but almost half the magnitude. Possible causes of this discrepancy in magnitude include the strut wake and load cell drift.

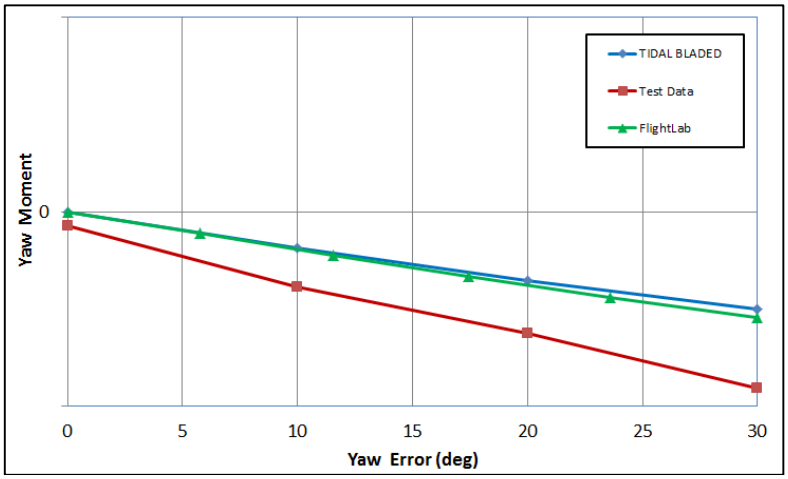

Figure 80 - Downstream Comparison of TIDAL BLADED Yaw Moment versus Yaw Angle Predictions against Test Data and FLIGHTLAB

To better understand the discrepancy in yaw moment magnitude, the variation of thrust with yaw for the downstream rotor configuration is shown in **Figure 81**. This also shows an unexpected behavior where rotor thrust increases as the yaw angle increases. Both Tidal Bladed and FlightLab shows similar trends to the upstream data of reducing thrust with increasing yaw angle.

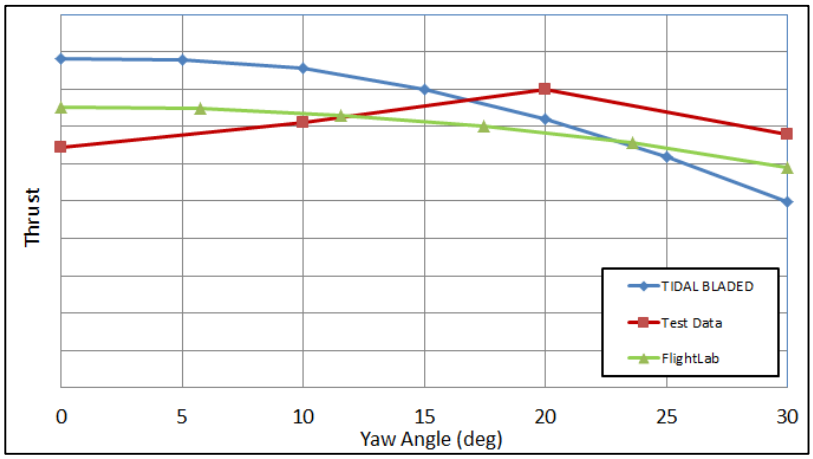

Figure 81 - Downstream Comparison of TIDAL BLADED Thrust versus Yaw Angle Predictions against Test Data and FLIGHTLAB

To investigate this unexpected thrust trend, a comparison of the C-Plane pitching moment at the load cell location for the downstream case is shown in **Figure 82**.

.

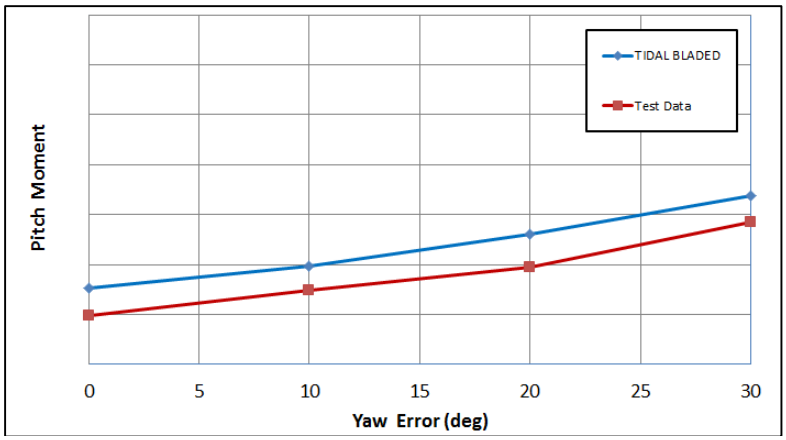

Figure 82 - Downstream Comparison of Tidal Bladed Pitch Moment versus Y-Axis Yaw Angle Predictions against Test Data

The trend of predicted pitching moment from Tidal Bladed is in agreement with test data. Since the mean pitching moment is a direct function of rotor thrust being applied at an offset distance from the load cell, a potential issue may exist in the thrust test data plotted above. A related issue may also be affecting the yaw moment test data plotted.

Investigations of the time-series yaw moment test data indicate high frequency content in the measurements. This high frequency content is potentially due to support structure vibration, and may also be a contributing factor to the yaw moment discrepancy between the structurally rigid simulation predictions and the test data. **Figure 83** shows the time-series yaw moment test data at 30 degrees flow angle for both upstream and downstream rotor configurations. Also observed in the downstream yaw moment data is a spike at the minimum point in the oscillating signal. This is not found in the upstream data and may be the result of blade passage through the strut wake. This spike is one contributing factor to the increased downstream mean yaw moment values.

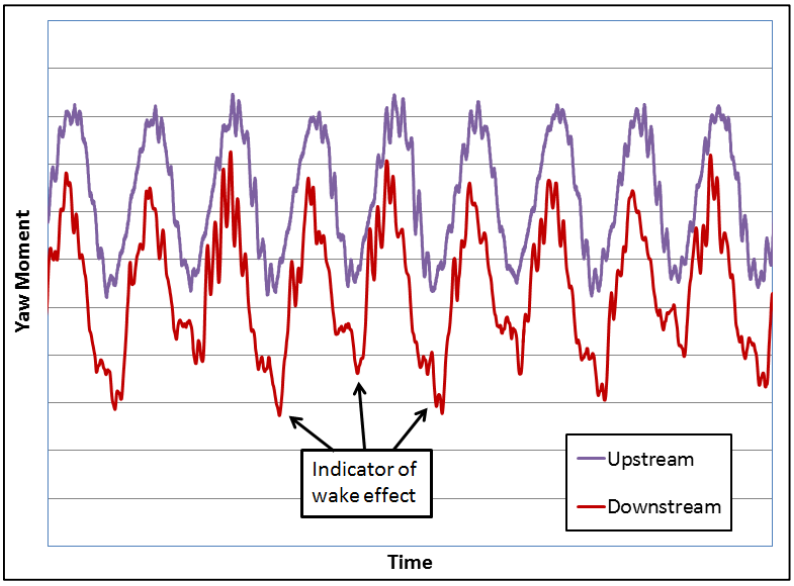

Figure 83 - Upstream vs. Downstream Yaw Moment Test Data at 30 Degree Flow Angle

The primary goals of the dynamic test were to validate computational stability simulations and loads avoidance, determine behavior during all anticipated modes of operation and failure events, and reduce technical risk in key areas of the C-Plane design. Testing the complete device required a significantly more complex model, controller, and sensor package. One particularly challenging aspect was developing the Lab View controller to maintain rotor synchronization. This controller allowed for the rotor to be accelerated or decelerated at specified rates while maintaining any specified phase relationship between the two rotors. Alternatively, the rotors could be run at different speeds in order to vary the thrust or torque differential between them in order to simulate a loss of torque control failure event.

Initial testing activities involved establishing the basic stability of the device and evaluating the pitch and depth response across a range of flow speeds. First, all sensors were zeroed and sensitivity studies were conducted. Secondly, the rotor thrust was balanced for synchronized rotors at the design speed to achieve near-zero yaw and sideslip using a trailing edge trim tab on the port

rotor. The trim tab was used to achieve finer adjustment than was possible using the 1 degree blade pitch increments in the interchangeable hub inserts.

Speed sweeps at the design tip speed ratio correlate very well with predicted pitch and depth response as shown in **Figure 84**. The slight dip in C-Plane pitch just above the initial dive speed is likely due to an adjustment made to the restraint line on the umbilical cable. Despite the lack of vertical shear in the tow tank, this validation is very useful for continued development of the passive depth control loads avoidance technique in the simulated environment.

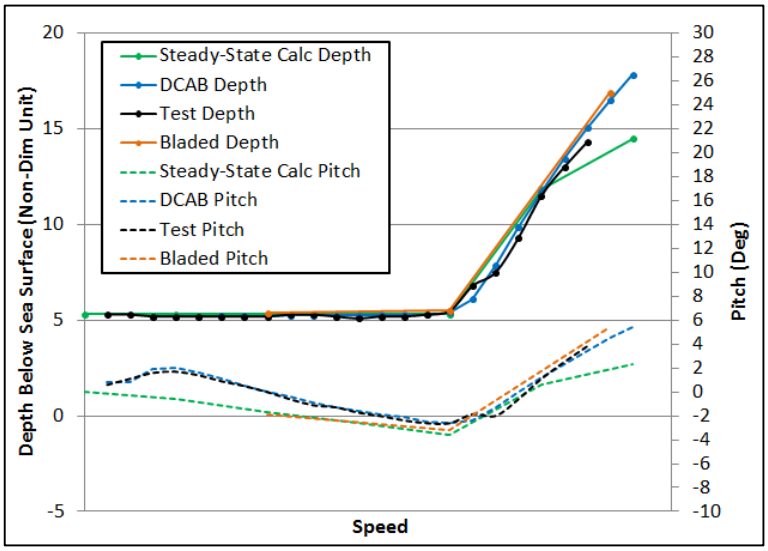

Figure 84 - Pitch and Depth Response

Testing included articulating the mooring anchor points up to -27.6deg with respect to the tow direction and collecting data over a range of speeds including reverse flow. **Figure 85** below shows the coordinate system for the yawed flow direction and C-Plane heading with respect to the mooring direction.

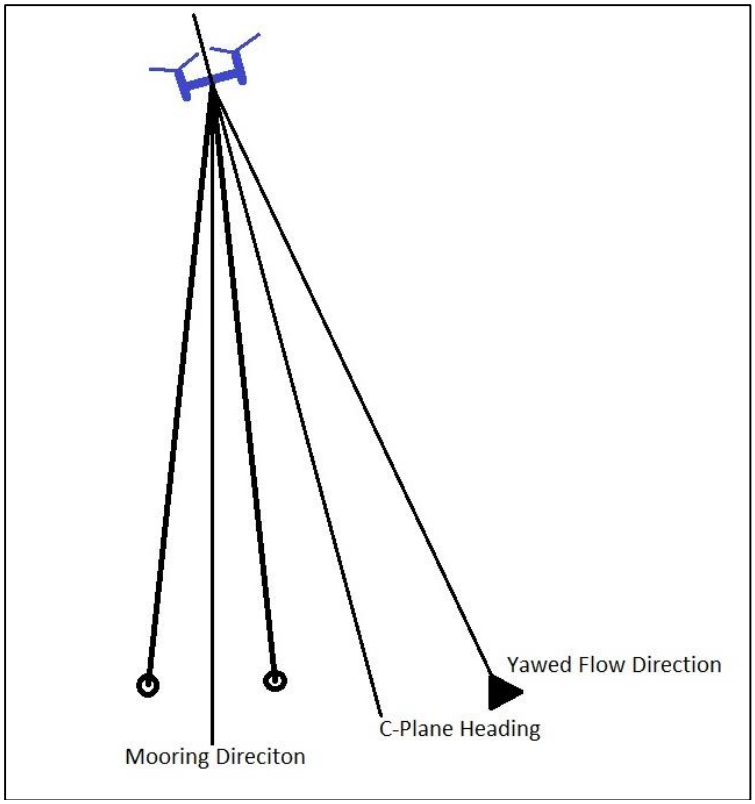

Figure 85 - Yaw Response to Flow Direction

Figure 86 shows the DCAB prediction and measured yaw response of the C-Plane with respect to the moorings. The C-Plane remains fairly well aligned with the flow direction, and becomes better aligned as flow speed increases. The discrepancy between the prediction and test data is due to a fairly high variation in the yaw test data as heading sensors primarily have to rely on inertial instruments due to magnetic disturbances from the basin and C-Plane electronics.

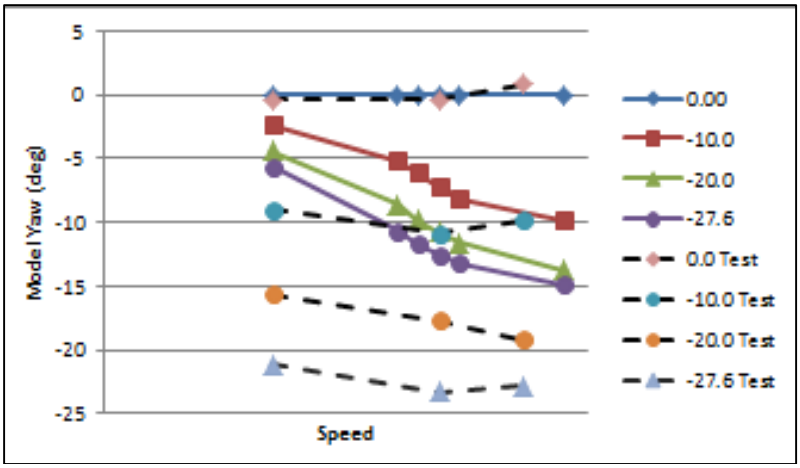

Figure 86 - Yaw Response to Flow Direction

The Tidal Bladed model definition and simulation methodology required refinement to accurately reproduce the test results. The Tidal Bladed skew wake model was important for capturing the coned rotor hydrodynamics for misaligned flow cases (yaw and pitch). Accurate modeling of the mooring attachment locations and model wet weight also proved to be very important.

Figure 87 shows the roll of the C-Plane over the same range of flow speeds and directions. The C-Plane is very roll stable; capable of staying within 5 degrees of level regardless of flow direction.

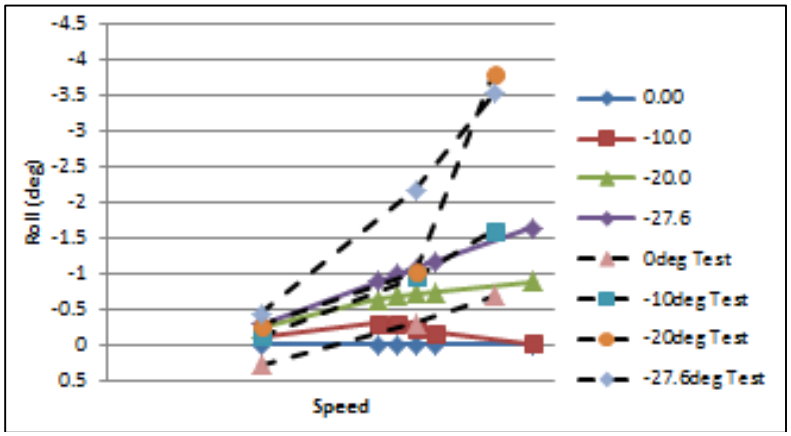

Figure 87 - Roll Response to Flow Direction

Tow tank testing has shown the moored C-Plane design to be very stable during all anticipated modes of operation over a wide range of flow conditions. The C-Plane has also demonstrated it has ample stability to safely react to a variety of failure modes including CG offsets resulting from

asymmetric flooding, torque and thrust differentials resulting from asymmetric drivetrain failures, and others.

This effort has also validated the ability of multiple simulation approaches to accurately predict the steady-state and dynamic stability of the C-Plane. In particular, the pitch and dive response are well characterized, which is useful for detailed design of a moored marine current turbine which utilizes passive depth control for loads avoidance. Testing of the tidal (reversing current) and single rotor configurations indicated a high level of stability and adaptability and provided valuable insight into and data for possible deviations from the baseline design.

2.6 Mechanical Turbine Design

During the grant period DA focused the majority of mechanical systems development on the hydrostatic drivetrain. The operational characteristics of this core technology shaped much of the design of other C-Plane components. In order to best understand the design and operation of a hydrostatic drivetrain design, DA entered into an agreement with Bosch Rexroth for development, simulation and testing of a 250kW scaled hydrostatic drivetrain. This was an excellent partnership as it leveraged Rexroth's profound experience in hydraulic systems, Hagglund's compact large radial pumps design and Aachen University IFAS's hydrostatic drivetrain test platform. The current IFAS test stand configuration can be seen in **Figure 88**.

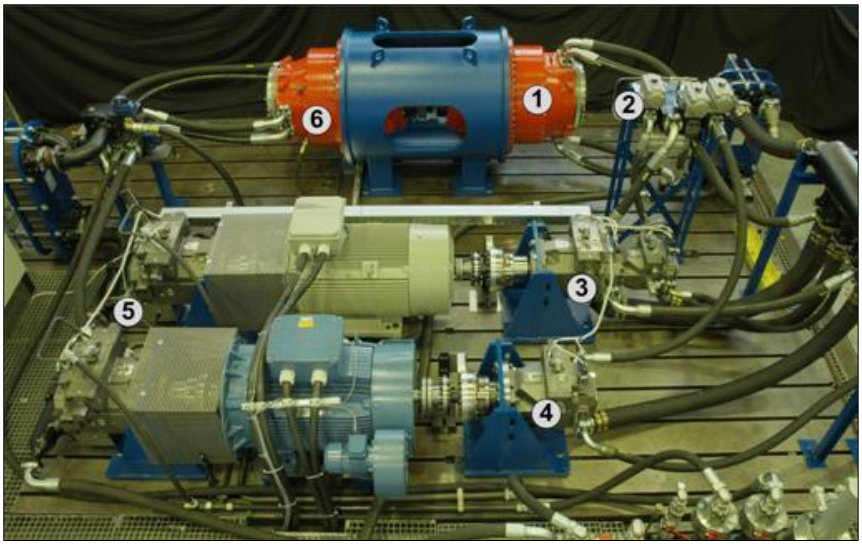

Figure 88 - Aachen University Hydrostatic Drive Test Stand

The objective of the scaled drivetrain simulation program was to provide data for comparison with those generated from the planned, scaled drivetrain test program. The scaled drivetrain test program is intended to verify the feasibility, performance and the expected properties of such a drivetrain, at approximately 250kW, tested in a laboratory environment. The scaled drivetrain

design for both the simulation and test utilized a Hagglunds pump and Rexroth generator drive motors of similar design and representative operation of the full scale system.

A comprehensive test plan was developed to evaluate the drivetrain performance under a variety of operational, steady-state, transient and fault conditions. In addition the test will evaluate the impact of stall regulation and high ratio dynamics. These test cases will allow comprehensive evaluation and measurement of the dynamics of the system, the controls to operate the system and the overall system efficiencies. The test plan and load cases were the basis for both the simulation work and the future test plan.

DA developed two operational torque profiles for operation of the hydrostatic drivetrain, passive depth control and stall control as inputs for the simulation work. Passive depth control assumes that the device will maintain a maximum apparent flow speed and thus reaches a torque and power limit at rated flow speed. The stall control drivetrain has a much higher flow speed limit, however as a consequence the maximum operation torque is approximately 2 times the maximum of the passive depth operation mode. The torque and power profiles of each operating mode can be seen in **Figure 89** and **Figure 90**.

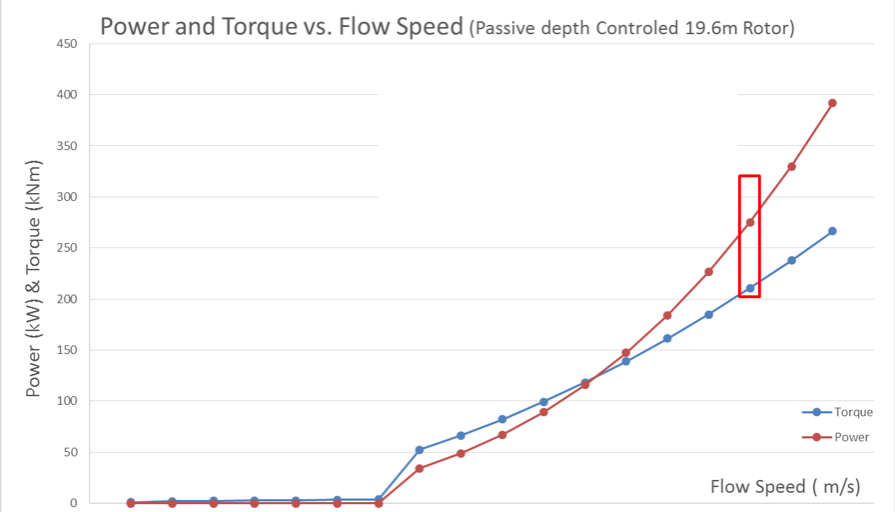

Figure 89 - Passive Depth Control Torque and Power Profile

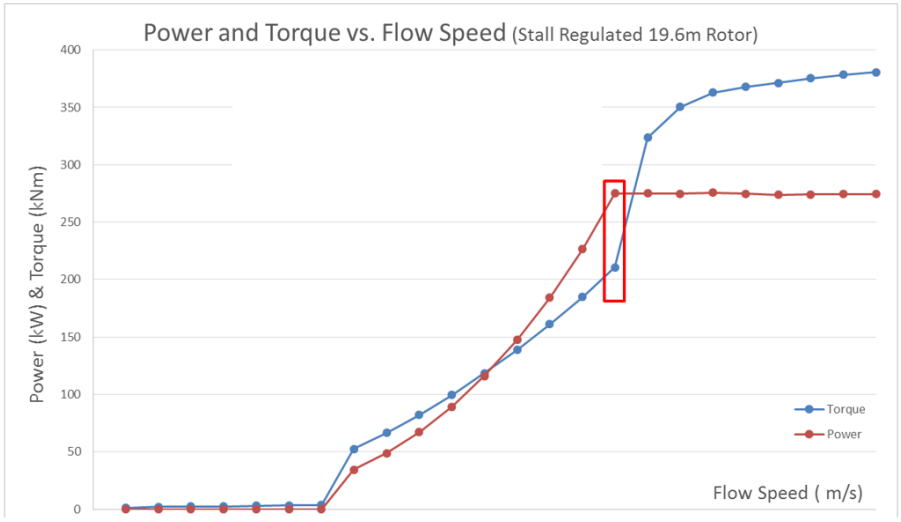

Figure 90 - Stall Control Torque and Power Profile

In addition, DA completed and delivered a dynamic torque model of a 19.7m, 250 kW rotor accounting for flow speed, tip speed ratio, wake loss, turbulence, and shear variation. These data and models served as the input to the Rexroth and Aachen University IFAS scaled drivetrain simulation. A graphical representation of these data can be seen in **Figure 91**.

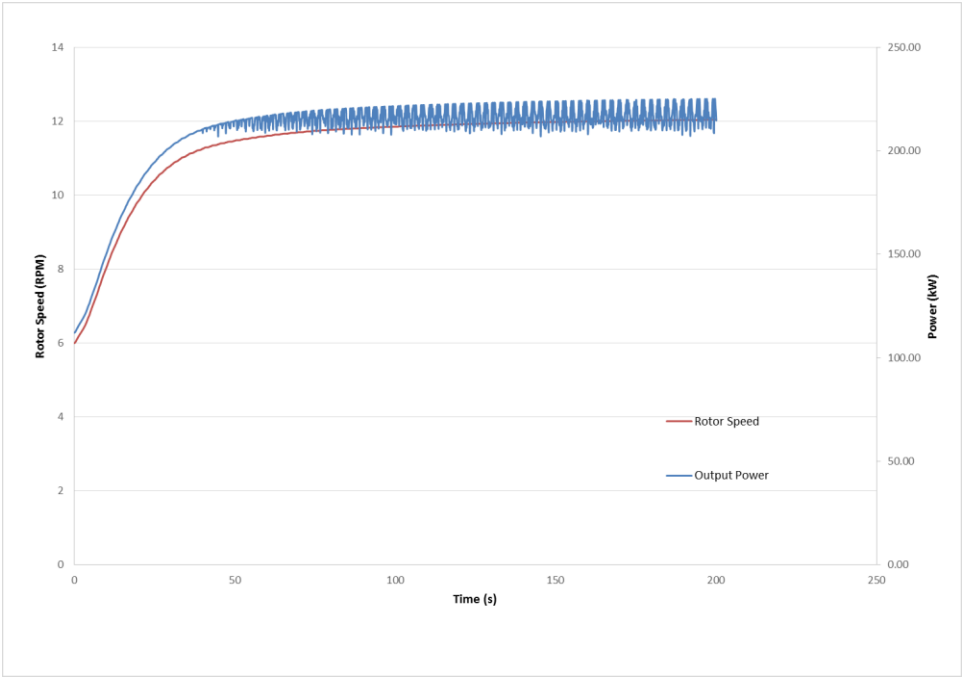

Figure 91 - Dynamic Rotor Power and Speed

Another major component used in the model was the slip induction generator. DA developed was a simplified model of the generator for use in the simulation. The generator is a standard off the shelf type design with no custom features, i.e. high slip, low in-rush, special environmental protections, or other considerations. Operating characteristics of the scaled generator are show in **Figure 92**.

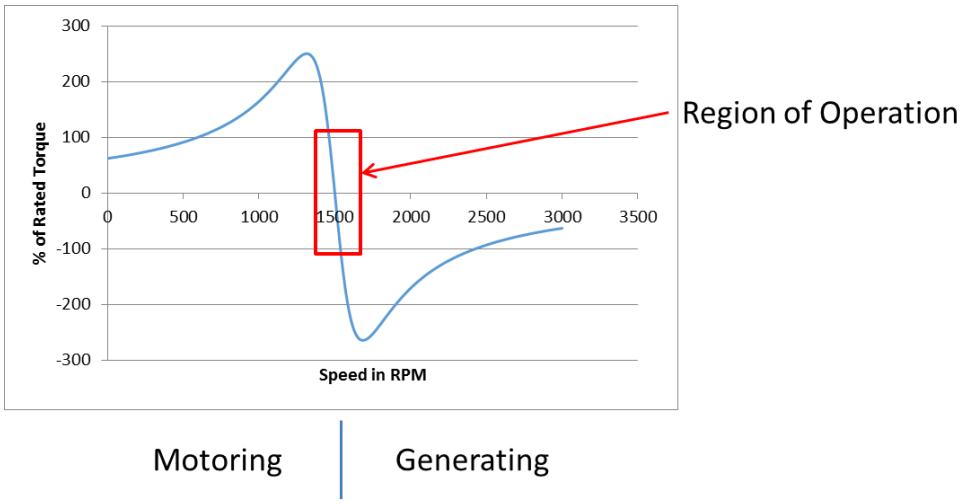

Figure 92 - Scaled Drivetrain Generator Operating Characteristics

The simulation work done by Aachen IFAS, under supervision by Rexroth, was done using a Matlab Simulink drivetrain simulation model. This model was developed by IFAS to generate system operating output data given defined system operating modes and changes of state. The simulation technique was previously validated against the test stand using a 1 MW drivetrain architecture developed for a wind turbine. A representation of this model and the components are shown in **Figure 93**.

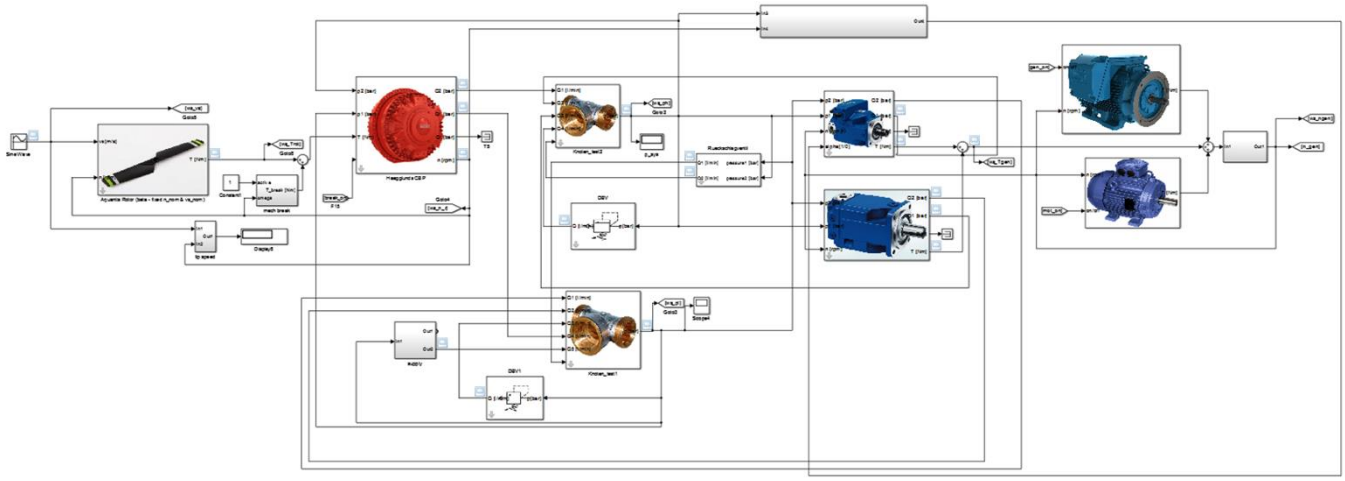

Figure 93 - Scaled Drivetrain Simulation Model

Rexroth and IFAS completed simulation of the hydrostatic drivetrain including varying inflow conditions and basic operating states, fault cases and other transient events. Their work also encompassed determining preliminary reliability and efficiency parameters associated with the system.

The final result of this effort was a comprehensive report providing the simulation model development, the operating conditions simulated, output from the simulation model and efficiency and operational implications. A graphical representation of the analysis process can be seen in **Figure 94**.

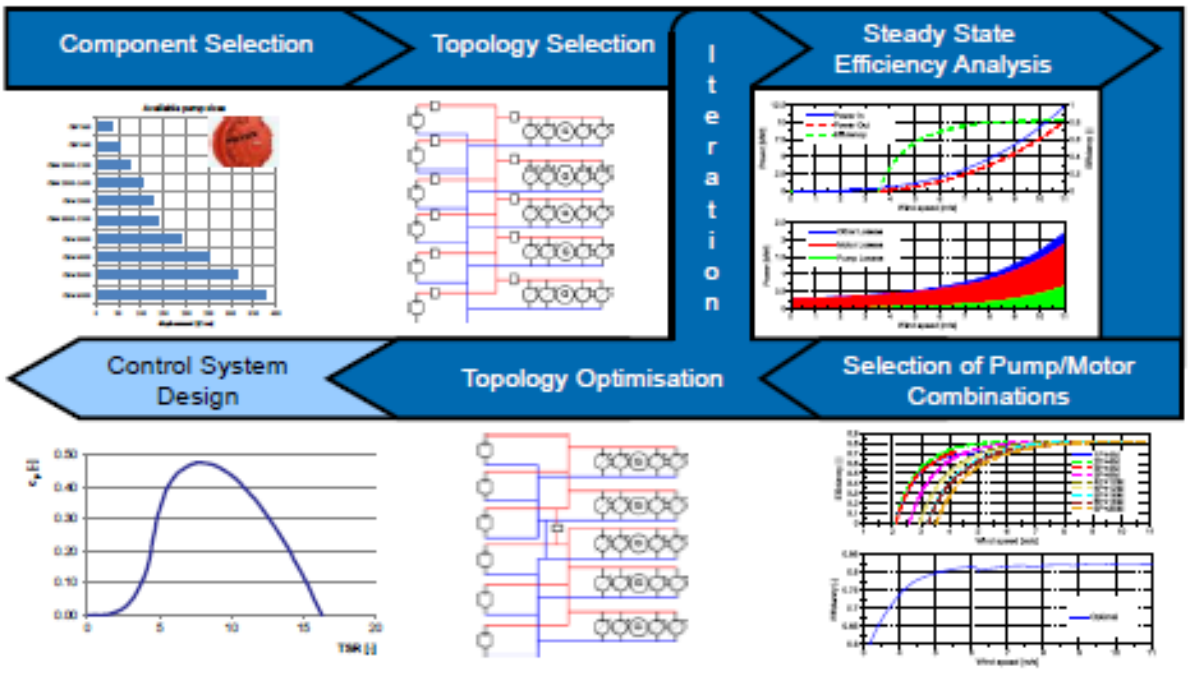

Figure 94 - Scaled Drivetrain Specification and Simulation Process

To aid and evaluate each step in this process, static and dynamic system simulations were used. The generation of three different drivetrain component layouts was conducted. The layouts were reviewed and analyzed based on the overall efficiencies and operating parameters (e.g. high pressure during operation or potential for over speed). One layout was selected for further investigation in a simulation environment. The control strategy was developed, as well as, strategies for start- up, stop and reactions to overload scenarios for the system. These strategies were subsequently tested in a simulation environment. Finally the results of the simulations were derived.

The three different drivetrain layouts are shown in **Figure 95**. All three configurations use the same pump configuration. On the motor side various combinations of fixed and variable displacement units were analyzed. Configuration 1 and 2 use the same total displacement, whereas the ability to vary the displacement is changed. In Configuration 3 the displacement of the smaller motor is increased. This leads to a higher maximally transferable power of this drivetrain. However, the system should be designed for a certain maximum input power and the drivetrains should be compared in regard to how each of them transfers the same amount of energy. So for configuration 3 the swivel angle is limited to make the installed displacement on the motor side equal for all three configurations.

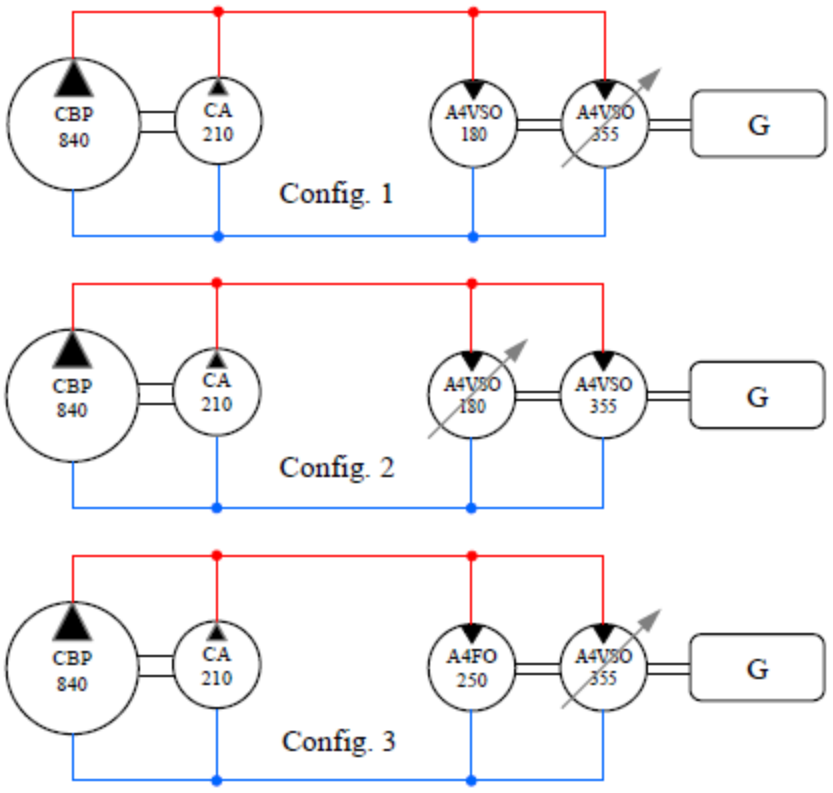

Figure 95 - Scaled Drivetrain Component Configurations

The calculated overall efficiencies are presented in **Figure 96**. As an operating point for each current, the optimal rotor speed, defined by the optimal TSR was chosen. Losses in the variable motors are higher compared to constant units so configuration 2 achieves the highest overall efficiency due to the smallest variable displacement. Accordingly configuration 3 shows the lowest estimates of the overall efficiency due to the higher variable displacement.

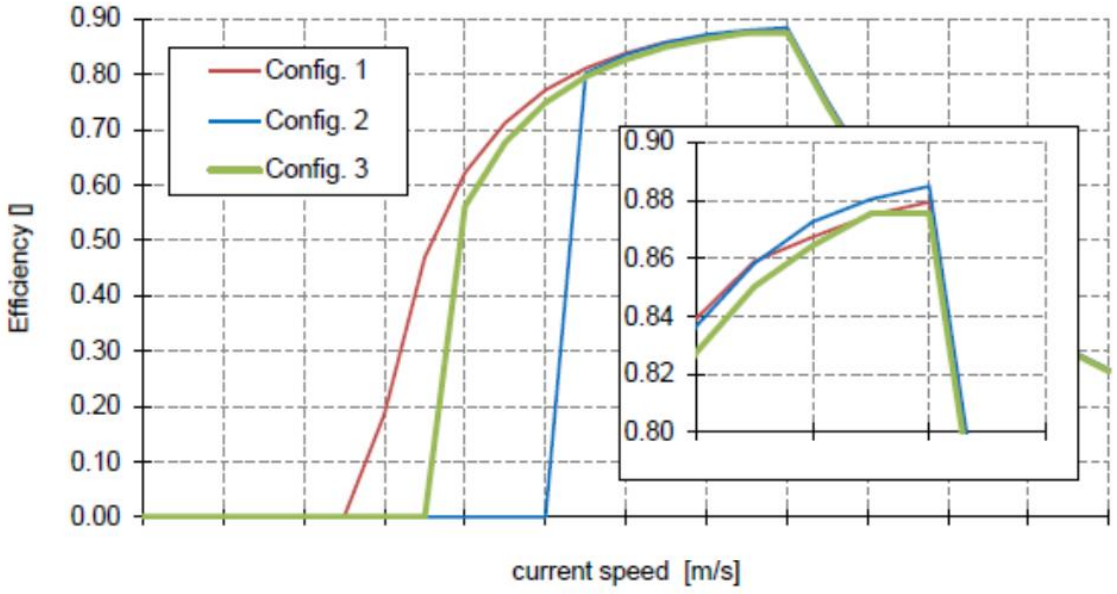

Figure 96 - Scaled Drivetrain Component Configuration Efficiencies

The optimal operating points for all three configurations are depicted in **Figure 97**. Due to the smallest constant displacement, Configuration 1 shows the lowest cut-in-speed about whereas configuration 3 utilizes the highest constant displacement that leads to a cut-in-speed of 1 m/s.

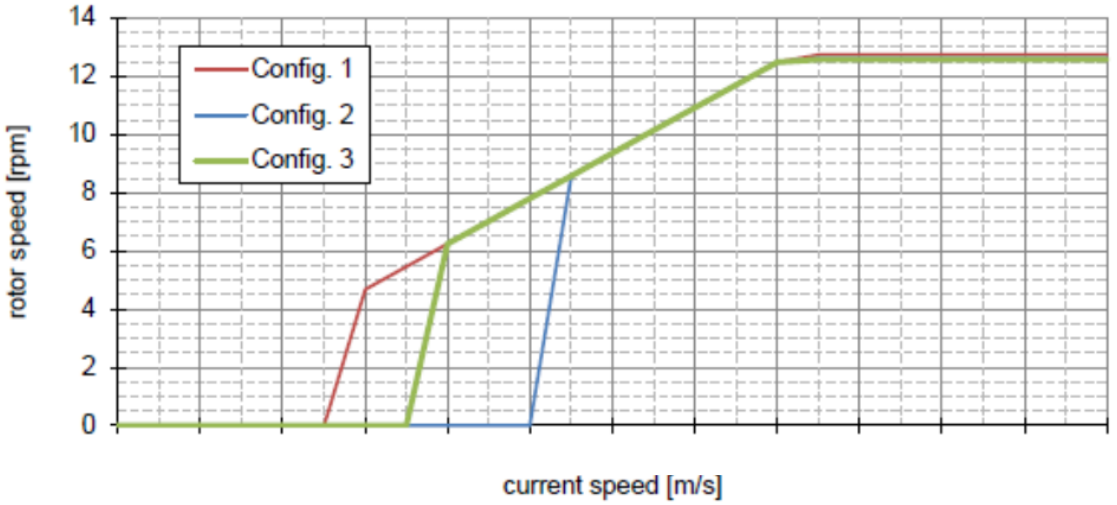

Figure 97 - Scaled Drivetrain Component Configuration Operating Points

The resulting power curves are depicted in **Figure 98**. Due to the smallest variable motor and the resulting losses configuration 2 shows the highest output power at the operating point with the maximum rotor speed and system pressure.

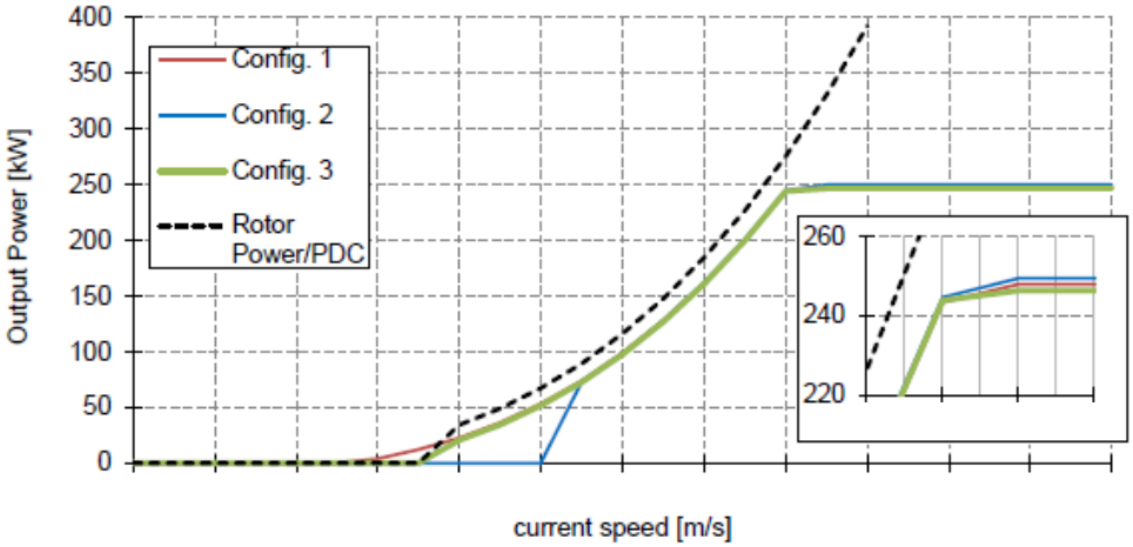

Figure 98 - Scaled Drivetrain Component Configuration Power Curves

For each current speed the corresponding output power and frequency of the current speed were multiplied. In doing so the output power for these operation points was weighted. The different drivetrain layouts were then compared. Finally for each configuration the weighted power values are summed up (**Figure 99**) to get the expected power output per year. At the rated operating point the power output of all three configurations is only slightly different. For lower current speeds configuration 1 shows a considerably higher efficiency (**Figure 99**) that leads to the highest estimated power output. Due to the highest variable displacement configuration 2 achieves the lowest estimate.

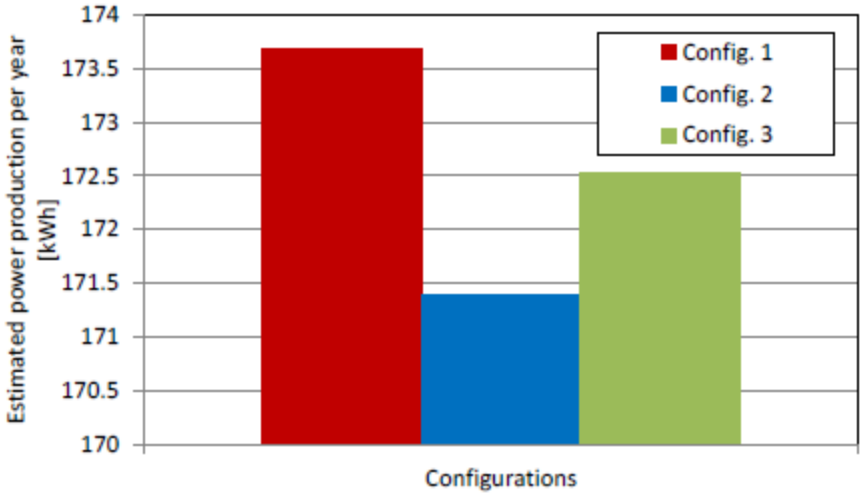

Figure 99 - Scaled Drivetrain Component Configurations Power Output Per Year

The differences in the estimates of the power outputs are comparatively low (maximum is 1 % between configuration 1 and 2), therefore more aspects were included to make a decision for a certain configuration. The drivetrain of configuration 1 reaches its maximum rotor speed at the rated operating point. Due the higher total displacement configuration 3 shows a wider range of possible operating points in the area around the rated operating point to handle overloads. Configuration 1 utilizes a constant motor with a displacement of 180 ccm. Such a displacement is not available within the Rexroth A4FO constant displacement motor series. To implement such a displacement, a variable displacement motor of the pricier A4VSO series must be used. A constant motor with a displacement of 250 ccm is available within the A4FO series. After considering costs and the ability to handle overloads, configuration 3 was chosen for further development within this project.

Control strategies that were investigated included a speed controller, a TSR controller with assessment of the current speed, and a TSR controller without assessment of the current speed (**Figure 100**). Left of the intersection point the rotor will tend to accelerate and right of the intersection point it will decelerate. The control system will drive the rotor to the intersection point, which also corresponds to the optimal rotor speed for the current flow speed. **Figure 100** shows the situation when the current speed increases. The new current speed follows a slightly different bell shaped curve. The previous steady state point *SSP*1 is now in a region of acceleration because the hydrodynamic torque is greater than the brake torque produced by the transmission. The rotor accelerates and moves to the new equilibrium condition *SSP*2. Therefore, it is clear that such a control strategy will ensure operation at the optimal TSR. The distinct advantage of this method is that it requires no input of the current flow speed.

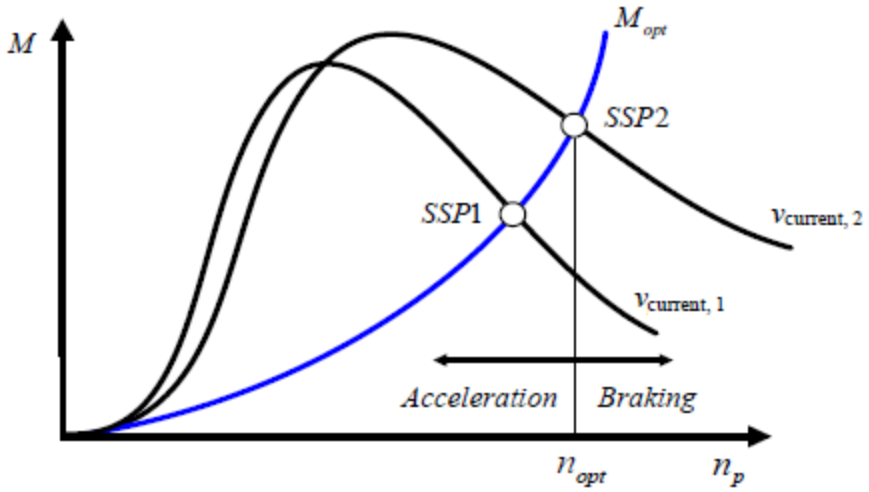

Figure 100 - Scaled Drivetrain Controller Options Speed Curves

The TSR controller without current speed control strategy stabilizes the turbine for each current speed at the optimal rotor speed, where the rotor absorbs the maximum amount of power. As the optimal tip speed ratio remains constant the optimal rotor speed increases proportional with the current and likewise the rotor input power increases. The resulting input power depending on the optimal rotor speeds is plotted in **Figure 101**.

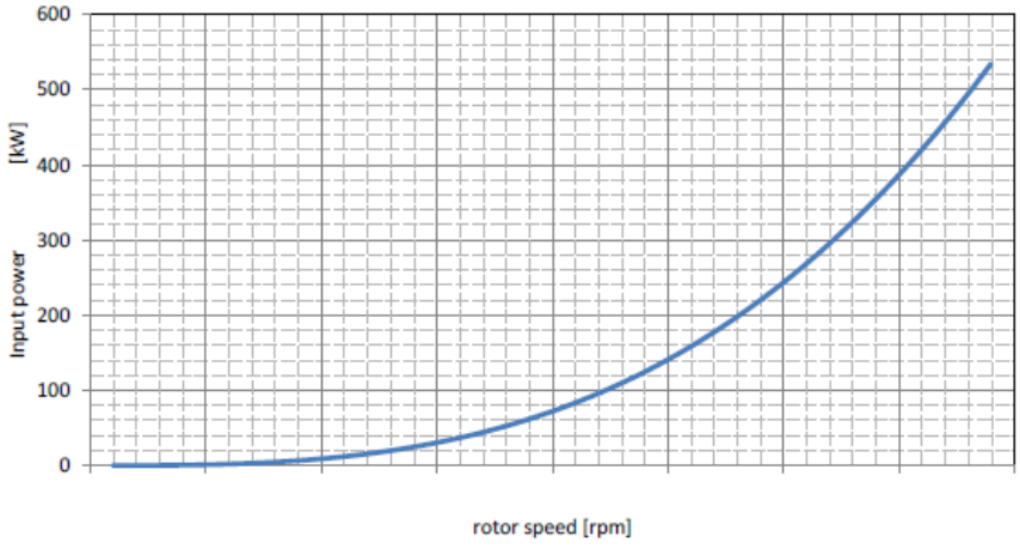

Figure 101 - TSR Controller without Current Speed Input Power and Speed Curve

The allowable input power of the drivetrain is limited to a certain level depending on the components e.g. the pumps, motors and generator. Therefore, a strategy to reduce the input power is needed to operate the turbine in overload scenarios. Most common systems use a pitch system to limit the input power, which is a method to react to overloads quickly by changing the blades' angle of attack. However, the proposed rotor design does not consider a pitch system. Instead "passive depth control" is considered. If the current speed increases above the rated current speed and likewise the input power, the turbine dives deeper in the water due to the increasing hydrodynamic forces. The turbine stops diving when it reaches a lower sea level where the current speed equals the rated current speed. This method of limiting the input power might react slowly to overload scenarios and a second more dynamic power control strategy may be needed.

As the hydrostatic drivetrain is capable of operating at variable rotor speeds, the input power can be limited by shifting the operating point into regions of lower input power. For a given current speed this means slowing down the rotor. But as the rotor speed for the maximum power is not the same as the rotor speed for the maximum rotor torque, slowing down the rotor at first leads to an increase in input torque. This leads to a higher system pressure compared to the desired level during normal operation. This issue can be seen in **Figure 102** where the rotor torque is shown for different current speeds. The maximum input power is assumed to be 275 kW and limited by the capacity of the generator and the electric hardware. The red line marks this limit, below which the input power is less than 275 kW. The optimal points of operation, where the rotor maximizes the input power, are marked by the green line. Under normal conditions the turbine is operated along this line ('Desired Control Curve II') by the proposed torque/pressure control, which means that for a given rotor speed the corresponding optimal braking toque is applied to the rotor shaft. Above the intersection of the green and red lines this control strategy would lead to operating points with an input power higher than the chosen limit of 275 kW. Therefore, the control strategy is changed and the turbine is operated along the red line controlling the input power. At the same time the 'passive depth control' should start working and the turbine should start diving deeper into sea, which leads to a decrease in the current speed. While the system dives the turbine is operated along the red line moving the operating point back towards the intersection. At the sea depth where the rated current speed is applied to the rotor, the input power is below the power limit and the control strategy switches back to the torque/pressure control along the green line.

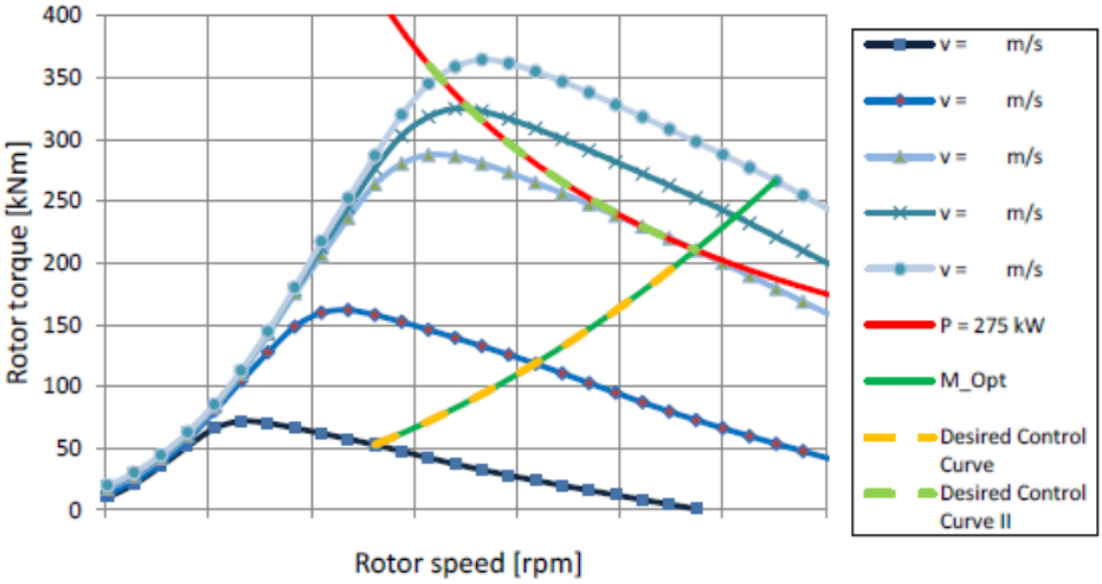

Figure 102 - Controller Options Torque and Speed Curves and Flow Speeds

For low rotational speeds the torque coefficient of the rotor (**Figure 103**) becomes very small or near zero. Consequently for a whole spectrum of low rotational speeds (resulting in a small TSR) the input torque remains too small to overcome the mechanical losses in the drivetrain e.g. rotor seal friction or mechanical losses in the pumps and motors. To overcome this issue the rotor needs to be sped up into regions of higher rotational speed (likewise regions of higher TSR) leading to higher torque coefficients and resulting in higher rotor torques. Once this region of small rotor speeds is passed, the generated input torque is sufficient to speed up the rotor itself. Therefore, a mechanism is needed that applies the necessary start up torque to overcome the losses during the initial startup phase until the rotor speeds up itself.

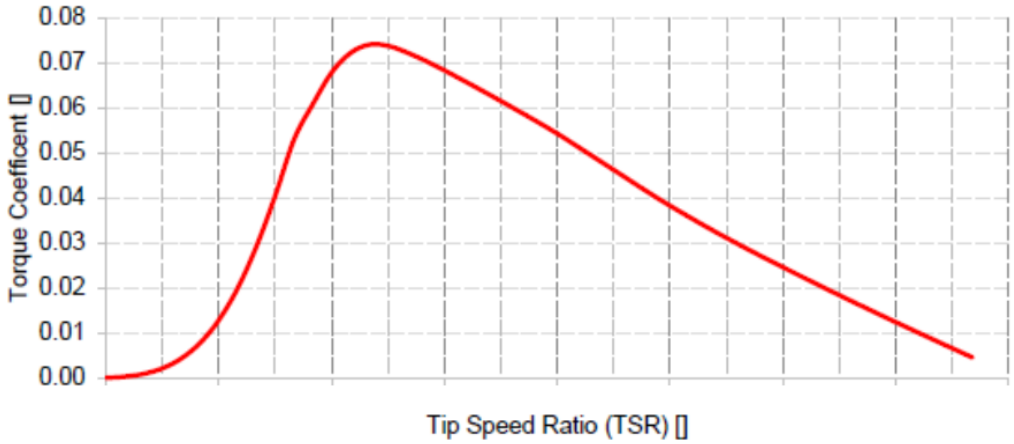

Figure 103 - Rotor Torque Coefficients

For the stop procedure of the turbine, two strategies are proposed that use the hydrostatic drivetrain to slow down the turbine and finally a mechanical brake to lock the rotor. The first strategy uses the pressure controller to generate the hydraulic braking torque whereas the second strategy uses the main pressure relief valve on the high pressure side.

The different control algorithms are shown in **Figure 104** including operation modes and when they are applied during operation. The initial state for the system is called "Standby". The system is not operating, the mechanical brake is locked and the generator is turned off. When the system's start-up is initiated ("Start-up" mode), one of the presented start-up strategies is performed. During start-up a control algorithm speeds up the rotor and generator. When the high pressure finally equals the optimal pressure, the control algorithm switches to a "pressure controller") and the turbine is operated under normal conditions ("Normal operation"). If the power at the generator shaft rises above 250 kW (regarded as an overload scenario here), the control algorithm switches to a "power controller" to limit the input power at the rotor ("Overload Operation" mode). Since the current speed is not measured, it cannot be detected, when the current speed has slowed down and the overload scenario ends. This issue is solved by comparing the pressures which are set by power controller and pressure controller. If the values are the same, the overload situation must have ended and the turbine can be operated under normal conditions again by the pressure controller ("Normal Operation" mode). The stop procedure of the turbine can be initiated regardless of the present operating point. To stop the turbine two procedures have been presented, which slow down the rotor and disconnect the generator from the grid. When the rotor speed is close to zero rpm the mechanical brake is locked and the system returns to the "Standby-mode".

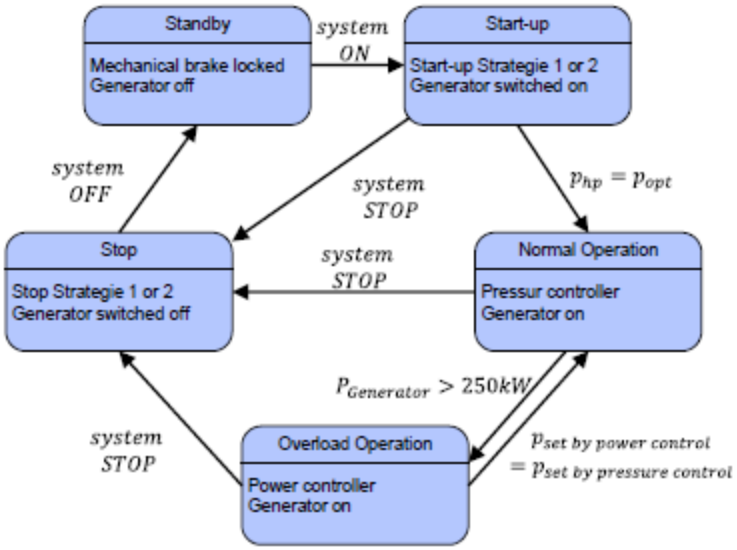

Figure 104 - Control Algorithms and Operation Modes

To operate a hydrostatic drivetrain system independently in the ocean for a long time additional components are required for different reasons. These are further safety installations (e.g. pressure relief valves or check valves), manifolds to collect or separate the oil flows, accumulators, additional (safety) valves, heat exchangers, boost pumps and oil filters.
Modeling of the basic components of a HDT was undertaken in the simulation software MatLab/Simulink/Stateflow. A one dimensional simulation considering the volumetric instead of the mass flow was carried out, a simplification often used in simulation of hydrostatic drivetrains. Finally a model of the whole drivetrain was set up including a dynamic model of the turbine, the hydrostatic drivetrain and a simple model of the generator. A control system for operation during the startup phase, standard operation, overload conditions and shut down was set up as well.

To set up the models the well-known equations for the components and measurement data of the losses in the pumps and motors are used. The data was measured using the hydrostatic test bench at IFAS. As the components used within this project are the same as the pumps and motors installed on the test bench, the data was applicable here. In case the displacement of a needed component differs to that component used for measurement, the loss data was linearly scaled up or down using the displacement as a scaling factor.

For the simulation of the drivetrain a simplified model was used and only necessary components for the startup, stop and normal operation phase were considered. A sketch of the system and the components considered is depicted in **Figure 105** and the basic model used within the simulations represents these components.

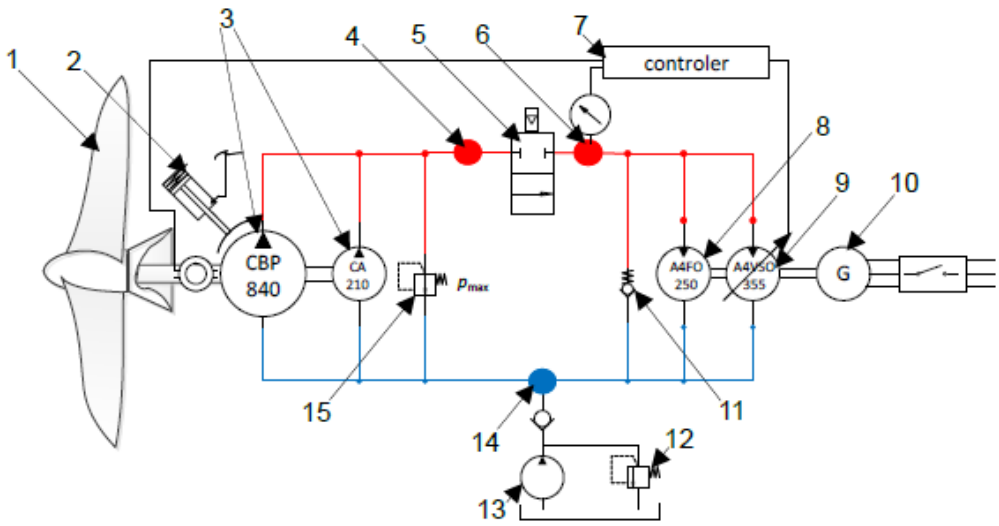

Figure 105 - Scaled Drivetrain Major Hydraulic Components

An efficiency map of the drivetrain is shown in **Figure 106** considering all hydraulic components. The efficiency is calculated by dividing the output power at the generator shaft by the input power acting on the rotor shaft. The efficiencies of the rotor and the generator are excluded. At high current speeds the pressure relief valve of the high pressure side opens and a certain amount of energy is lost resulting in a low efficiency (see blue marked area in the following figure). For the rated operating point n = Rated RPM and v = Rated m/s a maximum efficiency of 0.87 is reached. The power needed to operate all components of the periphery e.g. boost pumps is not considered. So the overall efficiency of an actual drivetrain will be lower (approximately 2 %).

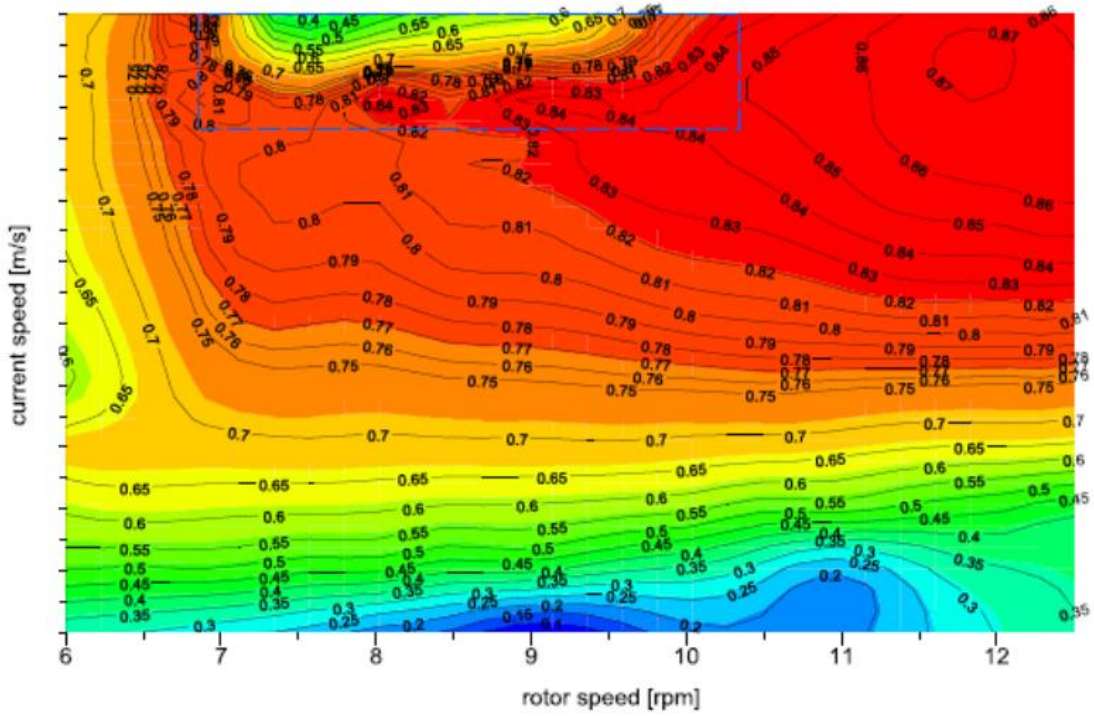

Figure 106 - Efficiency Map with All Hydraulic Components

Simulated operating environments using the simulation model included startup of the rotor with the grid, start up with the grid in an overload scenario, start up without the grid, an operating overload scenario and an over speed condition. In the previously discussed control scenario the input power was reduced by slowing down the rotor, which in turn led to a higher input torque and a system pressure in unwanted regions. Another option is to over speed the rotor. From **Figure 103** it can be seen that very high tip speed ratio results in a low power coefficient and consequently a lower input power. The maximum rotor speed is defined by the installed motor displacement. To operate the rotor at higher speeds the motor displacement must be increased. The minimum rotor speed is given by the related generator speed and the constant motor's displacement. As this parameter shall remain unchanged only the displacement of the variable motor is increased up to 500 ccm^3. This modification also affects the efficiency of the drivetrain resulting in an approximately 1% drop in peak efficiency.

The variable displacement motor has a poorer efficiency for low swivel angles. Due to the greater displacement, the variable motor is operated at lower swivel angles compared to the standard layout used within this project. This leads to a lower overall efficiency of this modified drivetrain compared to the standard layout and a mean loss in efficiency of about one percent. The results of the simulation are presented in **Figure 107**. The current speed is increased above rated speed resulting in an overload situation, an input power on the generator shaft greater than 250 kW and a high pressure of 240 bar. After 40 seconds the rotor is sped up leading to a reduction of the input power and the high pressure as well. Compared to the overload strategy both the generator power

and the high pressure are moved into desired areas, which is the main advantage of this strategy. However, the maximum rotor speed is still limited by the total motor displacement and so this strategy remains applicable only up to a certain current speed. Disadvantages are a lower overall efficiency and the costs for a variable motor with larger displacement.

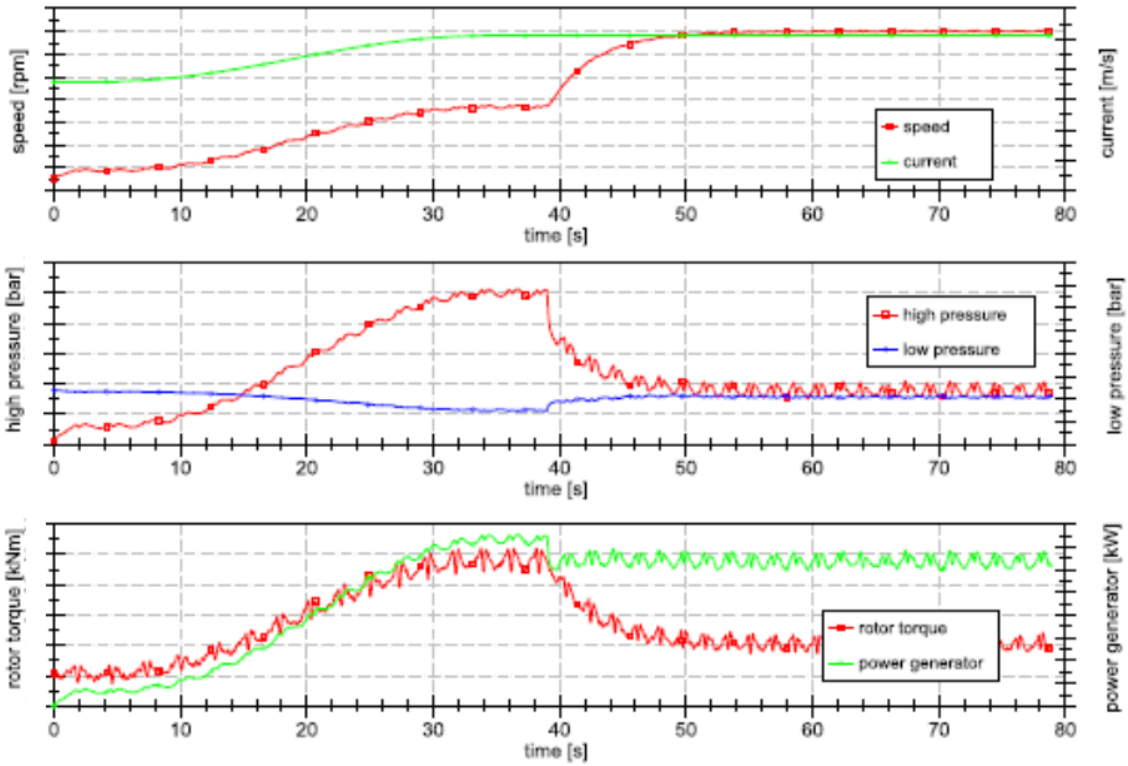

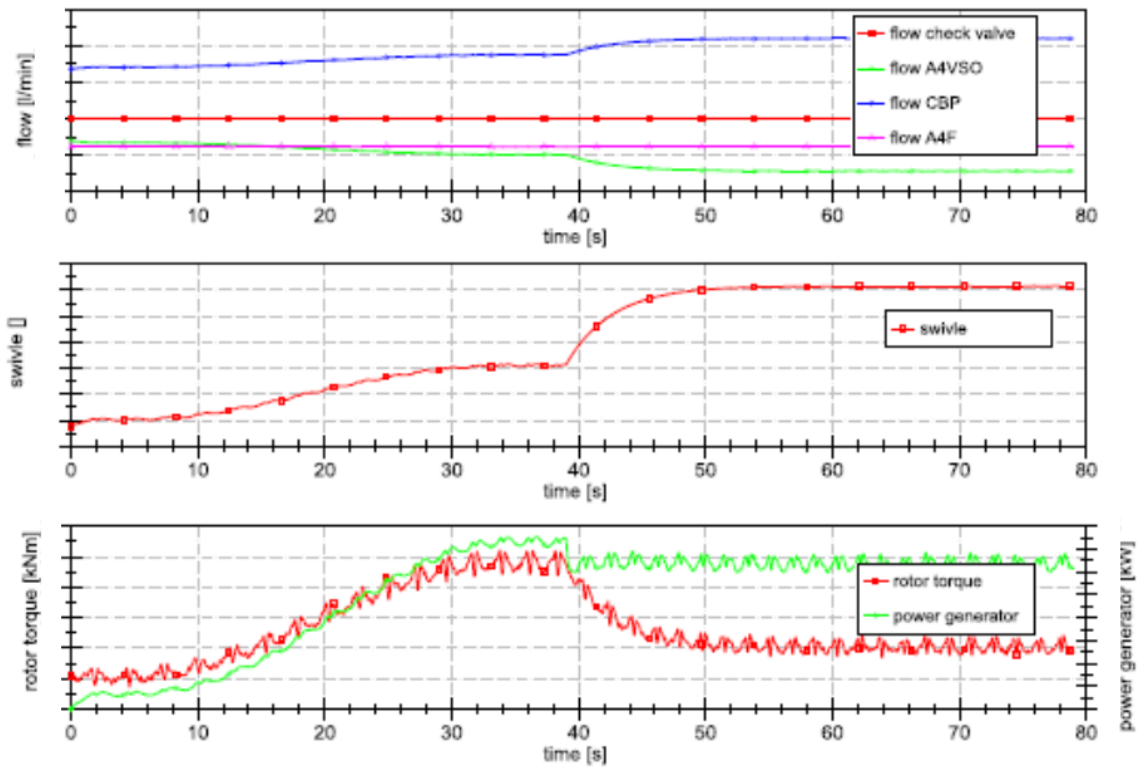

Figure 107 - Efficiency Simulation Results

Stopping procedures simulated in the model included: braking torque applied by the motors and braking torque applied by the pressure relief valve. In summary, both stopping procedures can be applied to the drivetrain in different situations. The motor strategy can change the system pressure dynamically and maintain a pressure that is sufficient for the present current speed leading to a smoother and less stressful deceleration process. However, in the pressure relief valve strategy to stop the drivetrain only the main valve needs to be closed and the generator is disconnected from the grid. This strategy can be applied in emergency situations as well. If the valve is kept open by the control system and closes otherwise, this stop procedure is the default state and is initialized either by the control system itself or when the control system breaks down. Therefore depending on the circumstances, one of the strategies should be applied, especially because the drivetrain layout does not have to be changed to run one of the two strategies and the needed hydraulic components are the same. Both strategies only differ in the control effort.

In **Figure 108** the simulation of a load cycle is shown. At first the turbine is sped up from cut in current speed. The rotor and the current accelerate and the control system operates the turbine along the proposed optimal control curve. After 55 seconds the current speed increases further resulting in an over-load situation. The control system reacts by controlling input power of the rotor and decelerates the turbine. Then the current speed decreases again and the overload scenario ends. The control system switches back to the pressure controller (around 95 seconds) and operates the turbine at the optimal TSR again. Finally a stop procedure is initialized.

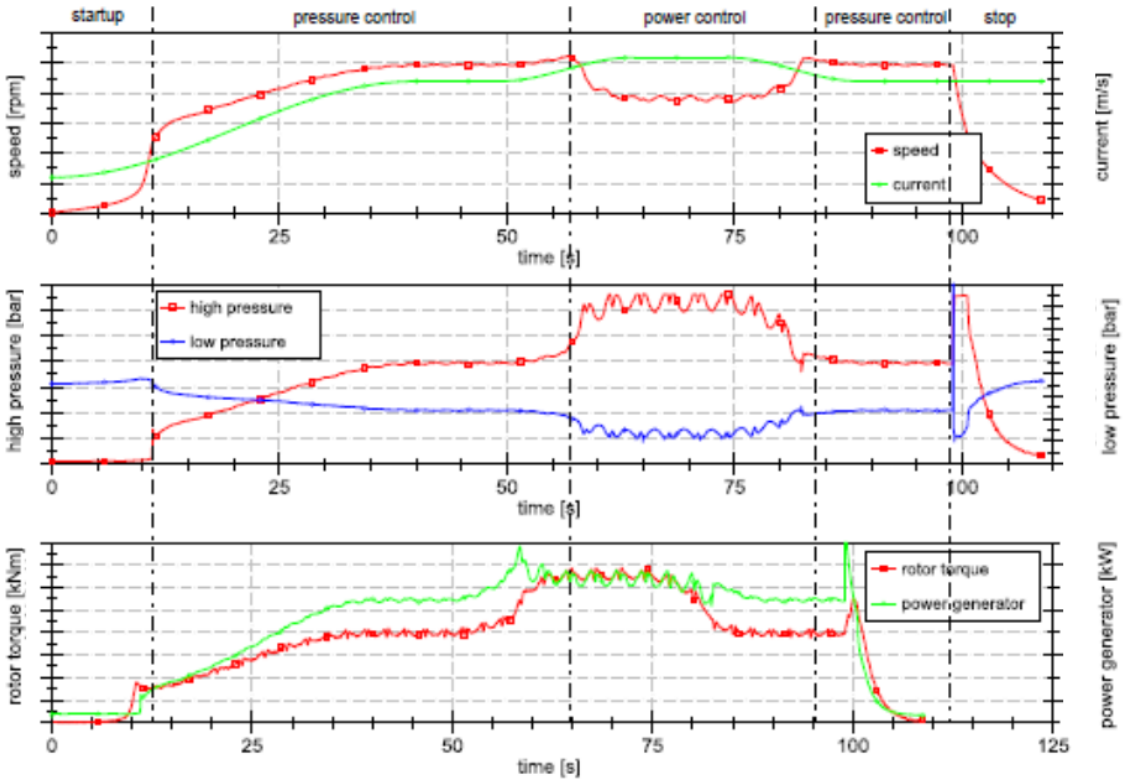

Figure 108 - Load Cycle Simulation Results

The analysis of the proposed drivetrain has so far been conducted using only simulations. To undertake further steps or to design a prototype the simulations need to be validated on a test bench. At IFAS a test bench for a 1 MW wind turbine drivetrain was developed and proven successfully. This test bench can be used for the necessary validations. Because the test bench was designed for higher input power the generator side needs to be modified to meet the requirements of this project e.g. the proposed motors, generator and the total output power.

The design of a HDT for a marine current power system with an electric output power of 250 kW was done for a specific location. Three different configurations of hydraulic pumps and motors were generated. After a first evaluation only one layout was chosen for further investigation.

An analysis of the selected configuration of the HDT was done by setting up a model of the system in Matlab/Simulink. The required data concerning the turbine and the generator was defined by DA. Data about the hydraulic components was supplied by IFAS. Different strategies for the startup, the stop and to react to overloads were developed and simulated. It was shown that the HDT is able to run well over its whole operating area and thus meets all requirements.

Another output of the simulation program was a complete bill of materials (BOM) outlining all the components required to achieve the functionality of the simulation drivetrain. The detailed

BOM listed all sensors valves pumps motors etc. and contains over 100 individuail items. In additon to the BOM the following hydraulic schematic (**Figure 109**) was also provided.

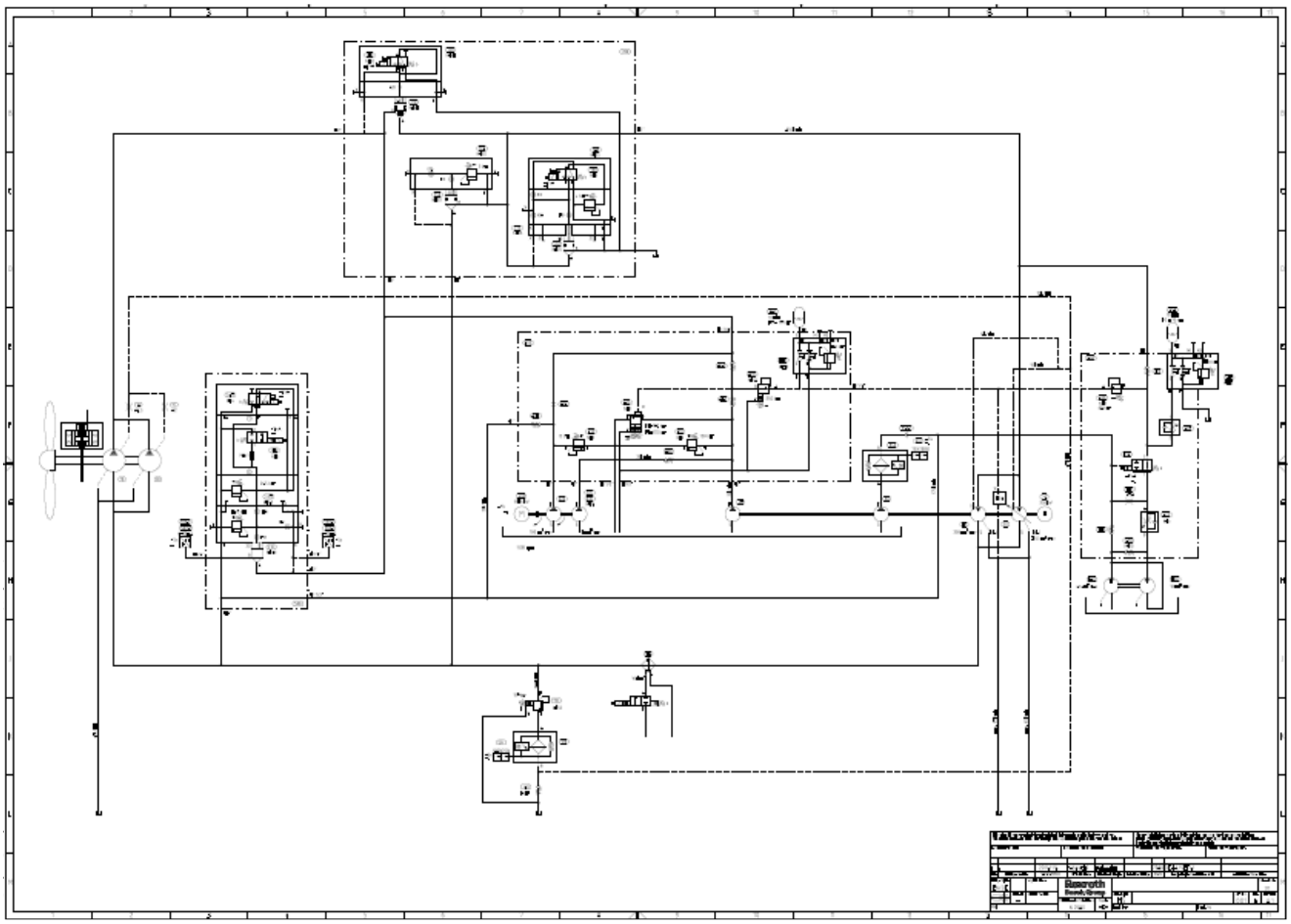

Figure 109 - Full Scale Drivetrain Hydraulic Schematic

Finally Rexroth provided a quotation for a 500 kW prototype drivetrain similar in architecture to the 250 kW test unit. The cost of a single prototype drivetrain was estimated with a production level cost reduction estimated at 35%. The quotation did not give detailed line items but the cost breakdown was given in the following cost categories:

- Hägglunds Pumps - 45% of total
- Torque Arm - 5% of total
- HPU / Manifolds / Skid / Piping - 35% of total
- Hydraulic Motors - 10% of total
- Controls / Motor Starter - 5% of total

This pricing information is useful for validating cost models and production cost of energy (COE) calculations.

Separate from the simulation and test program Rexroth was also tasked with design life estimation of the hydrostatic drivetrain. Using the flow histogram from the Gulf Stream resource and the drivetrain pump configuration the torque and pressure duty cycle can be evaluated for various pump arrangement. Rexroth evaluated its CBM 6000 pumps vs. the Aquantis C-plane duty cycle and found the life to be approximately 5 years. The result details can be seen **Figure 110**. This rather short rated life is a concern for the Aquantis device as the device has a design life of 20 years.

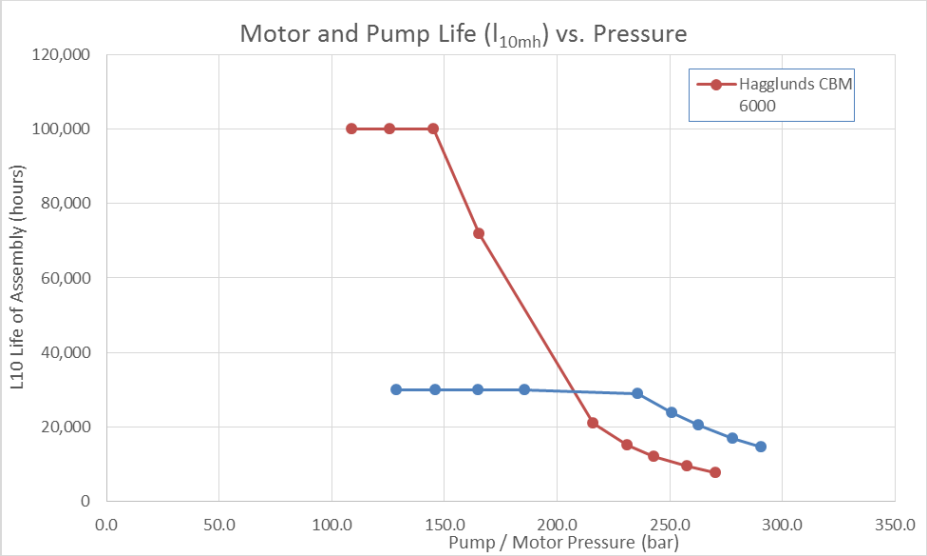

Figure 110 - Motor and Pump Life Estimate

The steep drop in calculated life at increasing pressure is due to a loss of oil film in the cam ring and roller interface. Increasing pump life is achievable through increasing the oil film thickness in the contact region. This oil film is dependent on surface velocity, pressure and oil viscosity. The C-Plane configuration input speed is fixed via the rotor diameter and increasing speed is not an option. Low speed operation is considered to be lower than 10 RPM so for most part, potential C-Plane designs operation will be in a very low speed regime. Therefore the easiest way to increase life is to reduce pump pressure, however decreasing pump pressure requires increasing pump size or reducing power rating. Additionally, increasing oil viscosity can help maintain oil film especially at low speed. Two ways to increase viscosity are to increase the bulk viscosity of the oil or reduce the temperature of the oil in the contact region. To reduce the viscosity of the oil in the contact region Hagglunds recommends using a flushing procedure that sends the cool oil directly from the cooler through the case. It was estimated this cooling loop would require ~ 4-5 gallons per minute flow rate. The drawback of increased viscosity is a 1-2% drop in efficiency mainly from the high speed motors.

The life calculations are L10mh calculations done using a common standard, ISO 281 “Rolling bearings -- Dynamic load ratings and rating life.” The quoted L10 mh values include modification factors that are multipliers of the standard life as calculated by the standard. The modification factors take into account better load distribution, material, lubrication, surface finish and other factors than assumed in the standard.

In addition to the low speed pumps, Rexroth also calculated the life of the high speed motors. However the motor life calculation only yields the life of the rolling element input shaft bearings and has a maximum calculable life of 30,000 hrs. There are advanced calculation methods that can better predict system life however they are difficult to implement and have not been performed.

As an alternative, the rolling element bearings can be replaced with fluid film or journal bearings which have infinite fatigue life. However fluid film bearings are an order of magnitude less efficient than rolling bearings. It is generally thought that the motors can easily achieve a 5 year design life.

In addition to the pumps and motors the life impact of the ancillary components (small pumps, valves, switches, etc.) as outlined in the hydrostatic drivetrain bill of materials must be taken into account. Given the system and ancillary component life it is clear that the hydrostatic drivetrain system would be significantly challenged to meet the original goal of a five year service interval.

Given the goal of producing hundreds of C-planes per year it is an important consideration that the major components of the device have a robust supply chain. After discussions with Rexroth and Hagglunds it became clear that the large input pumps would be the constraining item for production capacity. Hagglunds is the only manufacturer in the world for pumps of this size and they produce under 10,000 pumps per year and only a handful of CBM 6000's per year. A survey of other manufacturers reveals that while there are other suppliers there are none that have the size of the Hagglunds CBM 6000 unit. The largest size of competitors is less than half of the CBM 6000. Therefore creating a drivetrain design that does not have a single source of supply would significantly reduce the maximum size rating of a C-Plane device.

Using the information gathered through the development and analysis described in the preceding sections the proposed hydrostatic drivetrain was evaluated against a convention gearbox and generator approach.

Efficiency has long been known as the Achilles heel of hydraulic systems and while significant improvements have been made recently the peak efficiency calculated through analysis and validated by testing was shown to be approximately 81% for the hydrostatic system and slip induction generator. Alternatively, a modern wind turbine gearbox, permanent magnet generator and full power conversion with a peak of 92%. When compared across the operating range the off peak efficiency of the HST drops of substantially while the geared system stays relatively flat (**Figure 111**). The net result is for a given rotor diameter the HST system produces much less usable energy than a gearbox system. To produce an equivalent amount of power the HST requires a 6% larger rotor, which adds cost and loads (estimated at 14%) to the system.

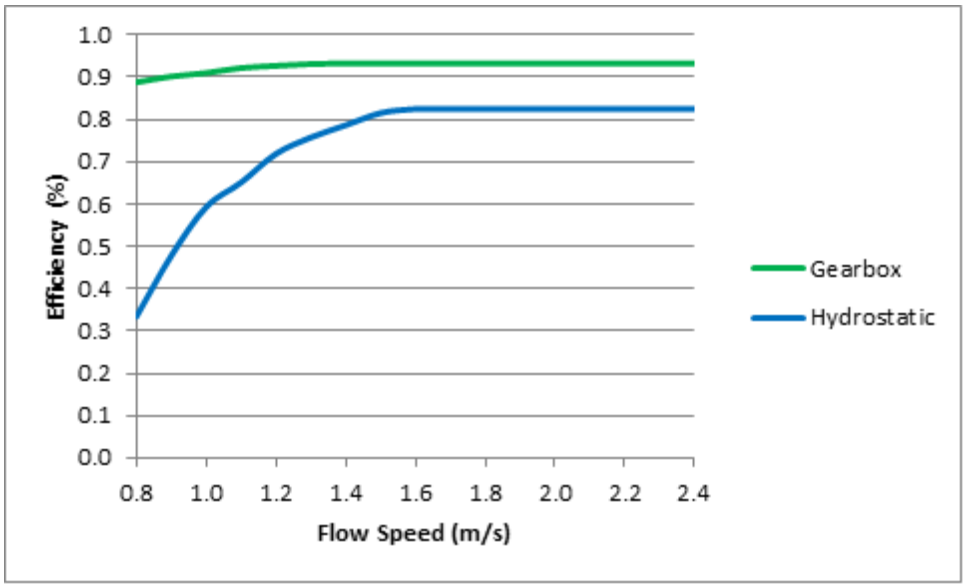

Figure 111 - Drivetrain Efficiency Comparison - Hydrostatic vs. Gearbox

System cost is another concern for renewable energy devices. Aquantis investigated the cost of the full drivetrain system for the hydrostatic and the gearbox solutions and concluded that the HST is 74% more expensive than the gearbox and power conversion topology. This is on top of the additional blade and structure costs to make up for the reduced efficiency.

System life and reliability was supposed to be the key metric that justified the additional cost and reduced efficiency of the HST. However upon further review of the system life calculations, the relatively high pressures at the operating conditions significantly reduced the life of the large pumps in the hydraulic drivetrain. Even in the best case scenario the L10 life of the pumps was approximately 10 years, requiring a mid-lifecycle replacement to achieve a 20 year design life. In comparison wind turbine gearboxes are routinely rated to 20+ yr. design life.

Design life is only part of the story, reliability and failures also account for a major portion of operations and maintenance expense. This is much harder to predict but given the complexity of the HST with multiple motors, valves, solenoids, sensors, etc. the system failures are expected to be a concern.

Robust supply is also a key parameter for the Aquantis device. Commercial COE predictions require large arrays to amortize the cost of vessels, grid connections, substations etc. Therefore many hundreds of drivetrains will be required to fulfill production demand. The production capacity of the main pump in the HST is single sourced and severely constrained as discussed above. Significant investment by the pump manufacturer would be required to meet the Aquantis demand. Alternatively wind turbine gearboxes of the MW scale are being produced by the thousands every year. Supply constraint is not anticipated to be a problem for a gearbox topology.

Drivetrain Design Conclusions:

- HST components can achieve L10 of 5-10 years with reduced pressure and optimized lubricants.
    - Significant system size, cost and efficiency impacts.
    - Large power ratings (>1MW) are limited
- Efficiency of pump systems is 10% lower than a comparable gearbox.
    - Larger rotor or reduced AEP
- Cost of hydraulic system is 74% higher than a current and comparable gearbox system.
- Large Hagglunds pumps are single sourced and have a limited production.

After significant review, the relatively low efficiency, high cost, design life and constrained supply chain have lead DA away from the hydrostatic drivetrain and towards more conventional geared solutions.

The expected advantages of the hydrostatic drivetrain did not materialize to be as great as expected when compared to a conventional gearbox and permanent magnet generator. The significantly lower efficiency forces much larger rotor blades to produce a given amount of power. The calculated life estimates of the pump were also much lower than expected when running at operating pressures. Finally the initial capital cost of the drivetrain was significantly more than a convention drivetrain solution.

The gearbox solution appears to be a more cost effective approach to convert the kinetic energy of the resource to electrical energy. In addition, leveraging previously developed wind turbine technology will significantly shorten the drivetrain development process and the Aquantis commercialization path. Aquantis envisions using a gearbox developed for a common 1.5 MW wind turbine as this is already being produced in high volumes and proven in the industry.

Task 3: Marine Composite Material Testing

This section covers the Statement of Project Objectives (SOPO) tasks 3.1 Spar Testing (with and without joints), 3.2 Pass-through-Spar-to-Hub Attachment, 3.3 Skin-to-Spar Attachment and 3.4 Identification of Critical Failure Modes.

DA has found that through various suppliers of composite materials and independent and academic test facilities there exists sufficient data on mechanical performance of marine composite material to allow for blade design to go forward with detailed testing to follow once the blade design has matured to a point where material systems can be identified with enough certainty to warrant a lengthy test program. As an alternative in the rotor development area DA has begun scoping the efforts required to conduct a MHK hydrofoil design and testing program. DA has also engaged with an industrial rotor designer and manufacturer for guidance on design of the C-Plane rotor.

DA continued efforts to work with manufacturers on suitable materials supply and manufacturability for the full scale rotor blades. It is planned that the rotor design will follow the following process (**Figure 112**):

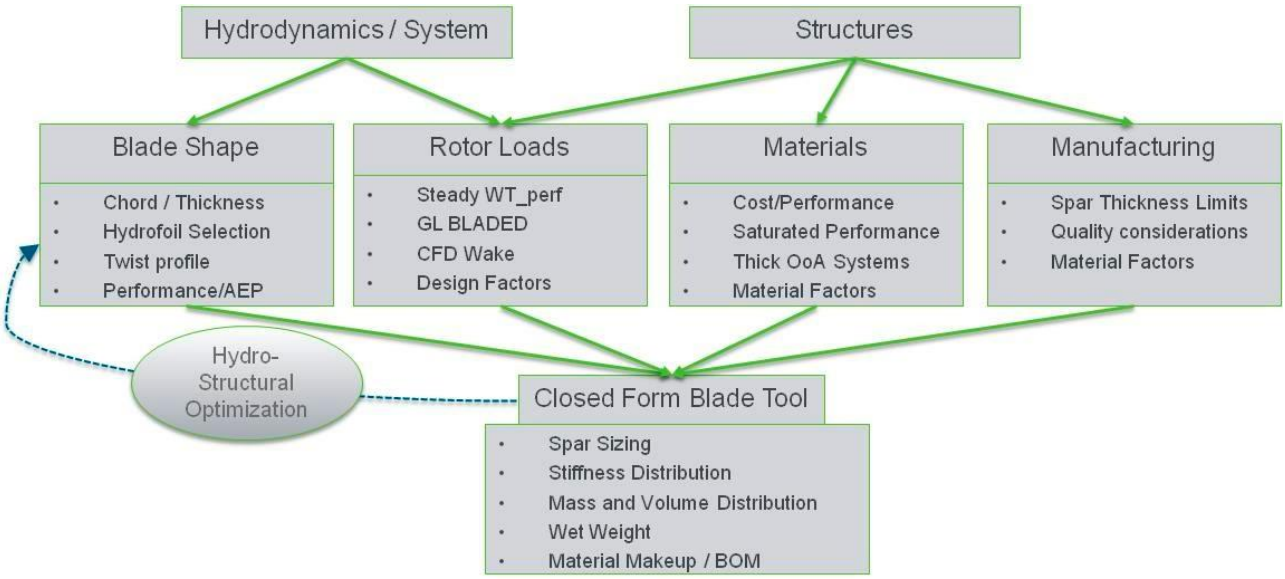

Figure 112 - Rotor Design Process

To investigate the impact of blade count, a parametric design study was conducted. This study assumed that for a two bladed rotor and a three bladed rotor the following parameters were equal when both rotors are designed for ideal axial induction: diameter, airfoil distribution, tip speed ratio, and solidity.

Using these design guidelines, a beam model was used to study the relationship of buoyancy and spar cap thickness to airfoil thickness for both the 2-bladed and 3-bladed rotors. A simplified blade structure was calculated for the 2-bladed and 3-bladed rotor blades at 30 stations along the blade span. This calculation routine took into account the spar width (linearly tapering and sized to fit the blade planform), blade thickness and flap-wise sectional bending moments. A spar thickness was calculated to provide sufficient strength to each section. A manufacturing limit of 6cm maximum thickness on the sparcap was imposed, and if a section could not converge with this spar thickness, the overall thickness of the blade was increased until the constraint was met. The 2-bladed design is able to achieve the desired T/C distribution for most of the span while the 3-bladed design requires increased blade thickness.

A second study evaluated wet weight and spar thickness at various sectional blade thicknesses for a given sectional moment load (near mid-span) by simplifying the blade sections into sandwich beams and performing a similar spar sizing study. This work found that for the given station, a three-bladed rotor would require increased thickness and/or provide a lower wet-weight.

To finalize this trade-off, DA needed to determine the relationship of hub mass to blade count, and the impact on fatigue loads and platform mass in the context of the wake strength from the upstream structure.

Using the 2-bladed configuration, a hydrodynamic design study was conducted to identify the largest feasible rotor diameter which would meet both the operational and braking torque constraints of the hydraulic drive system.

A preliminary structural analysis was conducted of the rotor blade using the aforementioned beam model after tuning it to finite element analysis results of previous blade designs. This study indicated the blade length has a good probability of being structurally feasible while still achieving high hydrodynamic efficiency.

In an ongoing effort to design and characterize "thick" MHK hydrofoil designs, DA and consultant partners have completed further analysis and design to optimize hydrofoils for high Reynolds number, fixed pitch operation and also benchmarked them against existing designs.

Given new information on hydrofoil sections and their performance DA re-focused on the structural blade design and attachment and contracted with leading large industrial company specializing in industrial MHK rotor design and manufacturing. This manufacturer is also a large supplier of composite materials with many years' experience in the marine composite sector. Preliminary structural analysis work can be seen in **Figure 113**.

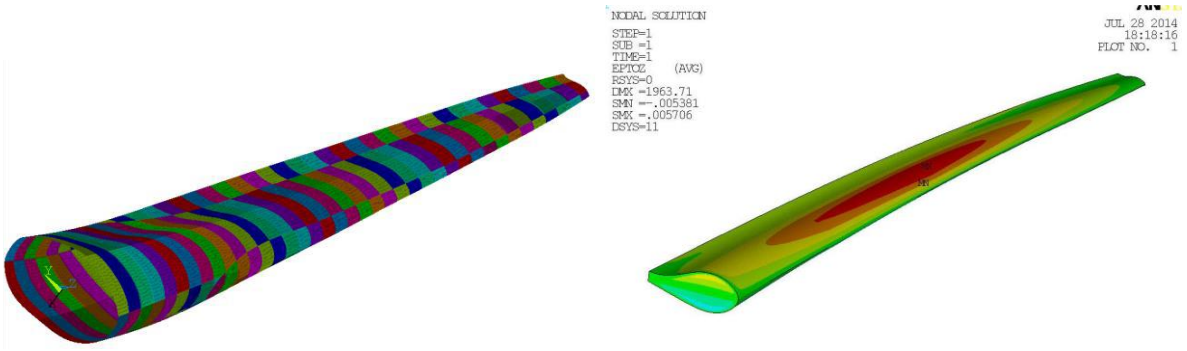

Figure 113 - Rotor Structural Analysis Preliminary Results

DA completed a preliminary review and analysis on a conventional MHK rotor blade at a diameter of 40.9m. Their study and analysis addresses the structural sizing of a composite blade for the C-Plane device. The key aim of this stage of the study was to establish an acceptable structural envelope for the blade given the supplied loads and initial blade geometry.

The study considered the structural design of the outboard part of the blade and also a bolted root connection to allow the blade to be connected to an interface at the blade root. The design was developed using a combination of composite materials expertise, bespoke blade design tools and experience of designing and building a variety of blades and rotors for sub-sea turbines.

The bulk of the blade length was sized using an in-house blade design program (BDP) which simulates the geometric and structural configuration of the blade and calculates static deflections and blade strains for a given loading case. Laminates can be optimized for all components of the blade to achieve required deflections or blade strains for a given load case.

The metal bolting for attaching the blade to the turbine and the composite blade root in the vicinity of the bolting were analyzed using spreadsheets developed based on bolt group theory and VDI 2230. Inputs to the calculations were taken from the relevant standards, or where not available, were taken from similar blade analyses previously undertaken.

The combination of blade geometry and Ultimate Limit State (ULS) loads were found to be unfeasible due to insufficient section depth in the blades to resist the applied bending moments.

A blade part cost was estimated, although this is being treated as a preliminary estimate and with optimization there is scope to reduce this.

The blade geometry was built with parametric box beam shape based on the blade shell. The divided geometry was imported to ANSYS and various properties were defined. The blade lay-up was driven by an Excel spreadsheet analysis tool which allowed very quick updates. Analysis results can be seen in **Figure 114**.

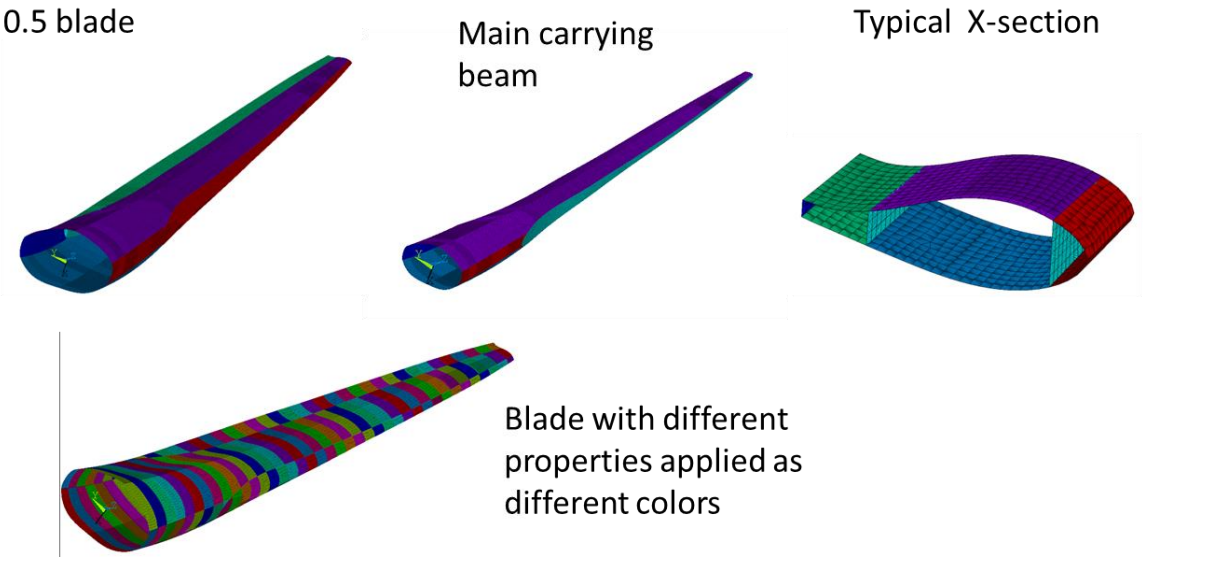

Figure 114 - Revised Blade Structure Analysis Results

Blade preliminary design results indicate the strain levels in the blade outboard of ~6m cannot be brought to the acceptable level. As an additional check, a 100% UD carbon composite (complete airfoil) part outboard of 7m was modeled. This indicated that the blade geometry and loads combination leads to an unsolvable design (within reasonable cost) and a new blade geometry is necessary (less slender -> shorter and more chord / thicker).

Task 4: Platform Design

Platform design has mainly been focused on the full scale system with respect to the impacts on the tow tank testing program and the design of the model for this program.

Platform design activities focused on that required for the scaled and full scale connecting structure between the nacelles. These designs were applied to the tow tank test program.

Platform design activities have continued to focus on the requirements for the dynamic tow tank test model. A complete test structure was designed, analyzed, manufactured and assembled for the dynamic tow tank model as shown in **Figure 115**, **Figure 116** and **Figure 117**. This effort has provided valuable lessons learned that can be applied to the full scale system.

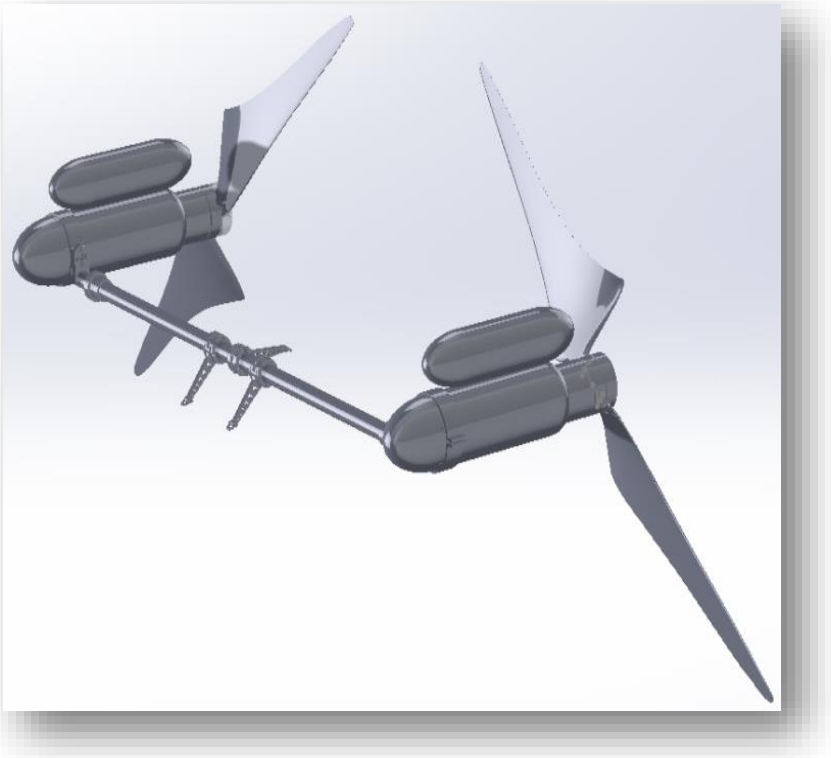

Figure 115 - Tow Tank Test Model Platform Design

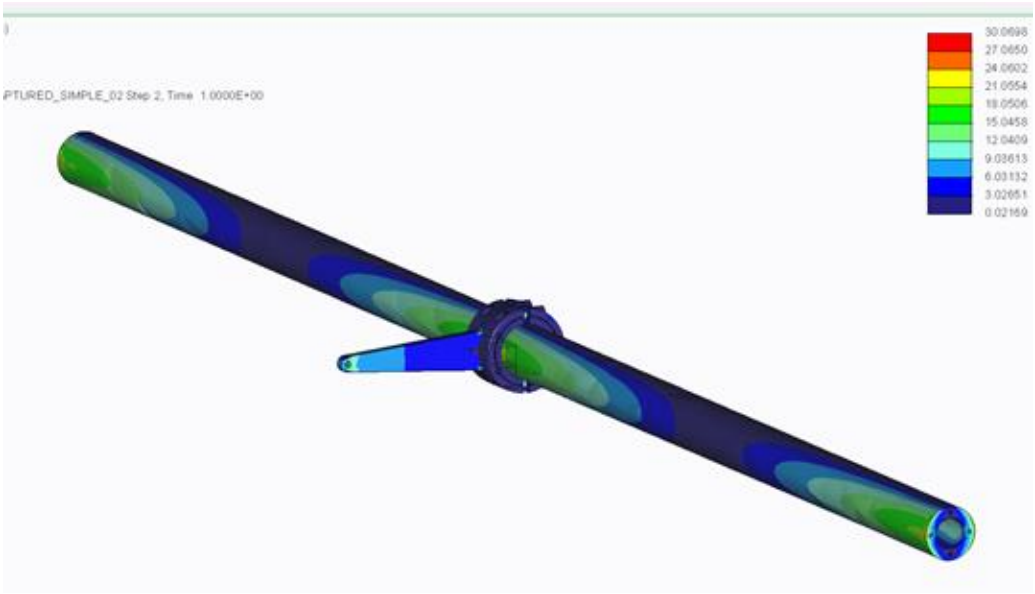

Figure 116 - Tow Tank Test Model Platform Analysis Results

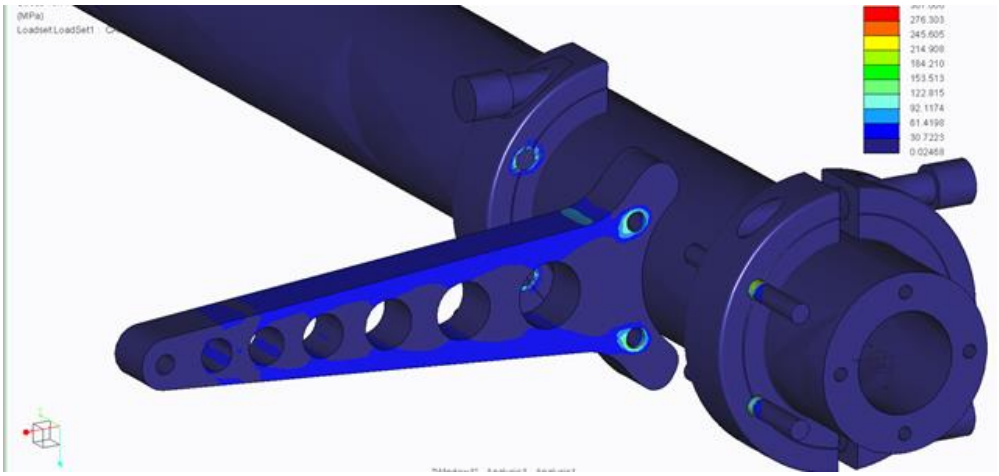

Figure 117 - Tow Tank Test Model Platform Detailed Analysis Results

Platform activities were limited to those undertaken in the manufacturing of the tow tank test model elements as seen in **Figure 118**. Tow tank testing provided significant and useful data for the future, full scale, platform design work. The final result of the tow tank test model platform design efforts can be seen in the figure below:

Figure 118 - Tow Tank Test Model Completed Platform

No detailed platform design work was conducted; however platform design parameters continue to be concepted and analyzed on a general scale in some of the Tidal Bladed modeling efforts. The concept work has centered on the gross sizes of structural members and the nacelle bodies as these have the most impact on the Tidal Bladed model.

Task 5: Hydrodynamic and Bearing Design

One of the challenging requirements of ocean current energy is the low flow speeds. The 1.6 m/s rated flow speed of the C-Plane device requires a 29 m rotor to generate 500 kw. This large rotor and operation in dense seawater generate enormous thrust forces, overturning moments and torques on the device during power generation. This creates a complex challenge for the mainshaft and rotor support bearing design as seen in **Figure 119**. Previously DA used the forces and moments generated by the rotor design to evaluate a wet (water lubricated non-metallic bearing) and standard dry (oil lubricated antifriction rolling element bearings). During the MHK grant period DA further evaluated the technical feasibility of the wet bearing concept through preliminary analysis, vendor recommendations, material selection and characterization testing. Specific considerations in conducting this design evaluation include: wear life, torque loss, coupling reliability, seal design, device dimensions and weight of the components.

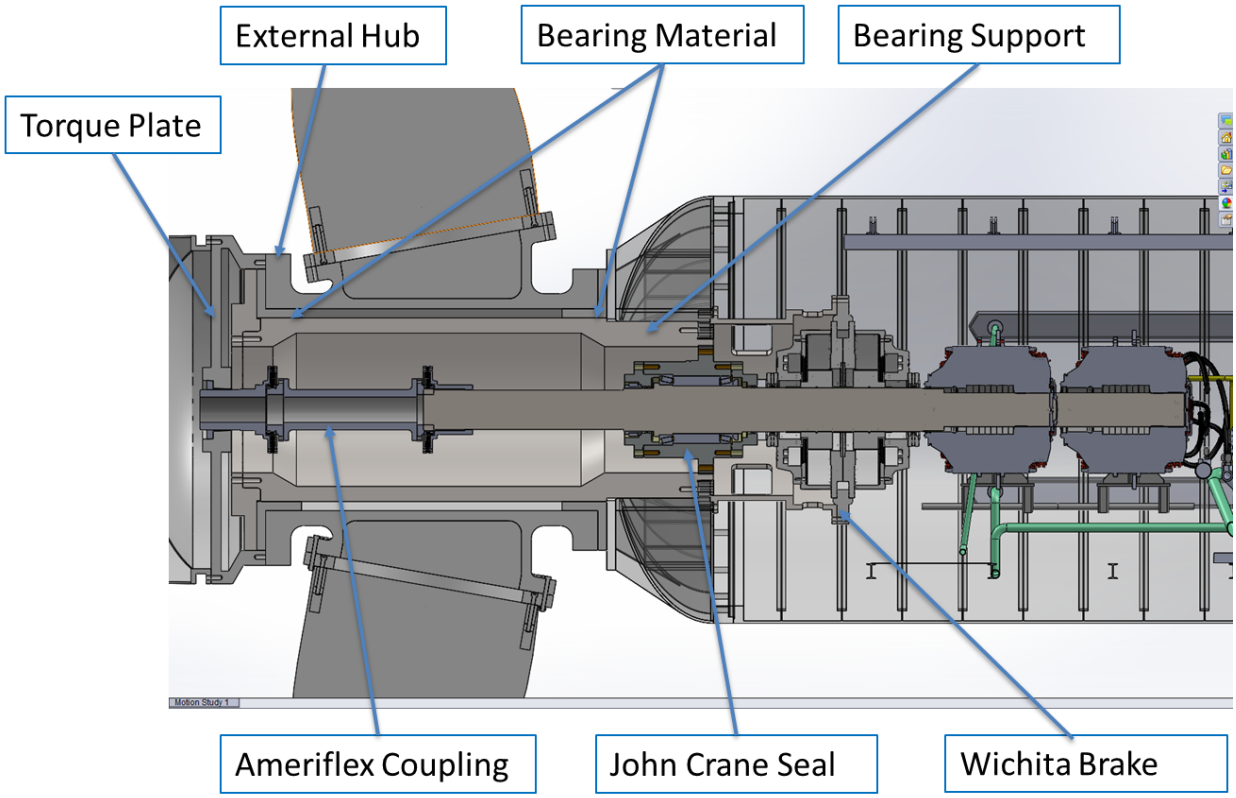

Figure 119 - C-Plane Rotor Mainshaft, Seal and Bearing Layout

The concept layout of the wet bearing and seal packages was developed for DA by partners Powertrain Engineers Inc. and ARL Penn State. Using the anticipated geometries and calculated rotor loads the bearings were sized using area and pressure calculations to determine initial wear and frictional losses. Preliminary stress analysis was also performed to investigate the ovalization and edge loading of the bearings. Using these first order calculations and geometry the preliminary

requirements of the bearings, including layouts and duty cycle, were developed for further investigation by various manufacturers. The proposed layout is shown in **Figure 120**.

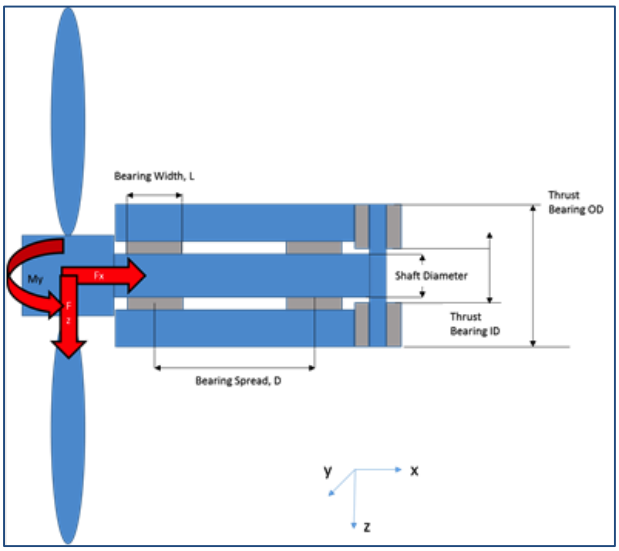

Figure 120 - Seawater Bearing Concept Layout

The seawater bearing is seen as a risk item due to the contact pressures, slow rotational speed and 95% operational duty cycle that requires an extremely low wear rate. Preliminary calculation of wear and frictional losses were done using material properties of ultrahigh molecular weight polyethylene (UHMWPE) as developed and recommend by the University of Florida tribology lab.

DA engaged multiple bearing material suppliers for material recommendations and analysis support of the C-Plane seawater bearing system including Duramax, Trelleborg, Kamatics, Thordon, GGB and Quadrant Plastics. Each manufacturer had a specific recommended material and guidelines for the design of seawater bearings. In general DA learned that higher surface speed and lower pressures allow hydrodynamic lubrication, and common guidelines for design are pressure of less than .5 Mpa and surface speed greater than 1 m/s. A common concern is the quantity of hours at low speed, start up and shut down. These conditions may require hydrostatic lift to eliminate wear. In addition, the bearing and support structure designs must allow for misalignment and edge loading due to off axis loading and may require compliant mountings. Preliminary bearing hydrodynamic analysis and wear results of the radial bearings for the full system duty cycle, performed by the leading manufacturer, indicate reasonable wear depth over life. No manufacturer was able to provide wear estimates for the thrust bearings.

The material selection proved very difficult as the C-Plane operating pressures are much lower than the standard operating pressures for the materials. The vast majority of suppliers for potential materials did not have typical design parameters or test data at the C-Plane operating conditions. This lack of data highlighted the need for material characterization testing at the C-Plane operating conditions. In response, DA and its industrial project partner selected the most promising materials and designed a characterization test that would evaluate each material at operating conditions similar to rated power generation in the Aquantis C-Plane. Materials that were down selected for further evaluation and testing include: Orkot TXMM, ultra-high molecular weight polyethylene (UMHWPE), Techtron HPV and Greene Tweed WR575. Properties for these materials can be found in **Table 5**.

Table 5 - Seawater Bearing Material Properties

Potential Vendors	Material	Density	Friction	Compressive Modulus	Hardness	Swell In Water	Max Dynamic Load	Max Sliding Speed	Wear Rate	Cost
		g/cc	-	Mpa	rockwell	%	mPa	m/s	1/Mpa	$/kg
Duramax Marine	DMX	-	-	-	-	-	-	-	-	-
University of Florida	UHMWPE	0.926	0.03	-	-	0.01	-	-	1.00E-09	-
Orkot Marine Bearings	TXMM	1.3	0.05	280	100	0.1	-	-	-	-
Thordon Bearings	SXL	1.16	0.15	440	85	1.3	10	-	-	-
Kamatics Corporation	Katherm T87s	1.39	0.02	875	85	-	276	0.25	-	-
GGB Bearings	GGB HPF	1.9	0.02	380	-	0.05	140	1	-	-
NA PTFE	PTFE	2.1	0.02	550	-	-	-	-	-	-

The material characterization and wear rate testing of the materials was specifically designed to test the conditions as found in the thrust bearing of the C-Plane. The design requirements for the bearing include high seizure resistance, low static friction coefficient, minimum possible dynamic friction coefficient, 5 year life and low wear rate. The testing program used common tribology abrasion testing equipment to arrive at wear rate data. The test used seawater as the lubricating fluid and the samples were run on a copper nickel alloy material to simulate the running surface of the main shaft.

The test procedure consisted of soaking the test specimens in seawater for 4 hours along with the loading and contacting disk. The loading was increased gradually with loading on the disk to the slide direction. The breakaway coefficient of friction was measured when the sliding load suddenly decreased. The dynamic coefficient of friction was measured after the initial wear in of the materials and the wear rate had stabilized. The stable wear rate of the material was calculated by measuring the wear depth in the material cross section and determining the volume of material removed. The surface roughness curve was measured before and after testing using a surface roughness measuring device.

An initial test was performed using the first material. Initial wear occurred until the sliding distance reached 45,000 m and after the initial wear the coefficient of friction was about 0.006 and the wear rate became stable. The stable wear rate was calculated at 1.51×10^{-10} 1/MPa.

This initial test showed promise that there exists a viable and stable material for the seawater bearing. However, additional testing should be conducted to better quantify the initial wear loss and more samples should be run to determine the repeatability of the test results. Other material specimens will be tested under the same conditions and the best material selected for the bearing. These data will inform the design process for a potential C-Plane seawater bearing application.

As a second path to a simple journal or plate DA engaged a leading designer and vendor of fluid film bearings. After discussion of the requirements and challenges of the project, Aquantis was provided a proposal for the design of an elasto-hydrodynamic lubricated (EHL) bearing where seawater forms a thin film to support the running shaft and reduce friction. This type of bearing would be an alternative to or used in combination with one of the bushing materials determined from the wear rate testing program. The proposal includes collection of operating data, bearing calculations, materials selection, specifications, manufacturing parameters, detailed design and analysis and drawings. This alternative will be evaluated with respect to the seawater bearing test material results and design and the alternative of using conventional rolling element bearing.

While the testing and manufacturer analysis show that the system could prove feasible, the economics tell a different story. The seawater bearing arrangement is much more costly than a standard anti-friction bearing arrangement. The system requires a large diameter to create the required surface area to minimize the bearing pressure and therefore large support structure. The structure has to be stiff in order to prevent ovalization and hot spots in the bearings. The structure adds significant mass and cost the system. The required clearance and wear rates of the bearing materials necessitate the use of a flexible coupling prior to the main shaft dynamic hull penetration seal. A coupling capable of operating in seawater with the required deflection capability is very expensive. Finally the mainshaft and seal in the seawater bearing arrangement still require a substantial antifriction bearing set to support the shaft. All these features add additional cost and complexity to the system. While the technology shows promise due to the cost and technical risk, Aquantis has made the decision to work on the seawater bearing as a technology development program and take it off the critical path of the prototype and initial production C-Plane.

COE MODELING

Prior to the MHK grant performance period, Aquantis developed a detailed LCOE model as a deliverable of the DOE AWP grant. This model explored all aspects of the C-Plane design including a detailed look at the powertrain, structures, rotors, mooring system, installation, and operations. The details of this model were discussed in the Final Report and presentation of the DOE AWP grant. Fortunately this model also served as a detailed starting point from which the Aquantis device cost of energy could be further explored for the various configurations (see **Figure 121**) and component optimization work performed under the MHK grant discussed here.

Over the course of the MHK grant, Aquantis explored various configuration and trade studies on the optimal commercial configurations of the Aquantis C-Plane. These studies included mooring

configuration, support structure architecture, power rating, control methodology, number of rotors, and powertrain topology. Each of these configurations were compared relatively using the AWP COE model inputs as a basis then scaling and updating areas as necessary..

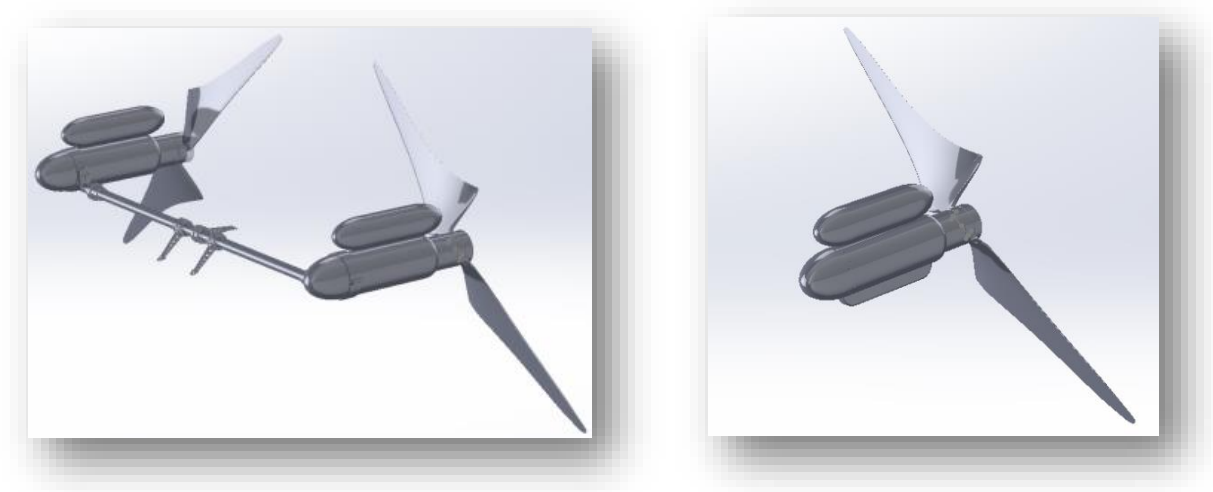

Figure 121 - Dual and Single Rotor C-plane Configurations

DA investigated the cost of energy between a single rotor configuration versus a dual rotor. The results of the investigation found for an initial commercial device, a single rotor turbine was competitive on COE and offered many other benefits.

The major cost driver is the structure required to support and separate the rotors. The large structure forward of the rotors also creates unsteady loading from its wake this increases the fatigue loading on the blades and main bearings driving up cost and weight.

Another major benefit is the handling, installation operations and maintenance of the turbine. The dual rotors and connecting structure is more the 2X heavier and 2X longer than the single rotor. A more maneuverable and retrievable device will significantly reduce the IO&M. In addition to being harder to maintain, the Dual-Rotor C-Plane will also incur reduced availability due to power-pods shutting down in pairs as one rotor cannot operate independently.

The drivetrain architecture was significantly researched and described in section 2.6 above. The impact of the major CAPEX increases for the hydrostatic drivetrain was investigated for LCOE. The net result of the increased rotor, structure, and drivetrain costs yield a 16% increase in relative COE for the HST when compared to the gearbox topology.

The final configuration that was down selected at the end of the MHK reporting period was a 500kW 27m single rotor, pitch controlled turbine with a conventional main bearing, gearbox and permanent magnet generator drivetrain. The LCOE of this configuration presented the most promising initial commercial cost of energy and allows for future COE reductions with larger

rotors and higher power ratings. The results of the LCOE for this device yield a LCOE of $0.112/ kWhr as shown in **Figure 122**.

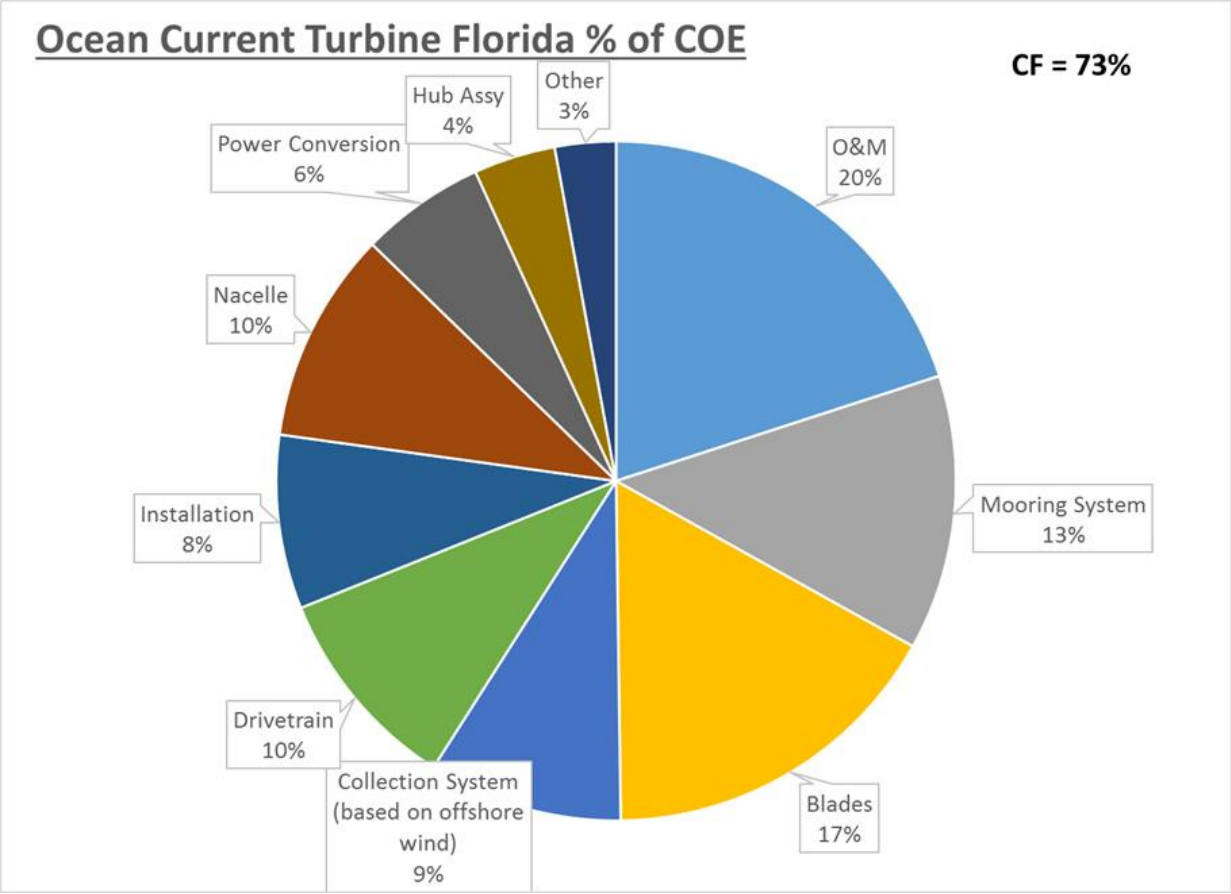

Figure 122 - Final Configuration LCOE

CURRENT PROJECT STATUS

DA renewed the cooperative research agreement (CRADA) with the Naval Surface Warfare Center – Carderock Division (NSWC-CD) to complete and deliver the final materials and a written record of the C-Plane DCAB analysis process; the results collected; and the correlation between it and the tow tank test data. Given the positive results obtained in testing a single rotor C-Plane system in the tow tank testing program and significant capital expense benefits to the project, DA has transferred its focus to this configuration. Recent efforts have involved refined Tidal Bladed modeling of the stability and loads properties of the single rotor system. In-house personnel and DA consultants DNV-GL (Garrad Hassan) and Helios Engineering, Inc. will continue their efforts on modeling the single rotor C-Plane in Tidal Bladed, conducting analyses, determining loads and stability and resolving challenges with the code.

The C-Plane tow tank test scaled model was returned from DA's project partner's facility to DA's

Santa Barbara, California facility for storage and possible future use. The dynamic towing rig is still located at the NSWC-CD facility partially disassembled and stored within the model test basin. No further testing is planned for the model or the dynamic test rig at this time. As a close-out of the tow tank model development efforts NSWC-CD will complete and deliver a summary of the test model control system developed and the components and software involved in it.

Rexroth and IFAS/Aachen University completed simulation of the hydrostatic drivetrain including varying inflow conditions and basic operating states. Their work also encompassed determining preliminary reliability and efficiency parameters associated with the system. Their work was summarized in a final report which DA analyzed. DA is currently evaluating the hydrostatic drivetrain with respect to conventional geared solutions before moving into detailed design.

DA will continue analyze the MHK hydrofoil sections using WT-Perf and CFD to optimize the geometry for performance. The hydrofoil sections include both an 18 and a 24% section. The end result of their work will be optimized hydrofoil sections that can be built into model test sections and performance tested in a wind tunnel. DA has conducted a checkout test of the proposed hydrofoil cryogenic wind tunnel test facility at NASA Langley. This test has proved the capability of the test facility to conduct the specific tests desired by using an existing airfoil test section.

DA will continue design work optimizing the blade including the barrel nut root attachment. Work will continue to resolve these challenges with revisions to the blade geometry, structure and materials. The final result will be an optimized design for both configurations taking into account the loads applied at the operating depth and the duty cycle.

DA and its project partner concluded initial wear rate testing of candidate materials for the seawater bearing. The initial testing showed all materials to be viable and stable for the seawater bearing with a coefficient of friction and wear rate below the design requirement. Additional testing will be conducted to further quantify the wear rate and a preliminary design prepared for comparison with conventional, rolling element bearings.

DA will continue to engage the expertise of commercial manufacturers of elastohydrodynamcally lubricated (EHL) bearings as a possible alternative solution for the C-Plane mainshaft bearing. Additional design and analysis will be completed to evaluate this option with respect to the seawater bearing and conventional rolling element bearings.

Given that the overall C-Plane system has been successfully tested in a tow tank environment, DA assesses that it is currently at TRL 5 in consideration of the DOE's TRL level ranking scale. DA assesses this TRL based on the DOE's definition of Level 5 being: "Laboratory scale, similar system validation in relevant environment" (US Department of Energy, 2011). The tow tank testing program simulated the dynamic, operating conditions of both a moored dual rotor and single rotor system in several modes of operation. The testing demonstrated the stability and operational parameter of the system that will be highly beneficial in modeling and designing a full-scale prototype for deployment in an ocean current or tidal resource.

PLANNED FUTURE WORK

Overall Project Direction and Commercialization Plan

Aquantis is developing and commercializing a single rotor device to address both tidal and ocean current markets in the U.S. and abroad. While there are more moorings to install per MW when using single rotor devices, the mooring hardware is proportionately smaller and easier to handle. The increased mooring installation cost is also offset by other benefits of easier deployment/recovery, improved maintenance access, and reduced downtime (a dual-rotor device must shut-down both rotors when one has a failure). Further benefits to business and technical development include reduced system complexity and prototype cost.

Naval Architecture

Consideration and recalculation of the C-Plane naval architecture parameters will be conducted as needed throughout the design process. These parameters will be maintained in the weight and buoyancy register, used as inputs for the Tidal Bladed loads analysis and recorded in the C-Plane loads document.

Hydrodynamic and C-Plane Dynamic Simulation Analysis

The full scale, single rotor, C-Plane system model and controller will continue to be developed and executed in Tidal Bladed. Loads results will be extracted from the operating condition simulations. The loads results will be used for detailed component design. DNV – GL have plans to modify Tidal Bladed to include fully dynamic mooring simulation and the inclusion of lift and moment coefficients on non-rotating model components such as the C-Plane's nacelle. From the analysis data, load mitigation strategies (passive depth control, stall regulation and dynamic braking) will be developed. The generated loads profile will allow rotor and platform extreme and fatigue load calculations to be conducted.

Mooring Analysis

The mooring system model will continue to evolve in the Tidal Bladed analyses yielding refined dynamic characteristics and tension loadings in the system. PCCI or an alternative firm will be further engaged to provide design input on the modified system and conduct OrcaFlex analyses, if required, to serve as a back-up and a check to the Tidal Bladed results.

Scaled C-Plane Model Platform and Mooring Fabrication- 1/25th

DA received shipment of the C-Plane model from its project partner for long-term storage at DA's headquarters in Santa Barbara, CA.

Platform Instrumentations: Inertial Measurement Unit, Transducers and Load Cell

The instrumentation was returned to the DA offices with the model for potential future use.

Scale Turbine Blades Fabrication - 1/25th

No further scaled blade fabrication activities are planned at this time.

Basin Test Towing Hardware

The dynamic test rig will be removed from the NSWC-CD tow test basin for other uses, remote storage or recycling.

Tow Tank Tests: Basin Evaluation

It is anticipated that the tow tank test data may be used periodically throughout the Tidal Bladed modeling efforts, as required, for results comparison.

Mechanical Turbine Design

As a next step the development of a test bench is proposed to validate the simulations. Accomplishing this requires a modification of the current hydrostatic drivetrain test bench at IFAS.

Hydrofoil and Rotor Development

DA will continue collaboration on the hydrofoil design and testing program. Senta Engineering will complete the hydrofoil design, analysis and final reporting for their scope. The hydrofoil testing program will be further scoped.

DA will continue work to resolve the structural issues associated with the conventional blade and root connection design. DA will define a target cost for the through hub spar blade to drive the design and develop a simplified evaluation tool that is necessary for the blade aero design input. DA plans to develop a simple tool to evaluate maximum moments transferred by the blade section that is elliptic shape based, based on the thickness/chord/materials data and provides a very quick and automatic estimation.

Platform Design

With the continued simulation of the full scale, single rotor C-Plane in Tidal Bladed planned DA will use this information as inputs for a preliminary design of the platform structure. The single rotor system offers significant platform advantages in reducing rotor wake effects on any structure and improving the system economics in terms of capital, operational and maintenance costs. The single rotor platform design will be reflected in updated CAD models.

Hydrodynamic and Bearing Design

The seawater bearing materials initial wear volume will be measured and stationary wear will be evaluated more precisely. Other material specimens will be tested under the same conditions and the best material selected for the bearing. These data will inform the design process for a potential C-Plane seawater bearing application.

DA will make further consideration of the proposal for possible execution on an EHL bearing design. This alternative will be evaluated with respect to the seawater bearing test material results and design and the alternative of using conventional rolling element bearings.

REFERENCES

US Department of Energy. (2011). *Technology Readiness Assessment Guide.* Washington, D.C.: U.S. Department of Energy.